NPS ARCHIVE
1967
BALL, E.

ACOUSTIC BACKSCATTER FROM A RANDOM ROUGH WATER SURFACE

ERNEST CHARLES BALL
and
JOHN ALGOT CARLSON

[redacted]

ACOUSTIC BACKSCATTER FROM A RANDOM ROUGH WATER SURFACE

by

Ernest Charles Ball
Lieutenant Commander, Royal Canadian Navy
B.A., University of Toronto, 1956
M.S.E.E., Naval Postgraduate School, 1966

and

John Algot Carlson
Lieutenant, United States Navy
B.C.E., Georgia Institute of Technology, 1962

Submitted in partial fulfillment of the
requirements for the degree of

MASTER OF SCIENCE IN PHYSICS

from the

NAVAL POSTGRADUATE SCHOOL
June 1967

NPS ARCHIVE
1967
BALL, E.

THESIS
B1744
C.1
[redacted]

ABSTRACT

Acoustic backscattering from a random rough water surface has been studied experimentally to test the application of two scattering theories, a statistical description and a resonance approach. The rough surface was created by wind agitation over an anechoic tank. The wave height distribution was measured with a resistive probe and the wave slope distribution by optical glitter detection using a photocell. The distributions of backscattered sound pressures were recorded for surface roughnesses and sound frequencies corresponding to a very wide range of roughness conditions. Both statistical and resonance theories have regions of applicability and regions where they fail to predict the backscatter. Backscattering may be considered to be due to these two mechanisms, since a summation of the predictions of the two theories fits the experimental data fairly well over the complete range of angles of incidence studied. A method of analysis is suggested to relate the doppler shifted continuous wave sound spectrum to the surface wave spectrum.

LIBRARY
NAVAL POSTGRADUATE SCHOOL
MONTEREY, CALIF. 93940

TABLE OF CONTENTS

Section		Page
1.	Introduction	13
	Historical	14
	Summary of Experiment	17
2.	Scattering Theory	19
	Statistical Theory	19
	Resonance Theory	29
3.	The Model Sea Surface	33
	Generation of Rough Surface	33
	Wave Height Statistics	33
	Theory	33
	Experimental	37
	Results and Conclusions	51
	Wave Slope Statistics	59
	Theory	59
	Experimental	61
	Results and Conclusions	70
	Surface Wave Spectrum	78
4.	The Backscattered Radiation	79
	Backscattered Pulse Distribution	79
	Experimental	79
	Comparison with Theory	99
	Backscattered Continuous Wave Spectra	109
	Experimental	112
	Observations	118

TABLE OF CONTENTS (continued)

Section		Page
	Analysis and Speculation	118
	Conclusion	128
5.	Summary	130
6.	Bibliography	132

LIST OF TABLES

Table		Page
3.1	RMS Wave Height cm.	59
3.2	Mean Square Slope	70
4.1	Beam Angles to 3 db Down Points	95

LIST OF ILLUSTRATIONS

Figure		Page
2.1	Scattering Geometry for Incident Sound	21
2.2	Scattering Geometry for Scattered Sound	21
2.3	Wave Energy Spectra for Fully Developed Sea	30
2.4	Resonance Interaction	30
3.1	Generation of Rough Surface in Anechoic Tank	34
3.2	Anechoic Tank and Wave Generator	35
3.3	Height Distribution for a Single, One Dimensional Sinusoidal Surface	36
3.4	Measurement of Wave Height	38
3.5	Surface Probe for Measurement of Wave Height	38
3.6	Wave Height Measurement System	40
3.6a	Equipment List	41
3.7	Wave Height Detector	42
3.8	Sampler Unit	42
3.9	Surface Probe Characteristics	44
3.10	Dynamic Calibration of Wave Height Measuring Device	46
3.11	Worst Case Extrapolation of Wave Height Measurement Device Frequency Response	48
3.12	Wave Height Measurement Calibration	50
3.13	Wave Height Distribution, Station 1, 1 Blower	52
3.14	Wave Height Distribution, Station 1, 2 Blowers	53
3.15	Wave Height Distribution, Station 1, 3 Blowers	54
3.16	Wave Height Distribution, Station 2, 2 Blowers	55
3.17	Wave Height Distribution, Station 2, 3 Blowers	56
3.18	Wave Height Distribution, Station 3, 3 Blowers	57
3.19	Typical Pulse Height Analyzer Output for Wave Height Distribution	58

LIST OF ILLUSTRATIONS (continued)

Figure		Page
3.20	Apparatus for Measurement of Wave Slope Statistics	60
3.21	Wave Slope Measuring Device	62
3.22	Wave Slope Measuring Device Details	63
3.23	Wave Slope Signal Processing Diagram	64
3.24	Wave Slope Signal Processing Apparatus	65
3.25	Typical Voltage Signal from Photocell	66
3.26	Typical Brush Recorder Trace, Wave Slope Signal	68
3.27	Upwind-Downwind Wave Slope Distribution, Station 1, 2 Blowers	71
3.28	Crosswind Wave Slope Distribution, Station 1, 2 Blowers	72
3.29	Upwind-Downwind Wave Slope Distribution, Station 1, 3 Blowers	73
3.30	Crosswind Wave Slope Distribution, Station 1, 3 Blowers	74
3.31	Upwind-Downwind Wave Slope Distribution, Station 2, 3 Blowers	75
3.32	Crosswind Wave Slope Distribution, Station 2, 3 Blowers	76
3.33	Energy Spectrum of Rough Surface	77
4.1	Electronic Apparatus for Analysis of Pulsed Backscattered Radiation	81
4.2	Transmitter and Receiver System - 70 kHz	82
4.2a	Equipment List	83
4.3	Transmitter and Receiver System - 450 kHz	84
4.3a	Equipment List	85
4.4	Shunt Gate	88
4.5	SCR Gate	88

LIST OF ILLUSTRATIONS (continued)

Figure		Page
4.6	Receiver Blanker Circuit	89
4.7	Detector Circuit	90
4.8	Regulated Power Supply	90
4.9	Calculation of Scattering Area	92
4.10	Positioning Gear for Transducer	94
4.11	Support Bridge for Transducer	96
4.12	Mean Square Pressure vs. Roughness Factor	98
4.13	Pulse Height Distribution, Station 1, 1 Blower	100
4.14	Pulse Height Distribution, Station 1, 2 Blowers	100
4.15	Pulse Height Distribution, Station 1, 3 Blowers	102
4.16	Pulse Height Distribution, Station 1, 1 Blower, 30^{o}	102
4.17	Backscattering Factor - Relatively Smooth Surface	103
4.18	Backscattering Factor - Transition Surface	104
4.19	Backscattering Factor - Transition Surface	105
4.20	Backscattering Factor - Rough Surface	106
4.21	Backscattering Factor - Rough Surface	107
4.22	Continuous Wave Spectra Measurement System	110
4.22a	Equipment List	111
4.23	Difference Spectrum - Smooth Surface	114
4.24	Difference Spectrum - Rough Surface, Normal Incidence	115
4.25	Difference Spectrum - Rough Surface, 60^{o} Incidence Looking Upwind	116
4.26	Difference Spectrum - Rough Surface, 60^{o} Incidence Looking Downwind	117
4.27	Graphical Construction of Doppler Spectrum, Upwind Direction	120

LIST OF ILLUSTRATIONS (Continued)

Figure		Page
4.28	Graphical Construction of Doppler Spectrum, Downwind Direction	121
4.29	Velocity of Surface Waves in Water	122
4.30	Backscatter from 0.2 msec Pulse at 48 kHz	124
4.31	Doppler Shift Energy vs. Wave Frequency	126

ACKNOWLEDGMENT

The authors are indebted to Dr. H. Medwin of the Naval Postgraduate School for his guidance and direction during the preparation of this thesis. His patient introduction to the theory of scattering and his appreciation of the pitfalls of experimental physics assisted immeasurably.

Sincere thanks are also due to Dr. G. Myers for his helpful discussion of the application of frequency domain methods to the analysis of backscattered signals.

The assistance of technicians W. Smith, R. Garcia, and H. Whitfil in the maintenance of electronic equipment assisted greatly.

ACOUSTIC BACKSCATTER FROM A RANDOM ROUGH WATER SURFACE.

1. Introduction.

Study of the limitations of acoustic propagation in the sea invariably reveals surface reverberation to be one of the chief noise sources. In recent years, many attempts have been made to produce a cogent theory to relate the scattered signal strength to parameters describing the sea surface, and these efforts have met with some success. However, results from measurements at sea show that no theory available at present can explain the scattering phenomenon completely.

Two principal theories, a statistical theory and a resonance theory are examined briefly to show the predicted backscatter. The major part of this work is devoted to experimentally measuring the pulsed and continuous wave backscatter from a rough water surface and to measuring the necessary surface parameters as required by theory. The results are compared with the predictions of theory and with results of other experimenters both in the laboratory and at sea.

Scattering theory has been developed largely with respect to electromagnetic radiation, yet the problem of acoustic scattering is completely analogous. Except for the phenomenon of polarization inherent in electromagnetic radiation, the reverberation problem in underwater acoustics is identical with the "sea-return" problem encountered in the operation of pulsed radar at low angles over a rough water surface.

Historical

Several works of recent years have pointed out the nature of the backscatter phenomenon. In 1956, Urick and Hoover (1) conducted experiments at sea near Key West, Florida under various conditions of wind speed and sea state. Their data brought out essential qualitative details of acoustic backscatter. They noted that at grazing incidence, (transducer beam nearly horizontal) backscatter increased as the surface became rougher. At normal incidence this effect was reversed, the backscattered energy decreased as the roughness increased. In addition, they noted the existence of a precursor in their echo traces at normal incidence which led them to predict the existence of a subsurface volume scattering layer. Measurement of backscatter by Garrison, Murphy and Potter (2) in 1959 in Puget Sound, confirmed the general shape of curves of backscattering coefficient vs. grazing angle, although the latter used wind speed rather than surface roughness as a parameter. (That they are related parameters is beyond question.) It is noted that the latter paper used Urick's and Hoover's postulated volume scattering layer as a possibly explanation of poor definition of curves obtained at low wind speeds. In addition, the effect of the curvature of acoustic paths was considered as a significant source of error for the long range method used in the experiment.

In 1961, Chapman and Harris (3), in deepwater north of Bermuda, extended the measurements at sea to the low frequency range using explosive sound sources. The backscattered echoes were recorded and played back through octave band filters. The curves of backscattered signal strength vs. grazing angle for all frequencies

showed dependence on grazing angle at large grazing angles and virtual independence of grazing angle at small grazing angles. This effect they, too, attributed to the existence of a volume scattering layer. Since this region of independence of grazing angle was seen to be at a higher level for higher sea states, the possibility of the volume scatterers being bubbles was raised, although it was noted that, in this respect, the data were inconsistent. The existence of the volume scattering layer was deduced from the return of echoes prior to the expected reverbation from the shock. This pre-cursor had a return time which demonstrated a diurnal variation suggesting that the scattering layer might also be biological in origin.

Scattering theory was developed in this period along two lines. Eckart (4) developed relationships between the scattering coefficient and the surface statistics of wave slope and wave height. Beckmann and Spizzichino (5) provided an excellent bibliography and summary as they examined the electromagnetic scattering phenomenon and related the scattered intensity, once again, to the surface parameters of wave slope and wave height. In the work of Beckmann and Spizzichino and Shulkin and Shaffer (6), the significance of a surface roughness parameter such as the Rayleigh roughness criterion is noted, and the suggestion is made that correlation of backscattering with wind speed may be observed for fully developed seas but not necessarily for other sea conditions.

In 1964, Clay and Medwin (7) examined the thesis that the volume scatterer might be bubbles and they calculated the bubble density required to produce such an effect. Barnhouse, Stoffel and Zimdar (8),

in 1964 conducted experiments to show that bubble populations greater than that necessary to provide volume scattering did exist in Monterey Bay, California.

An entirely different approach from the postulation of statistically distributed scattering surface facets is taken by Wetzel (9). As with Marsh (10), he deals with the relation between sea scatter and the ocean wave spectrum. He raises the question of a resonant interaction of electromagnetic waves with the moving water waves to show Doppler shifts. The theory is derived only for the scattering problem for relatively smooth surfaces.

The principal strength of the statistical theory appears to be for large grazing angles and for specular scattering (scattering in the mirror direction). However, the theory fails to predict the backscatter observed at or near grazing incidence. The theory that the acoustical scattering at grazing incidence is not a surface scattering but a volume scattering phenomenon begs the question as to a postulated mechanism since the same phenomenon occurs in the scattering of electromagnetic radiation from the same surface. Hence it appears reasonable to demand that theory contain a prediction of an inflection in the form of the curve of backscattering coefficient vs. grazing angle to explain the scattering at grazing incidence. It must be borne in mind that the theoretical curves used for comparison are asymptotic forms for "smooth" surfaces and for "rough" surfaces. Even so, the departure of experimental evidence from the asymptotic form for rough surfaces raises doubts as to the validity of the statistical model. Fante (11) has shown how curves of the correct shape can be found by modifying the assumption concerning the form

of the correlation function for the surface. Beckmann and Spizzichino have assumed a Gaussian correlation function because it is consistent with the known Gaussian slope distribution which accompanies the Gaussian height distribution. Fante has pointed out that an exponential correlation function gives the correct shape for the curve. However, the actual levels of backscattering predicted by Fante's modification of Beckmann's assumptions in a statistical scattering model appear to be seriously in error. The use of an exponential or Gaussian correlation function is discussed by Fung and Moore (19).

The resonance theory fails at nearly normal incidence, although the backscattering is predicted, as measured, at grazing incidence to be nearly independent of the grazing angle.

Summary of Experiment

It appeared from the summary of scattering theory that there was room for a number of experiments under controlled conditions to show how the several theories and hypotheses fit (or fail to fit) experimental data. This study is a consideration of backscatter only although the theory makes predictions for acoustic scattering at any angle. The backscattering problem, then, is confined to the situation where the receiving hydrophone is identical with or contiguous to the projector.

The statistical theory was tested by using pulse techniques. As seen from the theory, the backscattering coefficient is a function of the surface statistics and sound frequency through the definition of a roughness parameter. The surface statistics are the root mean square wave height, the root mean square slope and the correlation distance. The three statistics are not independent and in this

experiment the wave height and wave slope only are measured. The wave height is measured by a resistance probe and the wave slope by optical methods similar to the Cox and Munk (12) and Schooley (13) glitter photography methods. Sound frequencies of 20, 50, 70, 100 and 450 kHz were chosen so that the roughness factors approximated those experienced for a wide range of sea states for audio frequencies commonly used in underwater sound instrumentation.

The resonance theory was tested using continuous wave techniques. Differential amplifiers were employed to cancel out the effect of the signal from the projector directly incident upon the receiving hydrophone. The resulting signal was processed through a fixed bandwidth filter to study the backscatter spectrum.

2. Backscattering Theory.

At the present time the whole field of backscattering is in a state of uncertainty. Several theories have been postulated, but so far none has been sufficient to explain the observed phenomena for the full range of grazing angles. Two theories are considered in this thesis, the statistical approach as described by P. Beckmann and A. Spizzichino (5), and the "resonance" approach as used by H. W. Marsh (10), and L. Wetzel (9). A brief review of each is presented concluding with the expression for the Backscatter Factor. A comparison of the theoretical and experimentally observed results is made in Section 4.

Statistical Theory

In this approach to the scattering theory the random rough surface is described by the statistical distribution of its wave heights about a mean level and by a correlation function that relates the wave heights at the various points on the surface. The distribution of wave heights is assumed to be Gaussian with mean zero and standard deviation σ which is identically the root mean square wave height. The correlation function is here assumed to be

$$C(\tau) = \exp\ (-\tau^2/T^2)$$

where the parameter T is the correlation distance of the surface and τ is the distance between any two points whose correlation is desired.

The development of the statistical theory to be followed is a brief summary of the derivation given by Beckmann and Spizzichino (5), Chapters 3 and 5, for electromagnetic radiation. Acoustic scattering theory is completely analogous to the electromagnetic, the pressure field p replacing the appropriate scalar component of the electric field E.

It is convenient at this point to introduce the notation and geometry (Figs. 2.1 and 2.2) of the general scattering problem. The rough surface height is given by the function $\xi = \xi(x,y)$. The mean level of the rough surface is the plane $z = 0$. Cartesian coordinates x,y,z, with origin 0 and unit vectors $\hat{1}_1$, $\hat{1}_2$, $\hat{1}_3$, are used. The subscript 1 will denote all quantities associated with the incident field and the subscript 2 all those associated with the scattered field.

θ_1 = angle of incidence

θ_2 = angle of reflection

$\bar{r} = x\hat{1}_1 + y\hat{1}_2 + \xi(x,y)\hat{1}_3$ distance from origin of surface coordinates to scattering element

r_1 = distance from source to origin of surface coordinates

r_1' = distance from source to scattering element

r_2 = distance from origin of surface coordinates to receiver

r_2' = distance from scattering element to receiver

$\bar{k}_1 = k\hat{k}_1$ propagation vector of incident ray

$\bar{k}_2 = k\hat{k}_2$ propagation vector of reflected ray

$k = \frac{2\pi}{\lambda}$ propagation number

p_1 = incident pressure field at scattering element

p_2 = scattered pressure field at hydrophone

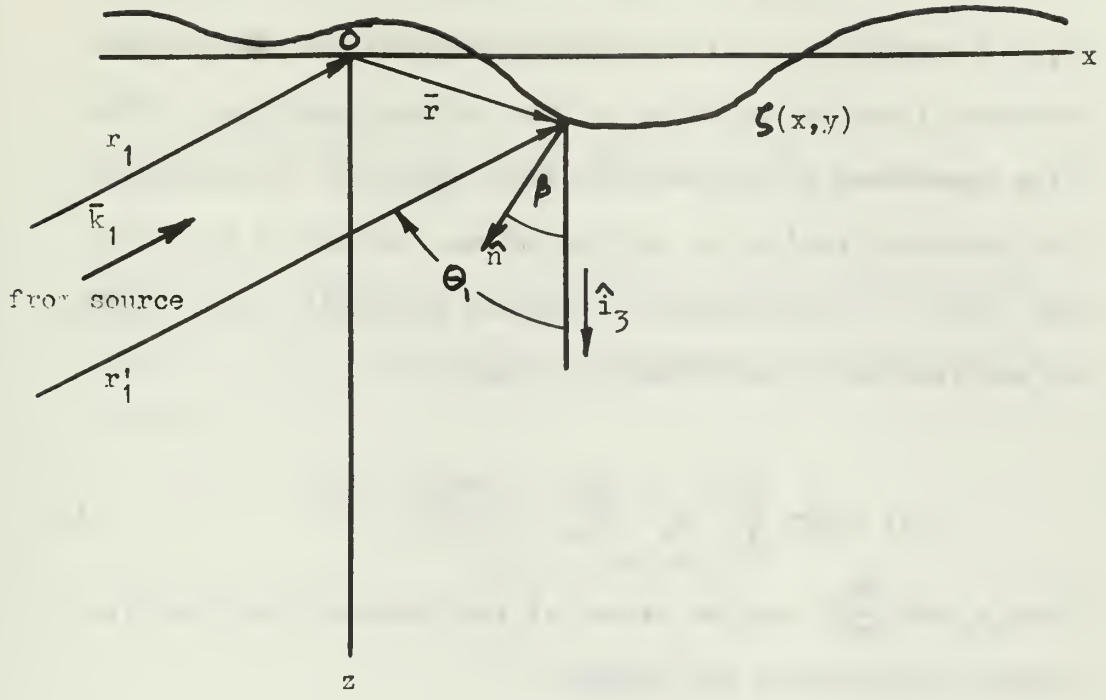

Fig. 2.1 Scattering Geometry for Incident Sound

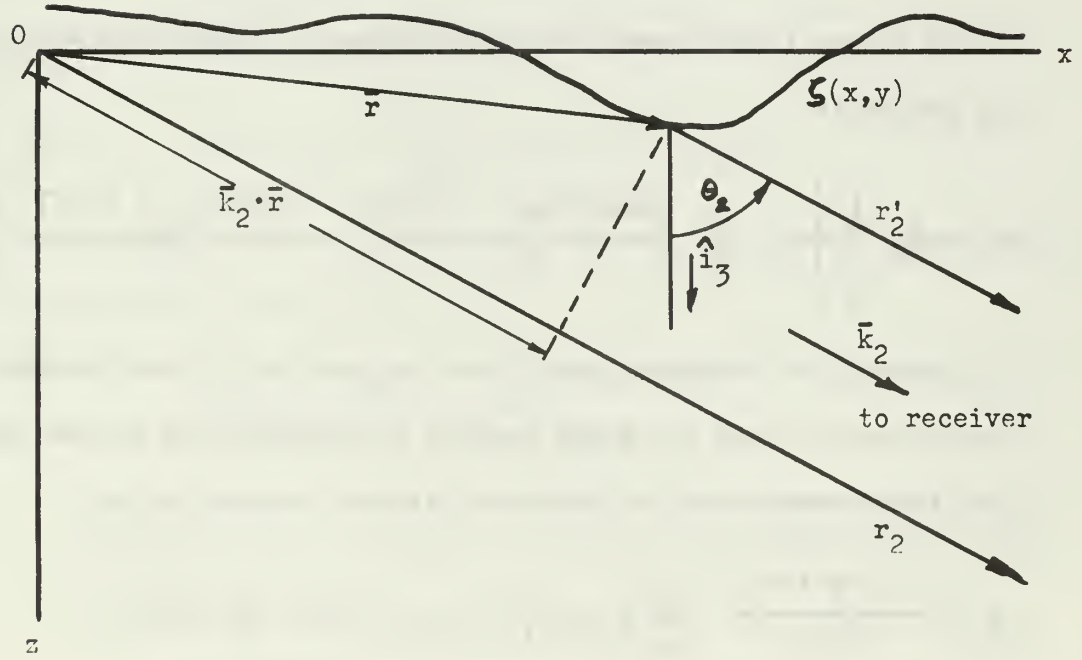

Fig. 2.2 Scattering Geometry for Scattered Sound

We will assume $p_1 = p_{10} \exp(i\bar{k}_1 \cdot \bar{r})$ where $p_{10} = P \exp[i(kr_1 - \omega t)]$ gives the amplitude and phase of the pressure field at the origin of the surface coordinates. The time dependence of the pressure field $\exp(-i\omega t)$ is suppressed. The pressure field p_2 at the hydrophone, assumed to be in the far field (i.e. the scattered rays are parallel), can be found by application of the Helmholtz integral.

$$p_2 = \frac{1}{4\pi} \oint_S \left[p_s \frac{\partial \psi}{\partial n} - \psi \frac{\partial p_s}{\partial n} \right] dS \qquad (1)$$

Here p_s and $\frac{\partial p_s}{\partial n}$ are the values of the pressure field and its normal derivative at the surface.

$$\psi = \frac{\exp(ikr_2')}{r_2'} \cong \frac{\exp[i(kr_2 - \bar{k}_2 \cdot \bar{r})]}{r_2}$$

and $\hat{n}$ is the inward normal from the surface. Making the substitution we arrive at

$$p_2 = \frac{1}{4\pi} \oint_S \left[p_s \frac{\partial}{\partial n} \left(\frac{\exp[i(kr_2 - \bar{k} \cdot \bar{r})]}{r_2} \right) - \frac{\exp[i(kr_2 - \bar{k} \cdot \bar{r})]}{r_2} \frac{\partial p_s}{\partial n} \right] dS$$

In applying the boundary conditions we make use of the Kirchhoff approximation that the plane surface conditions hold at each point and the assumption of a "pressure release" surface to get

$$p_2 = \frac{-i \exp(ikr_2)}{2\pi r_2} \oint_S p_{10} (\bar{k}_1 \cdot \hat{n}) \exp[i(\bar{k}_1 - \bar{k}_2) \cdot \bar{r}] \, dS$$

For simplification let $\bar{v} = \bar{k}_1 - \bar{k}_2$

$$\bar{v} = k[(\sin\theta_1 - \sin\theta_2 \cos\varphi)\hat{i}_1 - (\sin\theta_2 \sin\varphi)\hat{i}_2 - (\cos\theta_1 + \cos\theta_2)\hat{i}_3]$$

If p_{10} is assumed constant over the ensonified surface and zero everywhere else we integrate and find

$$p_2 = \frac{-ip_{10}\exp(ikr_2)}{2\pi r_2} \oint_S (\bar{k}_1 \cdot \hat{n}) \exp(i\bar{v}\cdot\bar{r}) \; dS \qquad (2)$$

Equation (2) enables us to compute the sound pressure field p_2 once the random rough surface is determined since $\bar{r}$ and $\hat{n}$ are functions of it.

If the surface is smooth [$\xi(x,y) = 0$]

$$\bar{k}_1 \cdot \hat{n} = -k\cos\theta_1$$

$$\bar{v}\cdot\bar{r} = v_x x + v_y y$$

and if the ensonified area is assumed to be rectangular, the scattered pressure field becomes

$$p_2 = \frac{ikp_{10}\cos\theta_1}{2\pi r_2} \exp(ikr_2) \; \text{sinc}\, v_x L \; \text{sinc}\, v_y W$$

where $\text{sinc}\, v_x L \equiv \dfrac{\sin v_x L}{v_x L}$ and $A = 2L \times 2W$

For specular scattering ($\theta_1 = \theta_2$, $v_x = v_y = 0$) from a smooth surface the pressure field p_{20} at r_2 is

$$p_{20} = \frac{ikp_{10} A \cos\theta_1}{2\pi r_2} \exp(ikr_2) \qquad (3)$$

Application of equation (2) to a random rough surface leads to the simple formula

$$p_2 = p_{20} \frac{F}{A} \iint \exp(i\bar{v}\cdot\bar{r}) \; dxdy \qquad (4)$$

where $F = \dfrac{1 + \cos\theta_1\cos\theta_2 - \sin\theta_1\sin\theta_2\cos\varphi}{\cos\theta_1 \; (\cos\theta_1 + \cos\theta_2)}$

This does not include the "edge effect" term which is negligible when the assumption $A \gg \lambda^2$ is made.

Since p_2 is a complex quantity the mean square scattered pressure $\langle p_2 p_2^* \rangle$ must be calculated before we can talk about the scattered intensity. The brackets $\langle\ \rangle$ denote the mean value and the asterisk denotes the complex conjugate quantity. $\langle p_2 p_2^* \rangle$ is related to the mean and variance at the scattered pressure field p_2 by the relation

$$\langle p_2 p_2^* \rangle = V[p_2] + \langle p_2 \rangle \cdot \langle p_2^* \rangle$$

The mean pressure $\langle p_2 \rangle$ scattered from a rough surface is now determined by taking the space average of equation (4).

$$\langle p_2 \rangle = \frac{p_{20} F}{A} \left\langle \int\int \exp[i(v_x x + v_y y)] \exp(i v_z \xi)\, dxdy \right\rangle$$

Since we have assumed a Gaussian distribution for surface wave heights the mean value of $\exp(iv_z\xi)$ is

$$\langle \exp(iv_z\xi) \rangle = \exp\left(- \frac{\sigma^2 v_z^2}{2} \right)$$

$$= \exp\left(-\frac{g}{2}\right)$$

where we define the roughness parameter

$$g \equiv \sigma^2 k^2 [\cos\theta_1 + \cos\theta_2]^2$$

The mean scattered pressure then becomes

$$\langle p_2 \rangle = p_{20} F \exp\left(-\frac{g}{2}\right) \operatorname{sinc} v_x L \operatorname{sinc} v_y W$$

This is the coherent component of the specularly scattered pressure field since it is in phase with the smooth reflected pressure p_{20}.

The variance of the acoustic pressure field p_2 is now needed so it can be added to the squared mean pressure $\langle p_2 \rangle \cdot \langle p_2^* \rangle$ to complete the picture of the total scattered intensity.

$$V[p_2] = \langle p_2 p_2^* \rangle - \langle p_2 \rangle \cdot \langle p_2^* \rangle$$

Substituting p_2 and p_2^* from equation (4) leads to

$$V[p_2] = p_{20}^2 \left(\frac{F}{A}\right)^2 \iiint\!\!\iint \left[\exp\left[iv_x(x_1 - x_2) + iv_y(y_1 - y_2)\right]\right] \times \quad (6)$$

$$\left[\langle \exp(iv_z(z_1 - z_2)) \rangle - \langle \exp(iv_z z_1) \rangle \langle \exp(-iv_z z_2) \rangle\right] dx_1 dx_2 dy_1 dy_2$$

This integration is performed by assuming the surface roughness is isotropic, changing to polar coordinates, and using the series expansion for the correlation function

$C(\tau) = \exp(-\tau^2/T^2)$ in evaluating $\langle \exp[iv_z(z_1 - z_2)] \rangle$.

$$\langle \exp[iv_z(z_1 - z_2)] \rangle = \exp[-g(1 - C)]$$

$$= \exp(-g) \frac{g^m}{m!} \exp(-m^2/T^2)$$

The result

$$V[p_2] = \frac{2\pi F^2 p_{20}^2}{A} \int_0^\infty J_o\left(\tau \sqrt{v_x^2 + v_y^2}\right) \left[\exp(-g) \sum_{m=1}^{\infty} \frac{g^m}{m!} \exp[-m\tau^2/T^2] \right] \tau \, d\tau$$

is integrated using equ. 14, Appendix B, Beckmann (5). The variance of the scattered pressure is then

$$V[p_2] = \frac{\pi F^2 T^2 \exp(-g) p_{20}^2}{A} \sum_{m=1}^{\infty} \frac{g^m}{m m!} \exp[-(v_x^2 + v_y^2) T^2/4m]$$

Finally the mean squared scattered acoustic pressure is

$$\langle p_2 p_2^* \rangle = \langle p_2 \rangle \cdot \langle p_2^* \rangle + V[p_2]$$

$$\langle p_2 p_2^* \rangle = p_{20}^2 F^2 \exp(-g) \left[\operatorname{sinc}^2 v_x L \operatorname{sinc}^2 v_y W + \frac{\pi T^2}{A} \sum_{m=1}^{\infty} \frac{g^m}{mm!} \exp[-(v_x^2 + v_y^2) T^2 / 4m] \right] \quad (7)$$

The first term is the coherent component of the scattering and is important only in the specular direction and, there only if $g < 1$. The second term, the incoherent component, is significant for all nonspecular scatter including backscatter.

For scattering in the specular direction, ($\theta_1 = \theta_2$ and $\varphi = 0$), the ratio $\dfrac{\langle p_2 p_2^* \rangle}{|p_{20}|^2}$ is important. Great simplification of equation (7) occurs since $F = 1$, and $\operatorname{sinc} v_x L = \operatorname{sinc} v_y W = 1$. This leads to

$$\frac{\langle p_2 p_2^* \rangle}{|p_{20}|^2} = \exp(-g) + \frac{\pi T^2}{A} \left[\exp(-g) \sum_{m=1}^{\infty} \frac{g^m}{mm!} \right]$$

The bracketed portion of the second term in the above equation is defined as $S(g)$. This factor takes on the extreme values of

$$S(g) \cong g \quad \text{for } g < .1$$

$$S(g) \cong 1/g \quad \text{for } g > 10$$

for the relatively smooth and very rough surface respectively.

For the smooth surface ($g \leq .1$)

$$\frac{\langle p_2 p_2^* \rangle}{|p_{20}|^2} \cong 1$$

For the rough surface (g>10)

$$\frac{\langle p_2 p_2^* \rangle}{|p_{20}|^2} \cong \frac{\pi T^2}{Ag}$$

or substituting for g and putting in terms of the mean square slope we have

$$\frac{\langle p_2 p_2^* \rangle}{|p_{20}|^2} = \frac{\lambda^2}{8\pi A \Sigma^2 \cos^2\theta}$$

For the backscatter case $v_x^2 + v_y^2 = 4k^2 \sin^2\theta_1$ and $F = (\cos\theta_1)^{-2}$ since $\theta_1 = -\theta_2$ and $\varphi = 0$. The surface backscattering factor is defined

$$S_B = \frac{\langle p_2 p_2^* \rangle}{|p_1|^2} \cdot \frac{r_2^2}{A} \qquad (8)$$

We can now find the equations for the backscattering factor (S_B) for a relatively smooth surface (g<<1) and a rough surface (g>>1).

For the relatively smooth case (g<<1) the first (coherent) term in the brackets of equation (7) is negligible for $\theta_1 \neq 0$; (it must be considered when $\theta_1 = 0$). Furthermore since g<<1 only the first term of the series need be taken hence

$$\langle p_2 p_2^* \rangle = \frac{p_{20}^2 F^2 \pi T^2 g}{A} \exp[-(v_x^2 + v_y^2)T^2/4 - g]$$

$$\langle p_2 p_2^* \rangle = \frac{16\pi^2 T^2 \sigma^2 p_{20}^2}{\lambda^2 \cos^2\theta_1 A} \exp(-k^2 T^2 \sin^2\theta_1 - g)$$

The backscattering factor S_B then becomes

$$S_B = \frac{16\pi^3 T^2 \sigma^2}{\lambda^4} \exp(-k^2 T^2 \sin^2\theta_1 - g) \qquad (9)$$

For the rough surface ($g \gg 1$) direct application of equation (7) is not reasonable because the second term converges too slowly to be of practical use. We must return to equation (6) and make the approximation

$$\langle \exp[iv_z(z_1 - z_2)] \rangle = \exp[-g(1-C)] \cong \exp[-g^2/T^2]$$

where $C \cong 1 - \tau^2/T^2$.

Using the same method of integration as before and noticing that the second term in the brackets (equivalent to $\exp[-g]$) approaches zero for $g \gg 1$ we neglect it and arrive at

$$V[p_2] = \frac{\pi F^3 p_{20}^2 T^2}{Ag} \exp[-(v_x^2 + v_y^2)T^2/4g]$$

For backscattering this is equivalent to $\langle p_2 p_2^* \rangle$ since the coherent term is negligible. Substituting in equ. (8) the backscattering factor becomes

$$S_B = (8\pi \Sigma^2 \cos^4\theta_1)^{-1} \exp[-\tan^2\theta_1 / 2\Sigma^2] \qquad (10)$$

where Σ^2 is the mean square slope.

In general, the data taken from backscatter experiments at sea appear to follow equation 10, decreasing rapidly with increasing θ_1 at angles of incidence up to 40^o measured from the normal. The equation does not however, predict the virtual independence of θ_1 that has been observed for angles of incidence greater than this.

Resonance Theory

In the resonance approach to backscatter the random rough surface is described by a wave energy spectrum. This spectral function E(f) is proportional to the surface wave "energy" per cycle bandwidth (cm^2/sec). The nature of the sea surface spectrum (Fig. 2.3) shows that there is very little energy in the band of frequencies below the characteristic frequency f_o, determined by wind speeds; that most of the wave energy lies in a small band of frequencies centered around f_o; and that at higher frequencies the curves fall as f^{-n}, where a common value for n has been found to be 5, Phillips (18).

Wetzel (9), in his approach to the problem, postulates that for the relatively smooth ($g \ll 1$) surface the major backscatter radiation does not come from the incoherent (scattered radiation arriving at receiver with uniformly distributed phase) component caused by the randomness of the scattering surface. Rather he suggests the backscattering is due to a resonant interaction between the incident radiation and some component in the water-wave surface. This interaction leads to a constructive interference which is physically similar to Bragg diffraction, and which, because of the surface wave velocity, manifests itself in a coherent doppler shifted frequency in the non-specular directions.

Using Bragg's Law

$$2L\sin\theta = n\lambda \qquad n = 1,2,3.....$$

one can compute the appropriate surface wave length for a given frequency of acoustic radiation and a known angle of incidence θ_1. For the first order effect (n = 1) the phase velocity for this

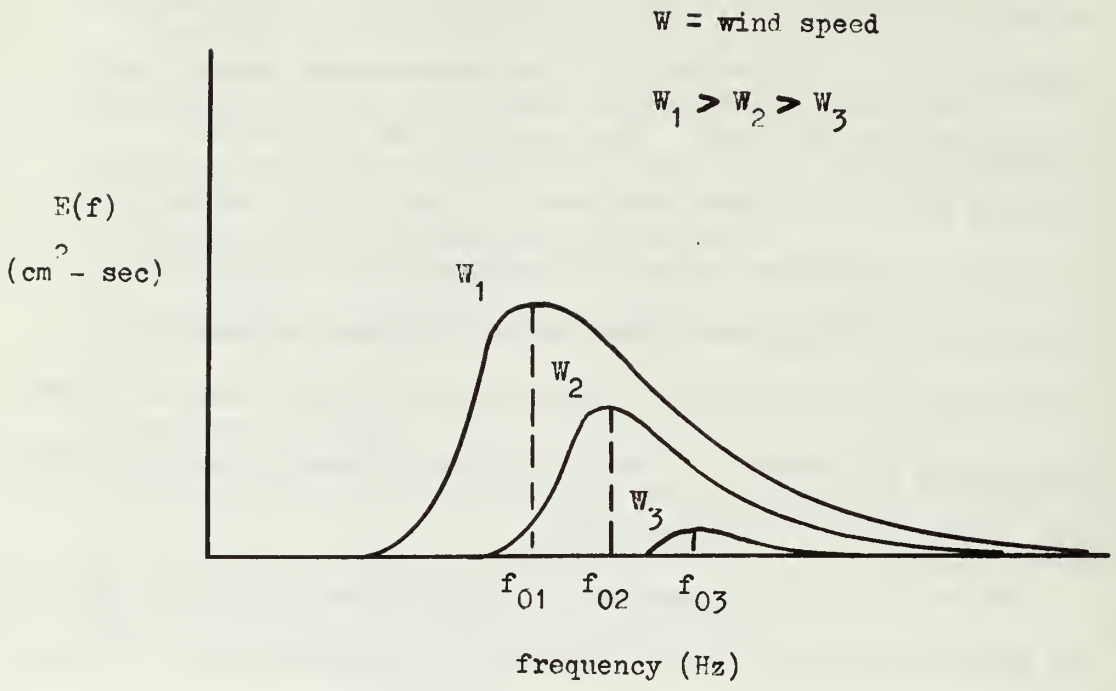

Fig. 2.3 Wave Energy Spectra for Fully Developed Sea

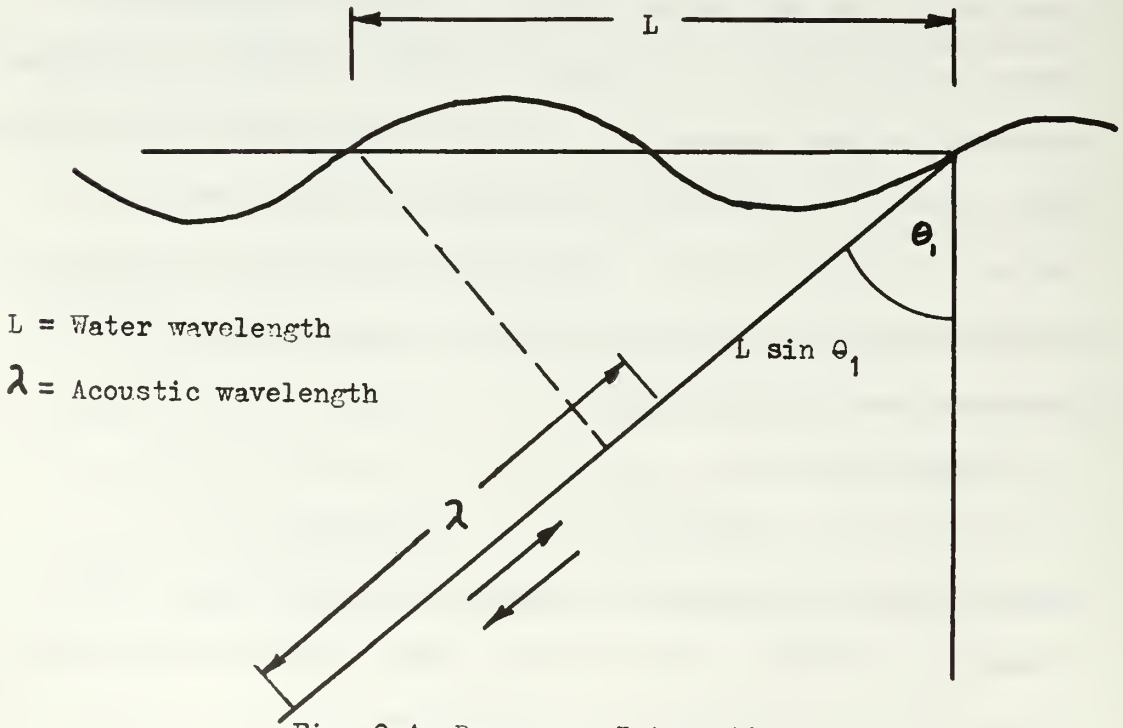

Fig. 2.4 Resonance Interaction

particular wavelength is then computed (taking into account surface tension if the wavelength is less than a few centimeters, Fig. 4.29) and the doppler shift calculated from the relation

$$\Delta f = 2V\sin\theta_1 f/c \qquad (11)$$

where V is the phase velocity of the surface wave.

Wetzel (9) derives an expression for the backscatter cross section per unit area, using the Kirchhoff approximations, and based on Chapter 3 of Beckmann and Spizzichino (5) modified slightly to include a term that Beckmann had identified as negligible. With this modification he arrives at the following expression for the backscatter cross section per unit area (Wetzel (9), equation 41)

$$\sigma_{bs}/A = k^4 g^{\frac{1}{2}} K_r^{-\frac{3}{2}} E\,[f(K_r)] \qquad (12)$$

where $K_r = 2k\sin\theta_1$ is the resonance wave number, A is the surface area ensonified, g is the acceleration of gravity, and $E\,[f(K_r)]$ is the value of the surface wave spectral energy at the resonance wave number. Substituting the values for K_r and g leads to

$$\sigma_{bs}/A = 11.07k^{\frac{5}{2}} E\,[f(K_r)]/\sin^{\frac{3}{2}}\theta_1 \qquad \text{cgs units}$$

Using the definition of the backscattering factor (8) it can be shown that this is equivalent to $\sigma_{bs}/A = 4\pi S_B$ or

$$S_B = \frac{.881k^{5/2}}{\sin^{3/2}\theta_1} \cdot E\,[f(K_r)] \qquad \text{cgs units} \qquad (13)$$

The level of backscattered sound predicted by equation (13) is examined quantitatively in Section 4 by comparing with the observed values. The values for $E\,[f(K_r)]$ are obtained directly from the wave energy spectrum measured (Fig. 3.33) for the surface by Cohen and Scheible (17).

In general Wetzel's equation (41) is a plausible explanation of the low level backscatter that has been widely observed for small grazing angles. However, at normal and near normal incidence it fails to give a reasonable prediction. The theoretical expression for the backscattering factor from the resonance theory appears to have a singularity at the normal incidence prediction but this is removed by the nature of the energy density in the surface wave spectrum which has no energy in the spectrum for a surface wave with zero frequency.

3. The Model Sea Surface

Generation of Rough Surface

All experiments were conducted in a fresh water filled anechoic tank 25' x 6' x 7' deep. The rough surface was produced by a combination of up to three centrifugal blowers. The tank surface was covered for a distance of ten feet from the point where the fan discharge struck the water surface vertically, by polyethylene sheets held in place by a slotted angle framework and plywood to form a plenum with its top 3½ inches off the surface of the water. This provided a short fetch for the wind to develop a rough surface. When it seemed necessary, a wire mesh "beach" was inserted one foot from the end wall of the tank to suppress standing waves in the water surface due to the small reflection from the end of the tank. The arrangements are shown in Figs. 3.1 and 3.2. Three locations or stations are marked in Fig. 3.1 to indicate the centers of areas of scattering used in the conduct of the experiments.

Wave Height Statistics

The statistical theory assumed that the rough water surface is a stationary random process and that the distribution of wave heights is Gaussian with zero mean and standard deviation, σ. It is desired to test this assumption from a theoretical point of view and then to test its validity experimentally by measuring the actual wave height distribution of several rough water surfaces.

Theory

For a simple sinusoidal surface in one direction, it can be shown that the probability density function for the height is

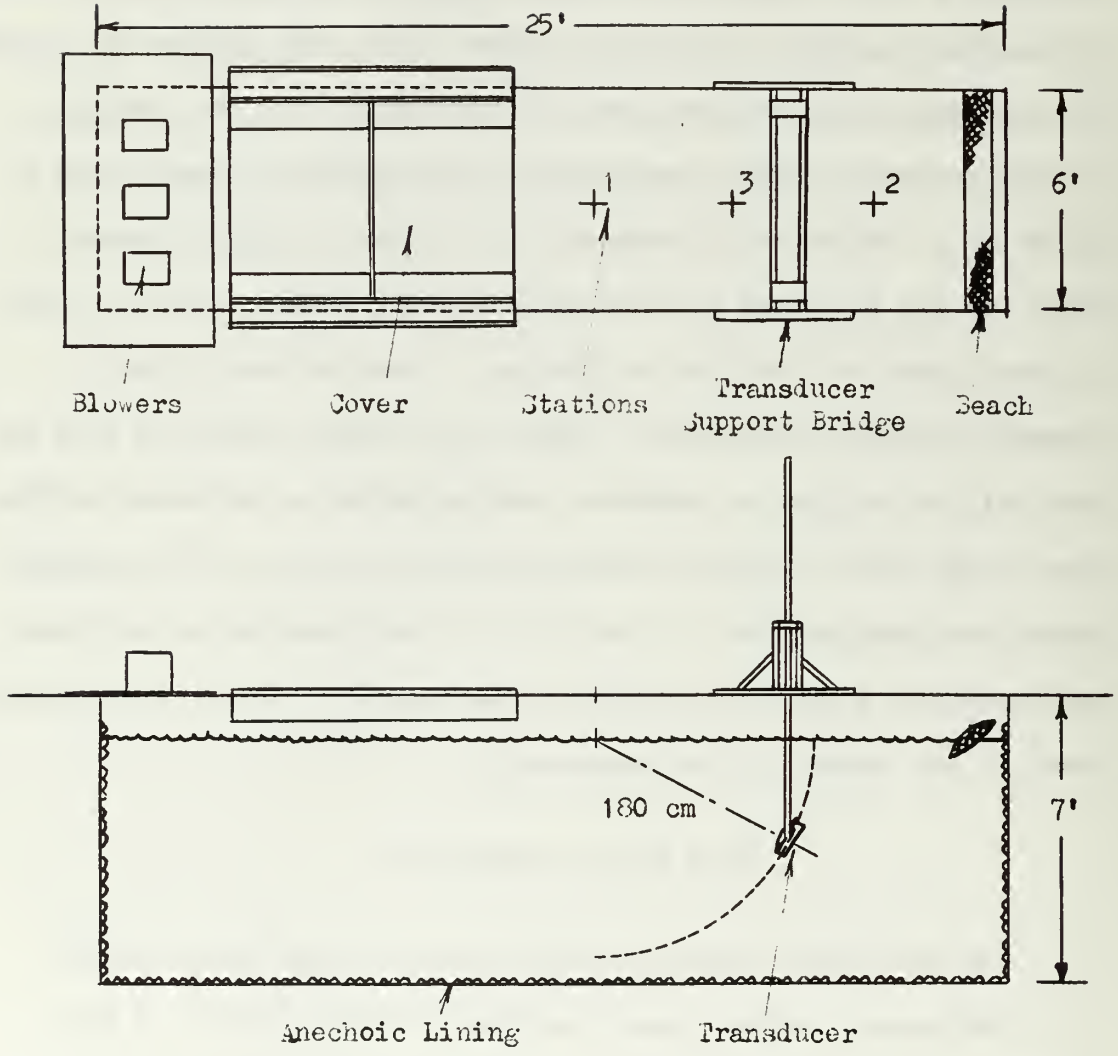

Fig. 3.1 Generation of Rough Surface in Anechoic Tank

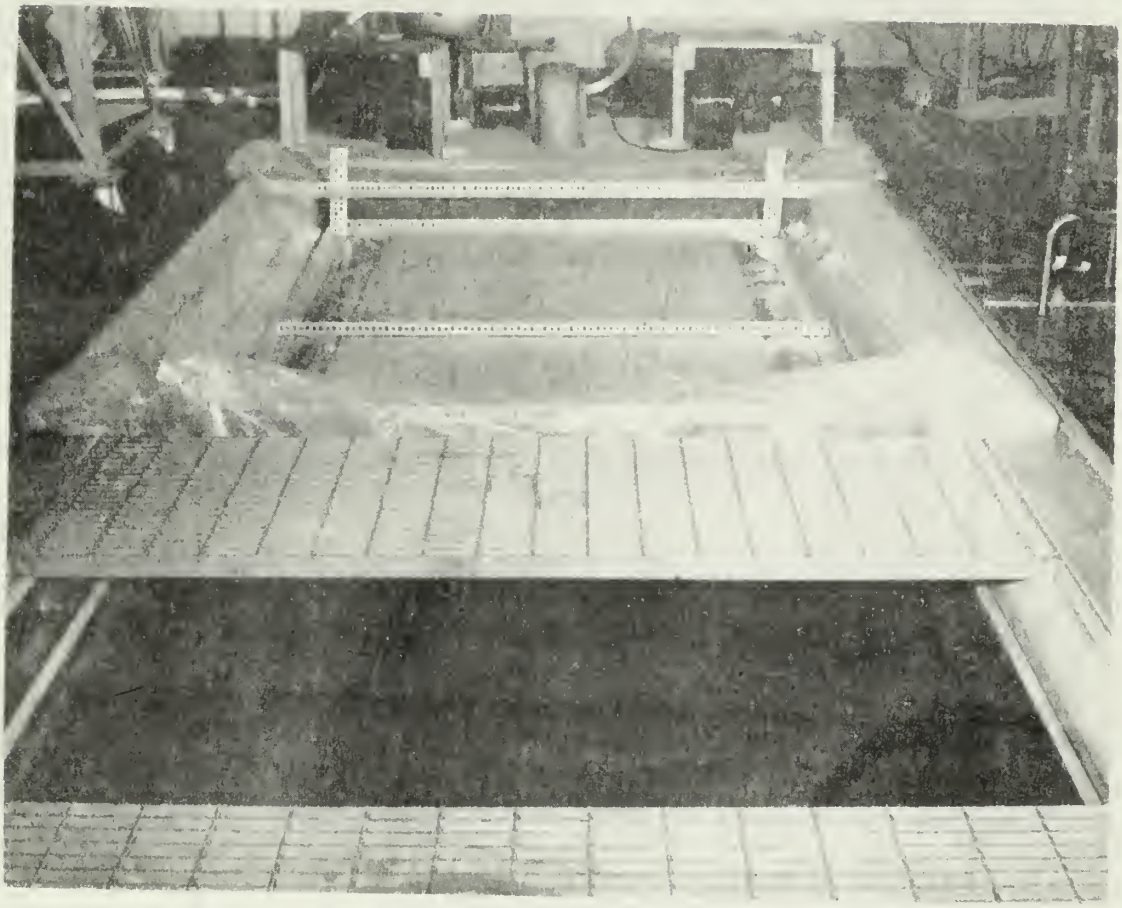

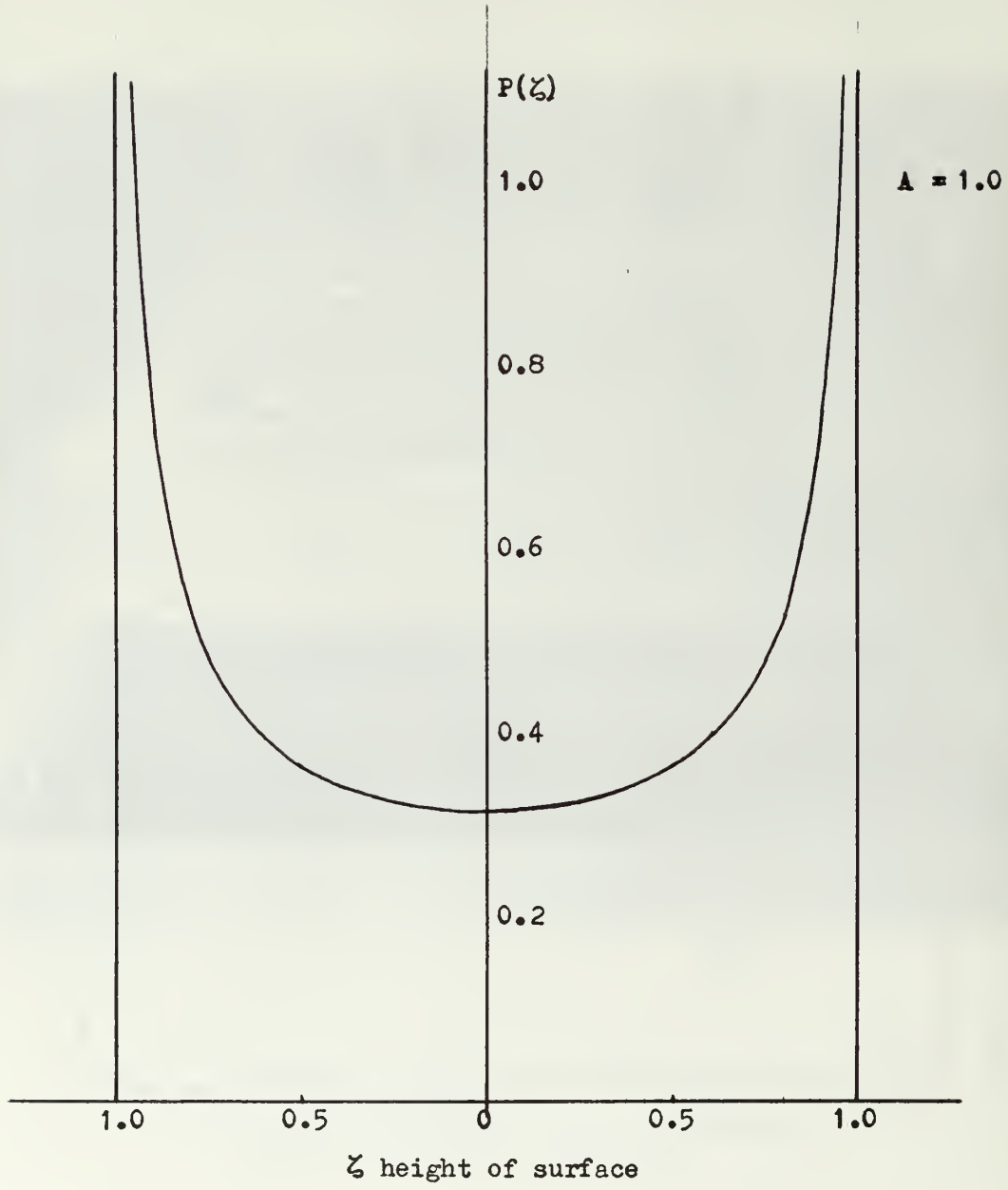

Fig. 3.3 Height Distribution for a Single, One Dimensional Sinusoidal Surface

bimodal and of the form

$$P(\xi) = \frac{1}{\pi \sqrt{A^2 - \xi^2}} \qquad \text{for } \xi < A$$

where A is the amplitude of the sinusoidal surface. The distribution is shown in Fig. 3.3, and is anything but Gaussian in nature. However, the evidence of our eyes and the study of wave spectra show that the surface of the sea is not a simple one dimensional sinusoidal disturbance. If we consider the height at any point to be due to the superposition of a number of wave motions, independent in space and time, the application of the central limit theorem shows that the values of wave height tend toward a Gaussian distribution. Cox and Munk (12) show the development of just such a distribution.

Experimental

Since the theory depends not on the mean wave height but only on the root mean square wave height, the stationary surface level is taken as zero and the variance of the height distribution is measured. Figs. 3.4 and 3.5 show the apparatus used to measure the distribution.

Probe. The probe is a piece of tinned copper wire, 0.80 mm in diameter and 25 cm in length, held with approximately 17 cm of its length below the surface of the water. The small diameter is necessary to minimize the formation of a wake behind the probe due to motion of the surface layer of water. The return is provided by a second electrode 3.14 mm in diameter and 45 cm in length, which is completely submerged at all times. This second electrode is connected to ground and in fact is parallelled by many other ground connections in the plumbing of the tank, so that its position and size do not affect the operation of the device to any extent. The impedance of the cell formed by the short surface probe and the ground return is

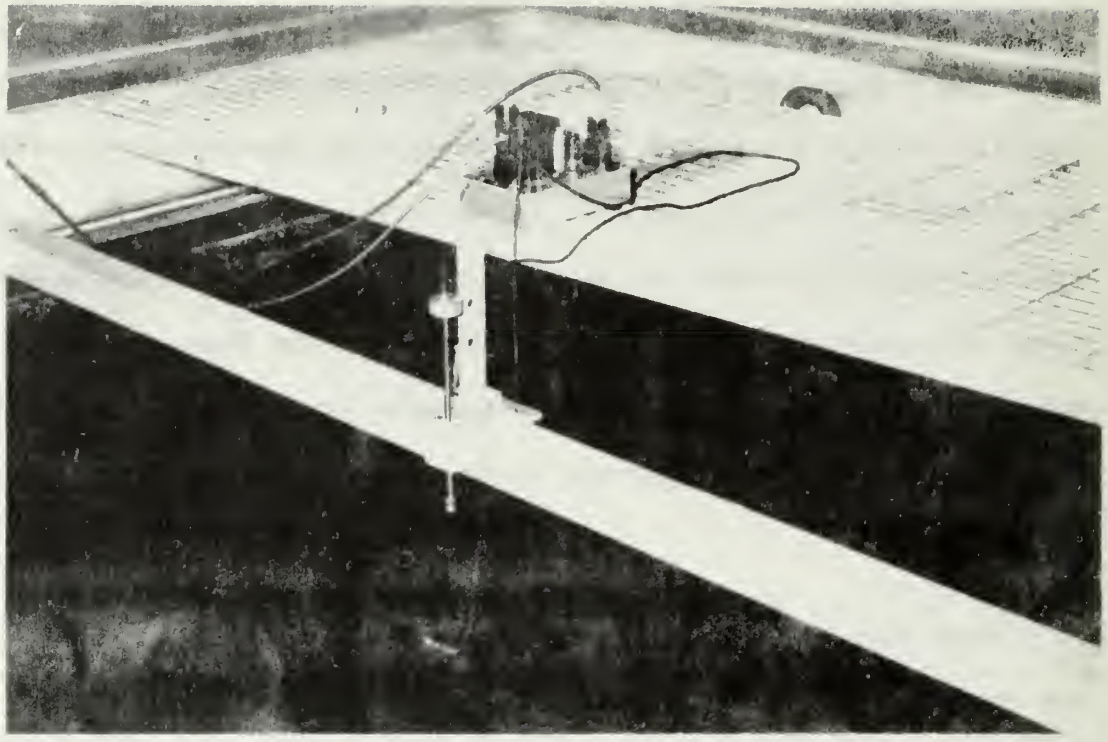

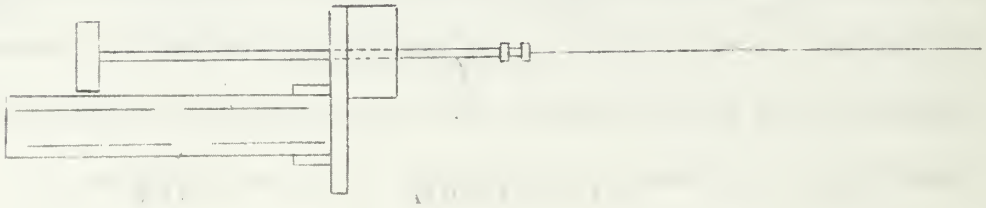

then a function of the amount of the probe below the surface and hence is a function of the wave height at the probe. The physics of the operation of the probe have not been thoroughly examined, although it is clear that conductive effects rather than capacitive effects predominate in its operation. Farmer and Ketchum (14) have given a theoretical derivation of the sensitivity of a device using similar methods, though of a much larger scale. What was clearly necessary, however, was an accurate calibration to determine the linearity of the device in measuring wave height and a frequency response test to determine whether the varying height of the water surface could be accurately changed into an electrical analog.

Electronics. Fig. 3.6 shows a block diagram of the system used in the determination of the wave height distribution. The device makes use of the output impedance of the oscillator by causing the output to be shunted by the variable impedance of the probe. This varies the output voltage of the oscillator. The resultant signal is an amplitude modulated 10 Hz carrier where the modulation contains the wave height information. The AC carrier is necessary to prevent the electrolytic polarization of the probe which would occur if DC were used.

The detector is a simple full wave rectifier followed by a π section RC filter as shown in Fig. 3.7. The filter must have a low pass characteristic in order to remove the carrier frequencies but not such a low cut-off as to cause undue phase distortion of the modulation signal. The differential amplifier is required to remove the large DC portion of the signal and to increase the signal level for the pulse height analyzer.

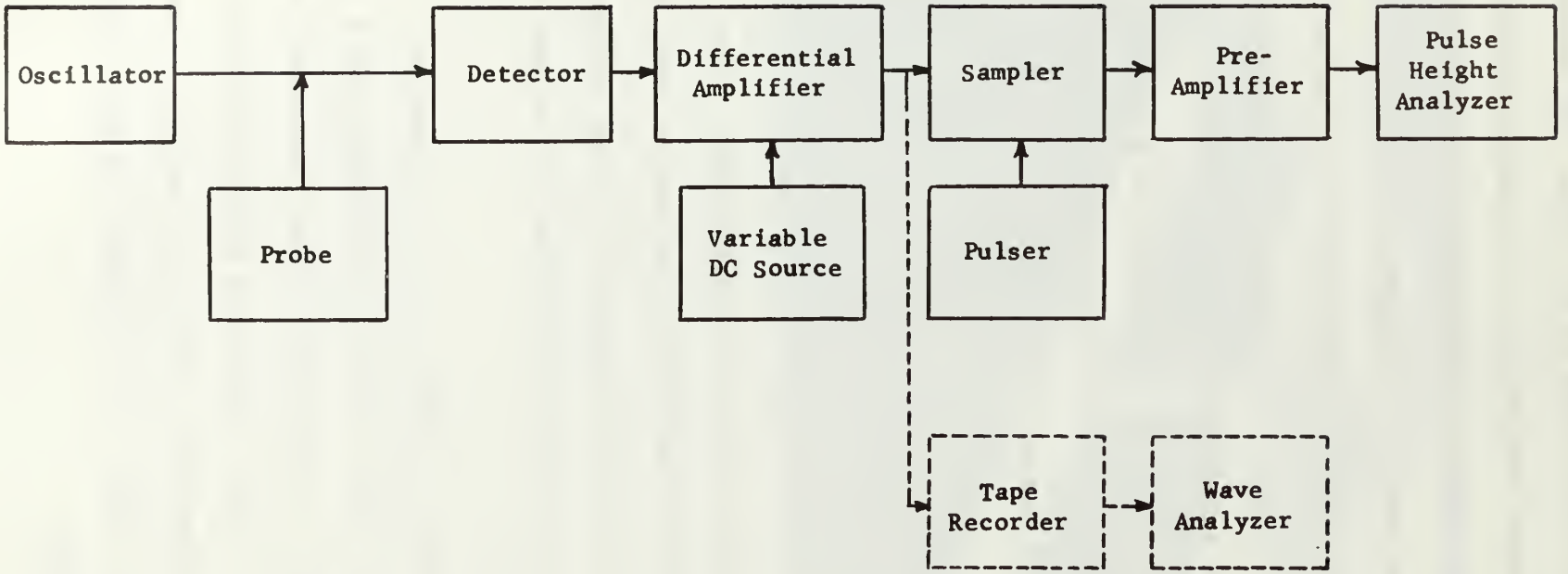

(Cohen and Scheible Apparatus [17])

Fig. 3.6 Wave Height Measurement System

Oscillator	HP 650A Test Oscillator
Probe	see Fig. 3.5
Detector	see Fig. 3.7
Differential Amplifier	Tektronix 1A7 in Tek 545 Oscilloscope
Variable DC Source	HP 467A Power Amplifier
Sampler	see Fig. 3.8
Pulser	GR 1217B Unit Pulse Generator
Pre-Amplifier	HP 467A Power Amplifier
Pulse Height Analyzer	RCLiac 128 Scaler Analyzer
Tape Recorder	PI-6200 Portable Instrumentation Tape Recorder
Wave Analyzer	GR 1900A Wave Analyzer

Fig. 3.6(a) Equipment List for
Wave Height Measurement System

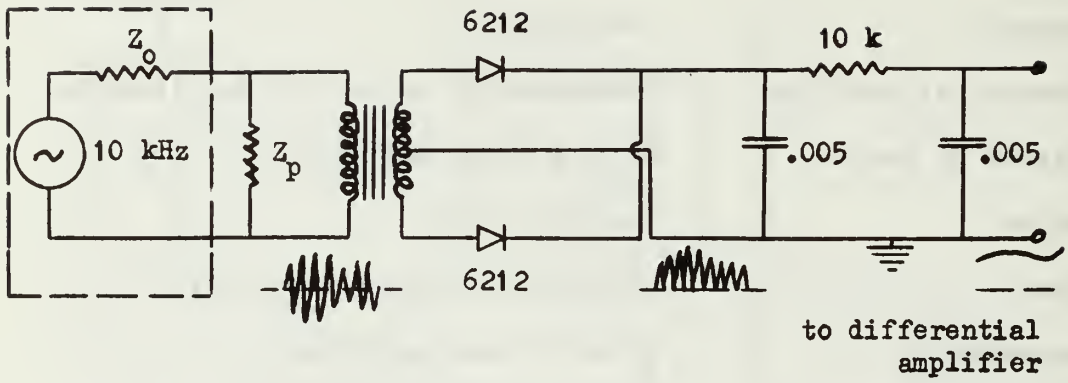

Fig. 3.7 Wave Height Detector

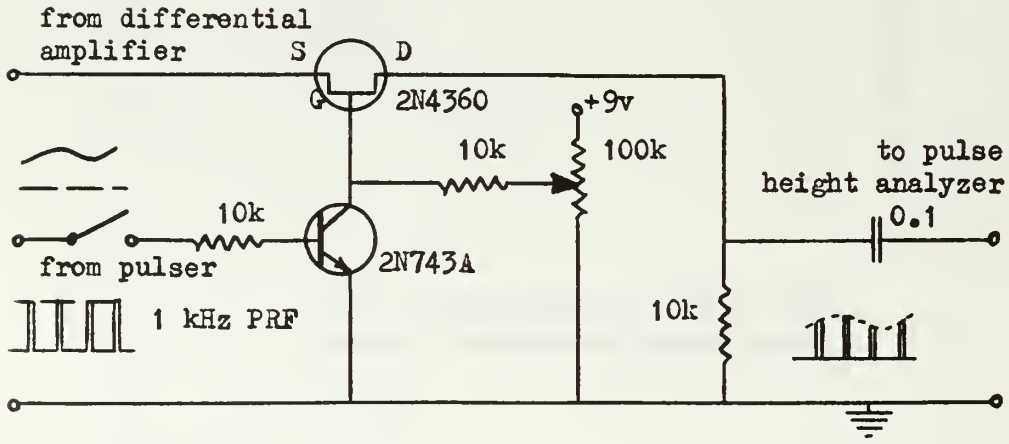

Fig. 3.8 Sampler Unit

The sampler consists of a field effect transistor which is controlled by a high speed silicon switching transistor, as shown in Fig. 3.8. The pinch-off voltage of the FET is removed when the pulse causes the switching transistor to saturate thus providing a very short rise time at the opening of the sampling gate. This fast rise time is required for the input to the pulse height analyzer.

The pulse height analyzer is a RCLiac 128 Channel Scaler Analyzer designed principally for nuclear physics applications. The scintillation crystal, photomultiplier and preamplifier section were removed and the input provided to the variable gain section through a separate isolation preamplifier. The analyzer is digital, providing a cathode ray tube output of the pulse height distribution both pictorially, as a frequency diagram or histogram, and as a decimal numeric readout for each channel. The analyzer detects the rise of a pulse and 1½ microseconds later it picks off and holds the input voltage. Simultaneously an internal 2 MHz counter is started and a rising ramp voltage is generated. When the ramp voltage exceeds the held input voltage, the count is stopped and a single entry is made into the cell in the ferrite core memory whose address is the count at stop time. The input is then re-enabled for the next pulse. The system dead time is 70 + n/2 microseconds, where n is the address of the memory core for the count. It is seen that the input pulses must have a sufficiently small rise time to rise to the full value in less than 1½ microseconds. In addition, the analyzer must be fed by some pulsing scheme other than allowing it to sample whenever the input is enabled, otherwise the sampling rate would not be independent of the pulse heights and the lower pulses would be

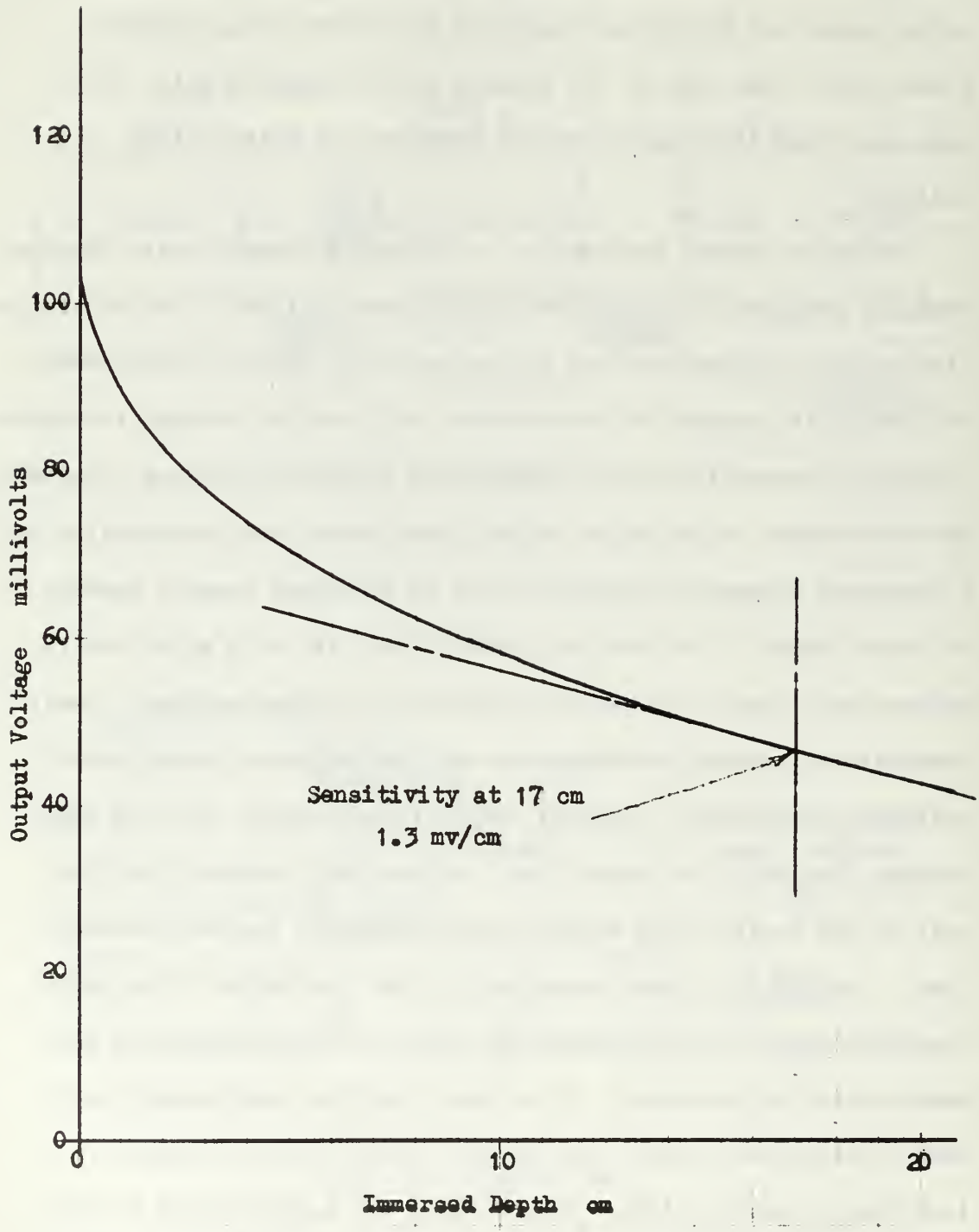

Fig. 3.9 Surface Probe Characteristic

favored. In this case, the sampling frequency for the wave heights was set at 1 kHz which is well beyond the limit dictated by the Shannon sampling theorem to prevent aliasing in detecting the highest frequencies in the wave height signal. Since the highest n is 128, the analyzer is limited to a maximum regular sampling frequency of 7.4 kHz.

Calibration. Examination of the characteristics of the output voltage of the wave height measuring device under slowly varying conditions showed that the output voltage vs water height was of the form shown in Fig. 3.9. It is clear that the relationship is anything but linear but over a small range such as the two to three centimeter variation expected in the model rough surface, the linearity is very nearly preserved. It is also noted that linearity improves as the immersed length of probe increases, but only at the sacrifice of voltage sensitivity of the device. Hence a compromise was made at an immersed depth of 17 cm at which the sensitivity of the probe with the supplied voltage at 2.0 volts was 1.3 mv/cm.

It is not sufficient to use a static calibration of the device, however, unless it is clear that the device will operate accurately over the range of frequencies in the surface wave spectrum. Since it seemed more practical to move the probe up and down in the water in a sinusoidal motion rather than to cause the water to move past the probe in a sinusoidal motion, the former course was chosen. Fig. 3.10 shows a diagramatic sketch of the apparatus used. The probe was driven vertically by a simple cam mechanism operated by a variable speed motor. The amplitude was fixed at about 3 cm by the cam arrangement but the frequency was continuously variable up to

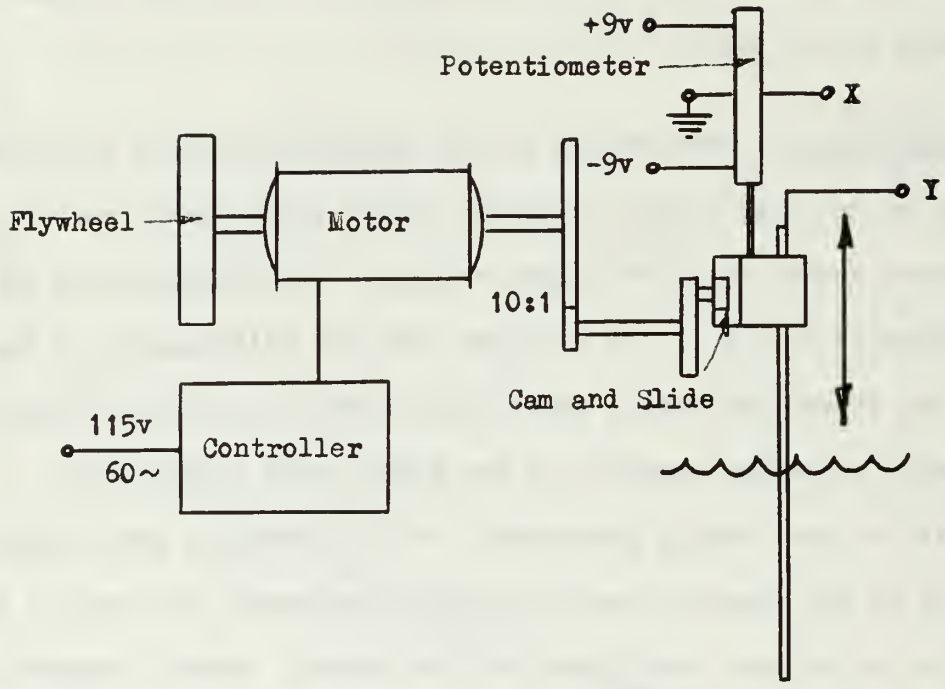

Fig. 3.10 Dynamic Calibration of Wave Height Measuring Device

8 Hz. The actual position of the probe was determined by a linear potentiometer supplied by a constant voltage DC supply. The potentiometer output was led to the X-input and the detected wave height led to the Y-input of a cathode ray oscilloscope. The resultant 1:1 Lissajou pattern was analyzed at several frequencies for linearity, sensitivity and phase distortion. It was expected from the static calibration that the linearity would be good, but the effects of surface tension to cause the inevitable meniscus about the probe causing a lagging response, were unknowns.

The results of the first calibration showed an unacceptably large phase lag at any frequency above 3 Hz. Since this phase lag could be caused by the characteristics of the filter in the detector as well as by the effects of surface tension it was decided to attempt to modify the detector. Fortunately it was found that simply reducing the time constants of the filter to the values determined by the parameters in Fig. 3.7, forced the poles of the transfer function of the system far enough out along the real line in the complex frequency plane to provide an acceptably low level of phase distortion. It was evident that the poles of the filter system dominated the pole introduced by the surface tension. After adjusting the filter parameters it was determined that at 8 Hz, the highest frequency at which calibration with the mechanical oscillator was possible due to limitations of the controller, the phase lag was 3 degrees. Since the system is essentially third order, the response can be extrapolated on a worst case basis on the assumption that all three roots of the system equation are identical. Fig. 3.11 shows such a construction as a Bode diagram to show the worst response in magnitude and in phase. It is seen that the response of the device

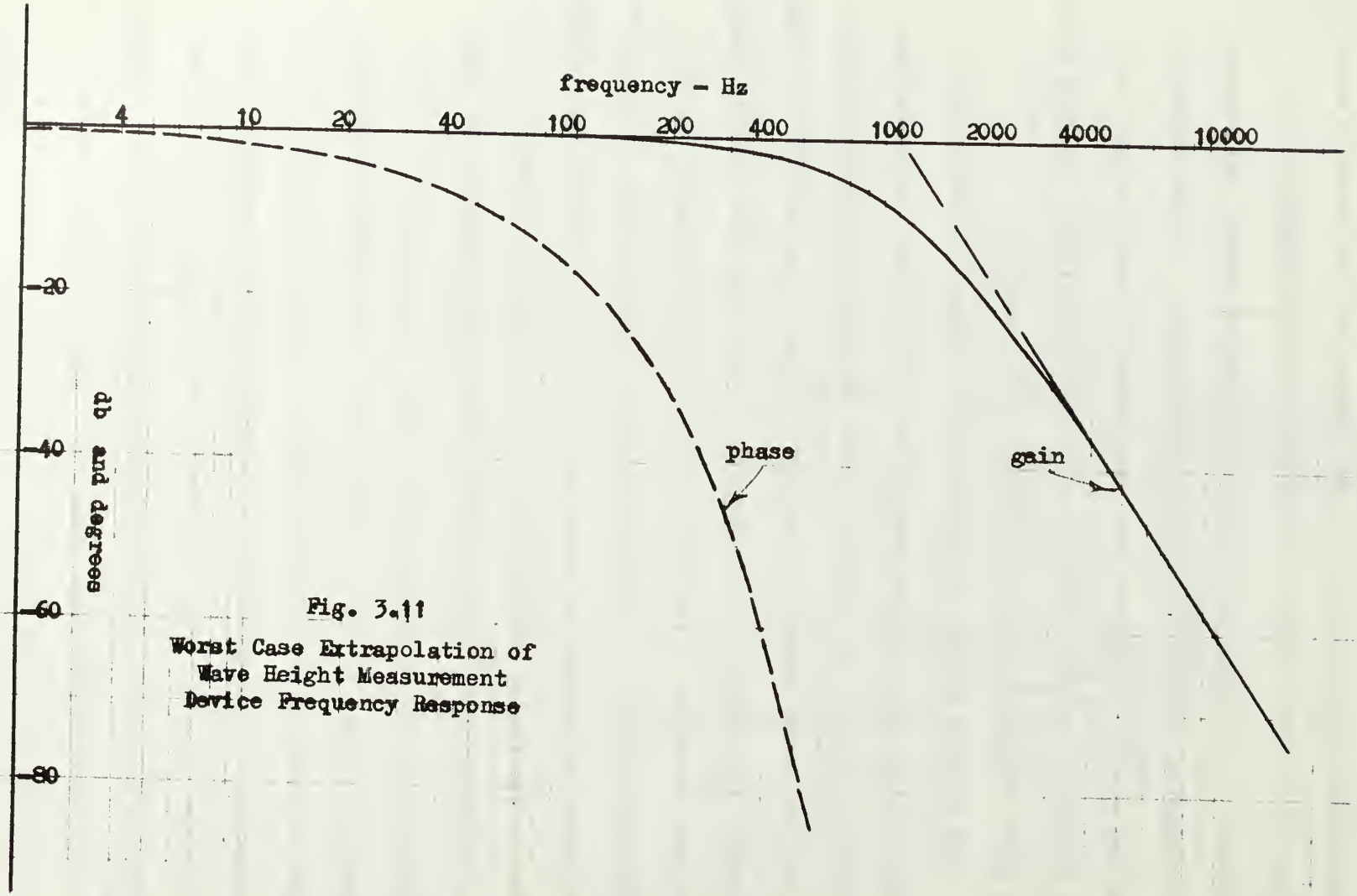

Fig. 3.11

Worst Case Extrapolation of
Wave Height Measurement
Device Frequency Response

is accurate to less than 1 db at frequencies up to 100 Hz at the very worst and is probably much better. It should be noted that the filter characteristics decided upon to optimize the frequency response of the device were not the best for suppression of the 20 kHz ripple in the detected signal. However, the change in the standard deviation of the wave height distribution due to the ripple is quite small (1.4 mv) and can be corrected using the summation principle of variances for the sum of random variables which are uncorrelated.

The conclusion of this dynamic calibration procedure is that the response at frequencies expected in the surface wave spectrum is flat, without phase distortion, and that it is sufficient to calibrate the device under static conditions and to apply that sensitivity to the entire spectrum. The pulse repetition frequency of the sampler was 1 kHz and the sampler pulse length set at 25 microseconds. The device was calibrated statically in smooth water by adjusting the immersed depth of the probe by turning the 20 pitch adjusting screw. The attached scale, which can be seen in Fig. 3.5, indicated the number of turns of the screw and the head of the screw was indexed to ensure the accurate setting of an integral number of turns. A typical calibration curve is shown in Fig. 3.12. It will be noted that the calibration yields a sensitivity in channels/cm, an odd unit perhaps, but convenient in the processing of wave height distribution data from the pulse height analyzer.

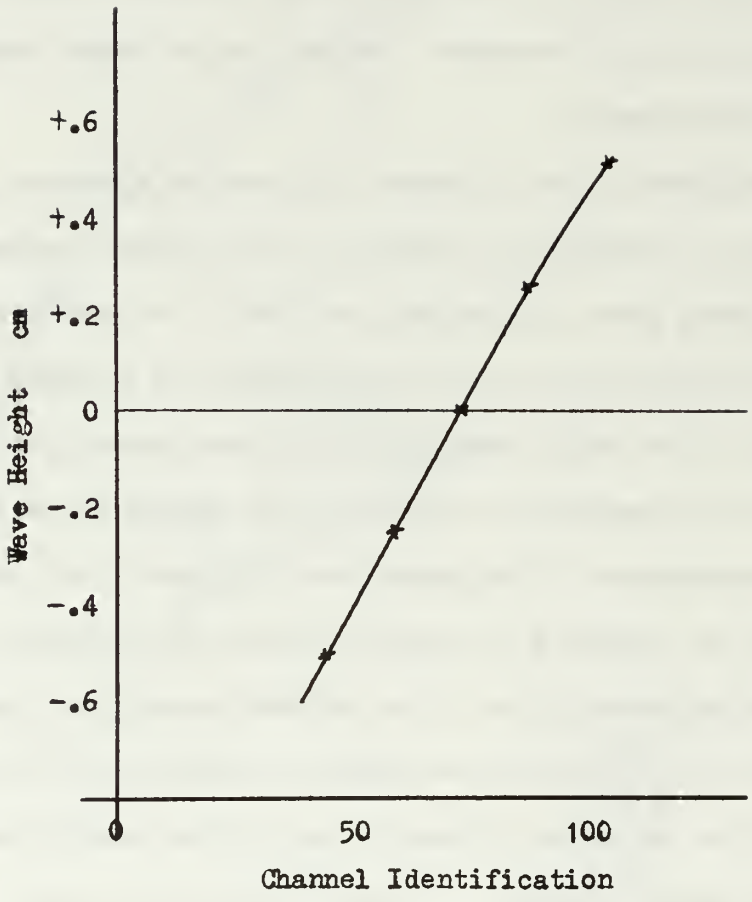

Fig. 3.12 Wave Height Measurement Calibration

Results and Conclusions

The wave height distribution was studied at three stations in the tank (see Fig. 3.1). The process is assumed random, homogeneous and stationary, that is the height distribution statistics are constant in time and over the area ensonified in the scattering experiment. It is further assumed that the statistics of the time distribution are the same as for the spatial distribution. Measurements of the samples of wave heights were taken for 197 seconds giving a distribution of 2.0×10^5 samples of wave height in that period. In each of the stations, the wave height was measured with combinations of one, two and three blowers operating.

Capillaries were evident at station 1 with two and three blowers operating, but these had died out almost completely by the time the wave motion had reached station 2, eight feet further downwind. Figs. 3.13 to 3.18 show the height distributions at each of the three stations. The measured distributions are compared with Gaussian curves with the same (zero) mean and standard deviation, normalized to have unit area. Table 3.1 summarizes the measured wave height at each scattering location (stations 1 and 2) as well as at station 3 which was the site of the continuous wave scattering experiment. The RMS wave height was calculated from the distribution data by the general purpose computer (CDC 1604 - FORTRAN) using the sensitivity calculated from the static calibration curve taken at the time and station where the wave height was recorded. A typical polaroid photograph of the pulse height analyzer readout is shown in Fig. 3.19.

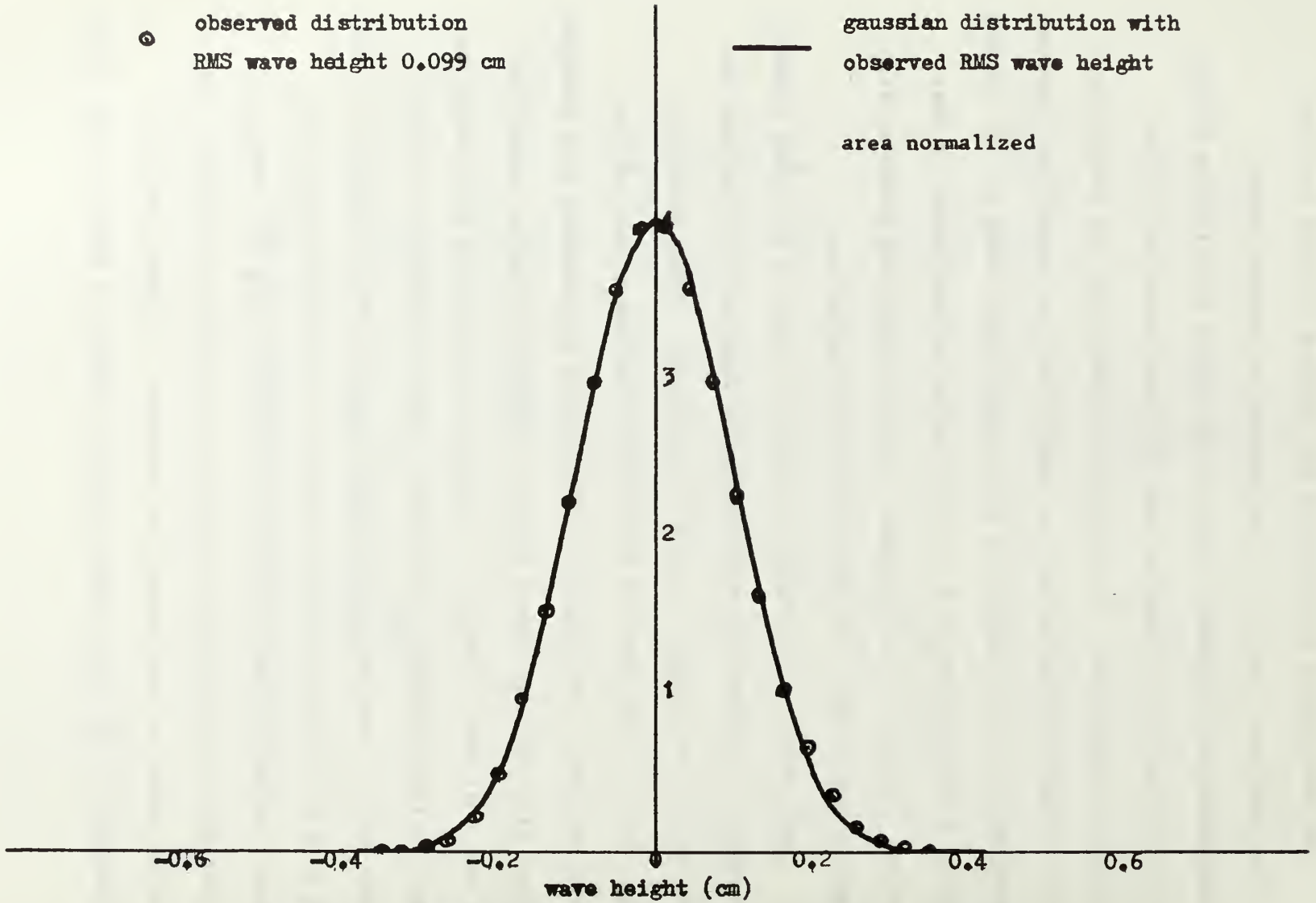

Fig. 3.13 Wave Height Distribution Station 1 1 blower

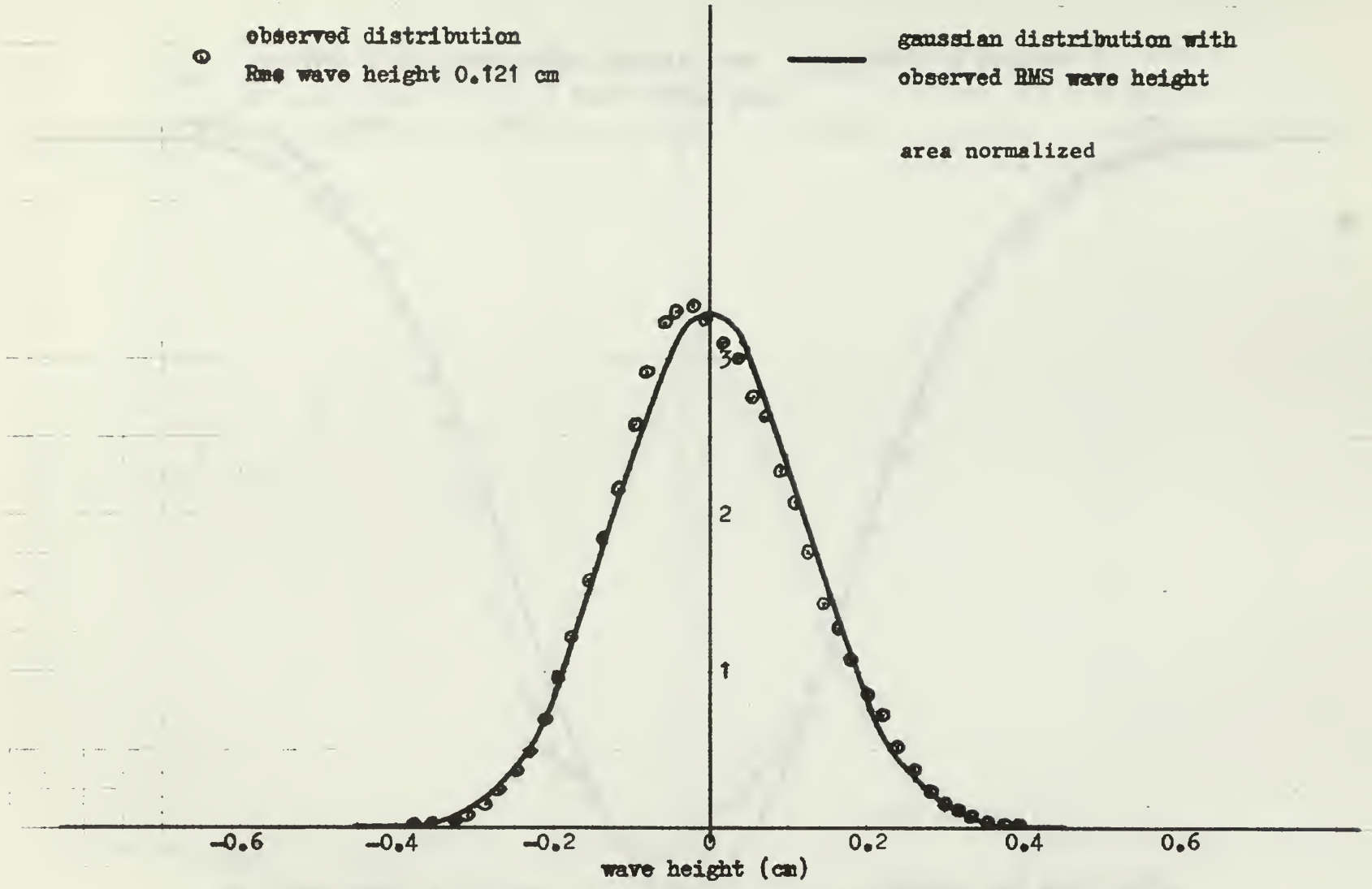

Fig. 3.14 Wave Height Distribution Station 1 2 blowers

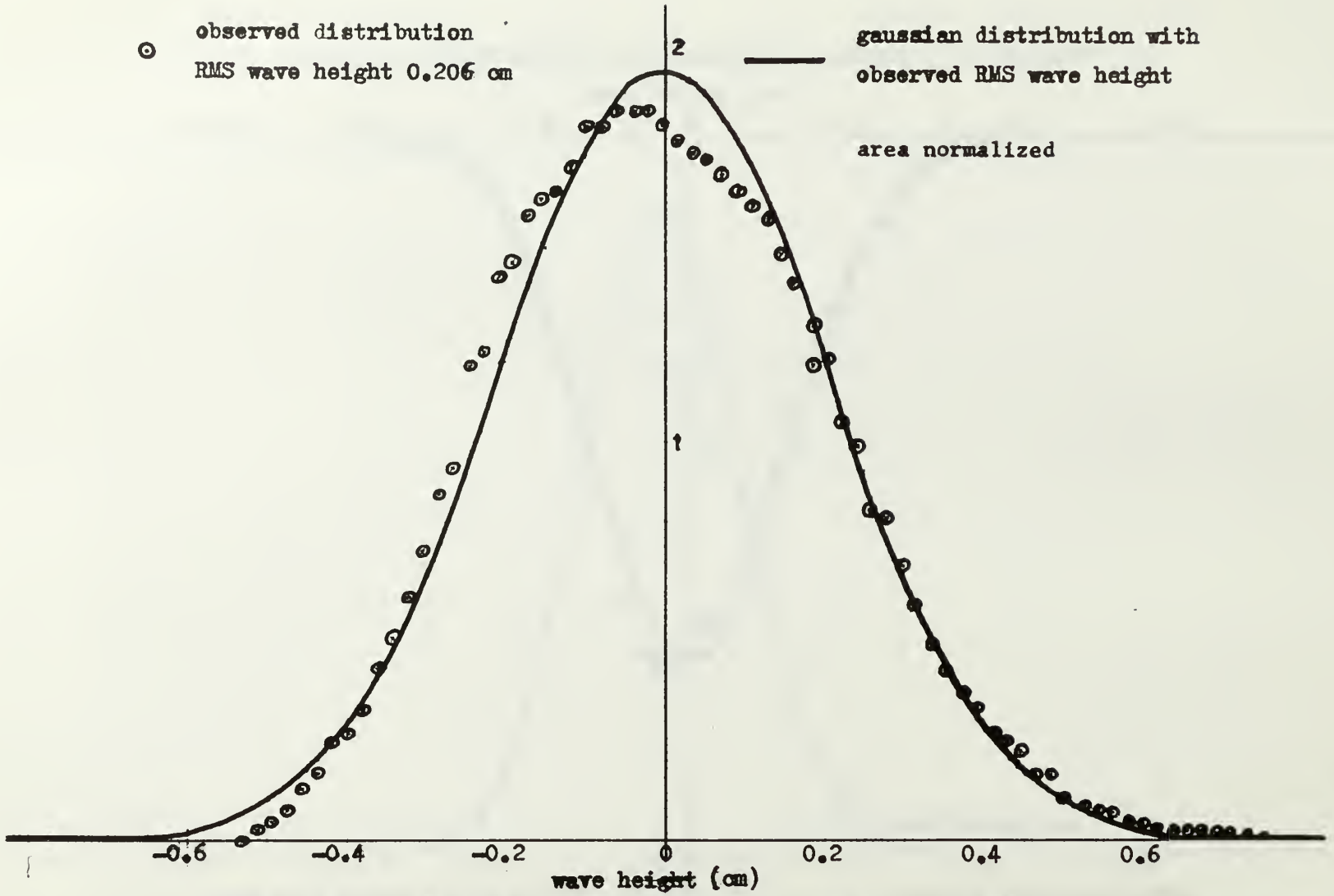

Fig. 3.15 Wave Height Distribution Station 1 3 blowers

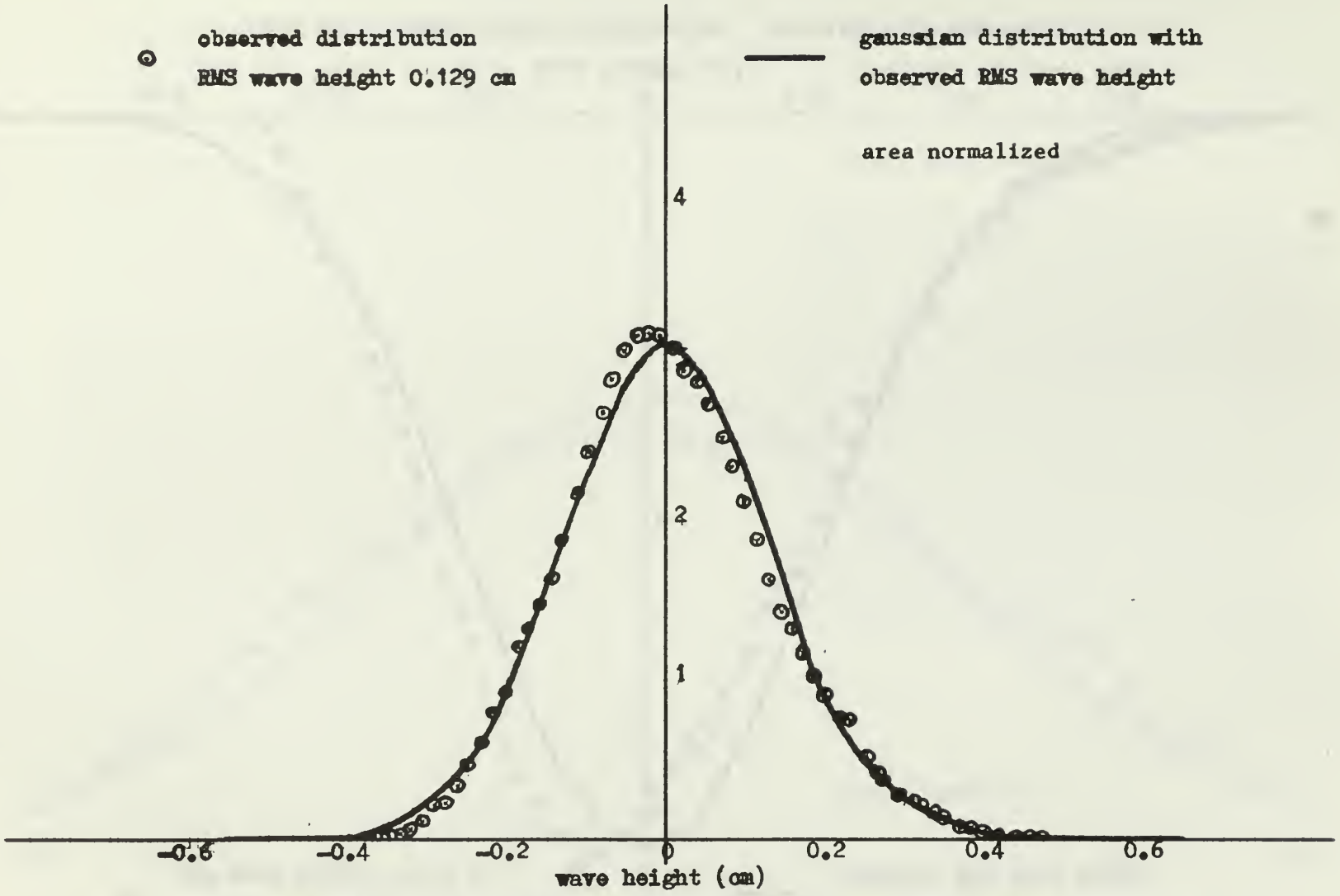

Fig. 3.16 Wave Height Distribution Station 2 2 blowers

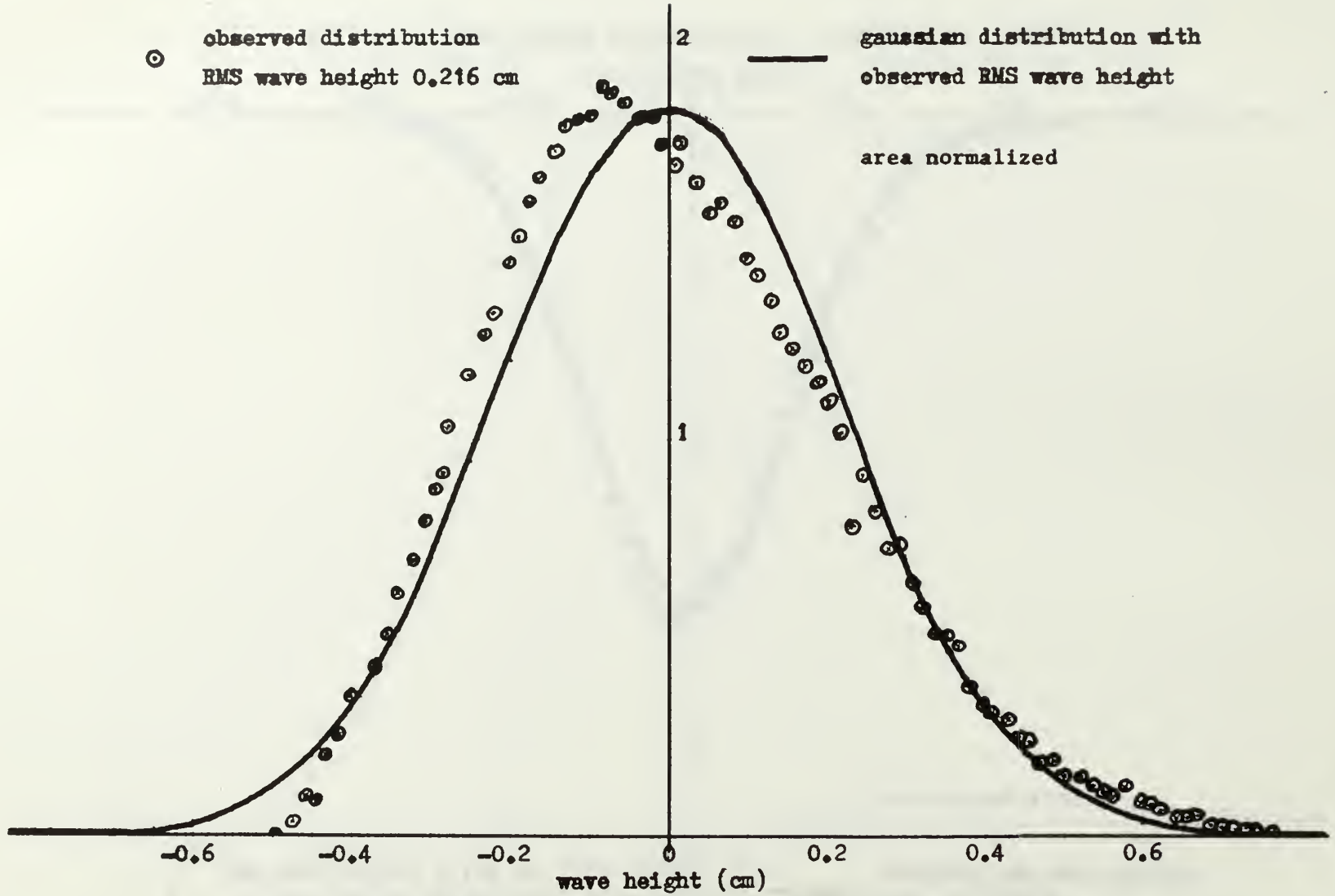

Fig. 3.17 Wave Height Distribution Station 2 3 blowers

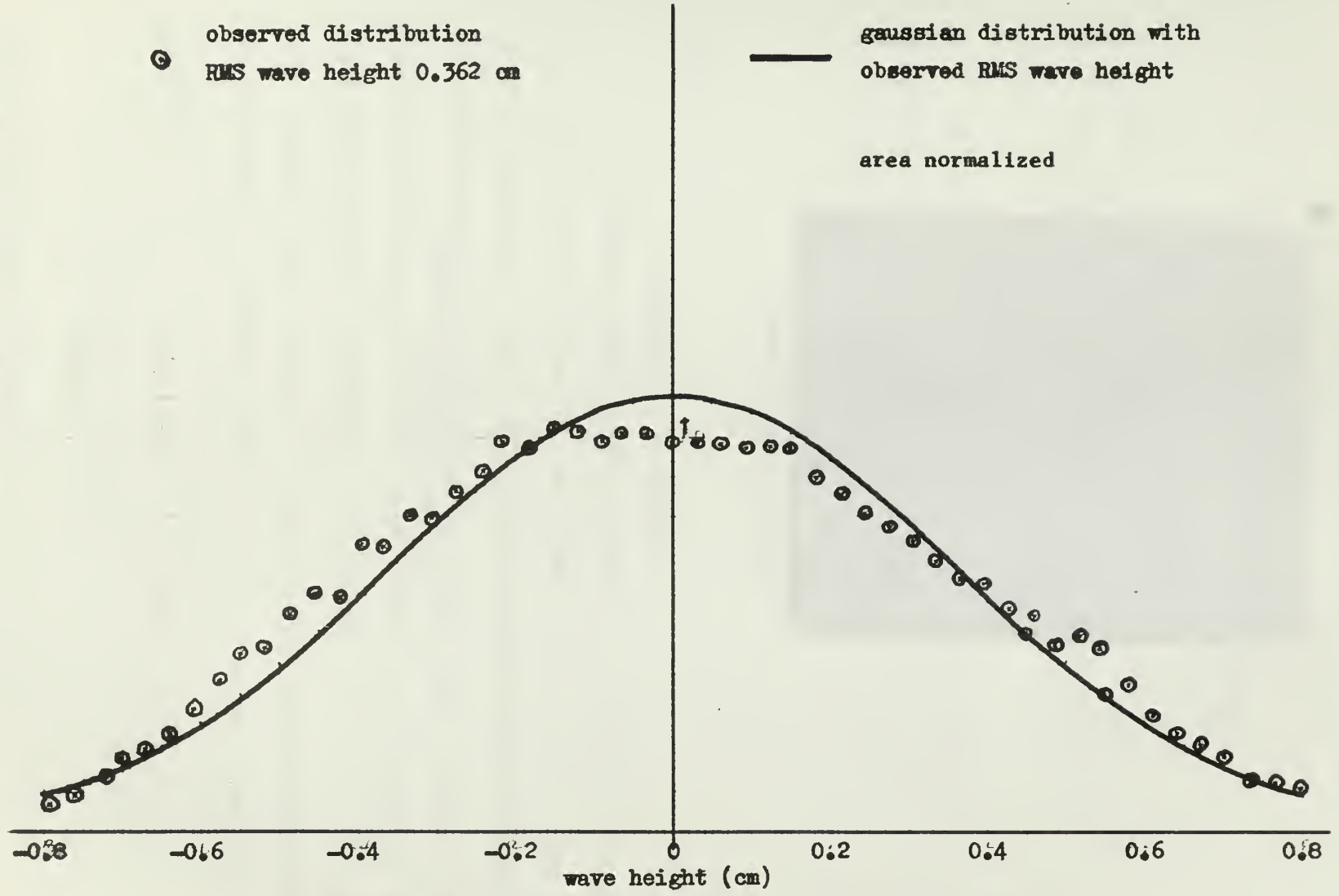

Fig. 3.18 Wave Height Distribution Station 3 3 blowers

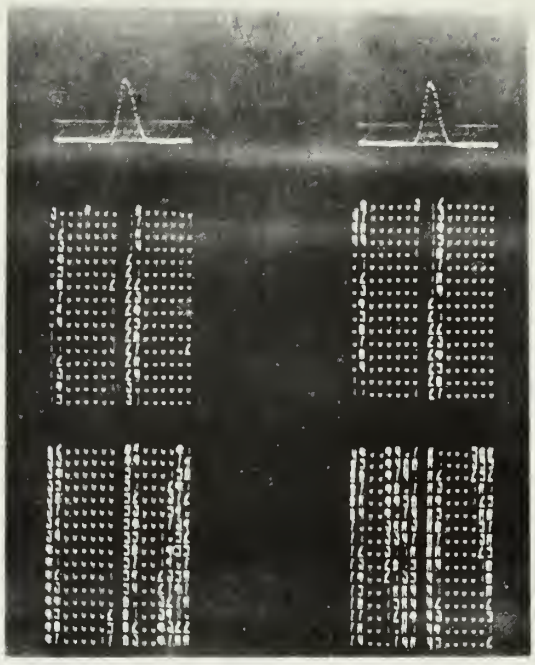

Station 1 - 2 Blowers

Fig. 3.19 Typical Pulse Height Analyzer Output for Wave Height Distribution

TABLE 3.1

RMS WAVE HEIGHT - CM

	1 Blower	2 Blowers	3 Blowers
Station 1	0.099	0.121	0.206
Station 2	-	0.129	0.216
Station 3	-	-	0.362

The assumption in theory that the wave height distribution is Gaussian is very nearly correct for the wind agitated water surface in the tank.

Wave Slope Statistics

Theory

In describing a random rough sea surface it is often more convenient to work with the slopes of the surface rather than with the heights above a mean level. In Appendix D of the book by Beckmann and Spizzichino (5) it is shown that a surface whose waveheights are normally distributed has its wave slopes normally distributed if the correlation function is Gaussian. More specifically, if the correlation function is $C(\tau) = \exp(-\tau^2/T^2)$ and the wave height distribution has zero mean and standard deviation σ the mean square slope turns out to be

$$\sum^2 = \frac{2\sigma^2}{T^2} = \frac{1}{2} \tan^2 \beta_o$$

where β_o is the RMS slope angle.

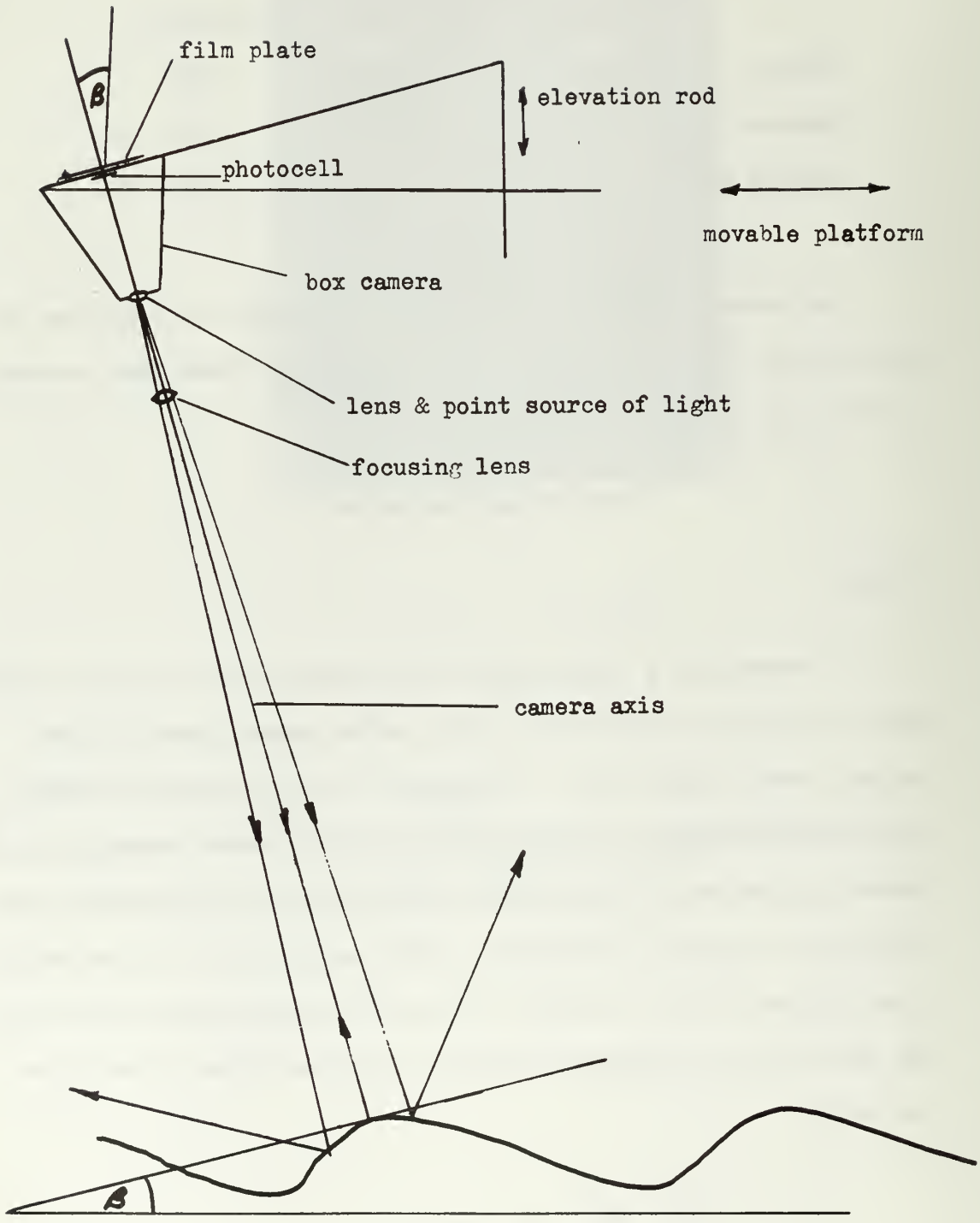

Fig. 3.20 Apparatus for Measurment of Wave Slope Statistics

Experimental

The method used in obtaining the statistical distribution of the water surface slopes was a modification of a simple optical method described by A. H. Schooley (13). Rather than obtain the statistical distribution of the wave slopes from a series of "glitter" photographs (an extremely time consuming method), the following technique, as illustrated in Fig. 3.20 , was adopted.

A simple box camera was constructed with a Hoffman type 55C (.2" x .2") photocell placed at the center of the film plate position. A 100 watt zirconium arc point source of light was placed next to the lens of the camera (Figs. 3.21 and 3.22) and was assumed to be coincident with it. A convex lens was placed approximately 12" in front of the point source in order to concentrate the light intensity in a spot of diameter approximately 20 centimeters on the water surface. Provision was made so that the camera axis, passing through the lens center and the photocell, could be oriented to any angle from 0 to 20 degrees with the vertical. The whole apparatus was mounted on a movable platform over the tank with the camera lens at a height of 62" above the water. Measurement of the water surface slope was accomplished by adjusting the elevation rod so that the camera axis was at the slope angle desired. The inclined camera was then positioned horizontally so the measurement could be taken at the center of the scattering area (defined in Fig. 3.1).

Every time a wave facet of the roughened surface was perpendicular to the axis of the camera (i.e. set at the slope angle desired) light from the point source was reflected to the photocell. The voltage of the cell, being proportional to both the intensity of light falling

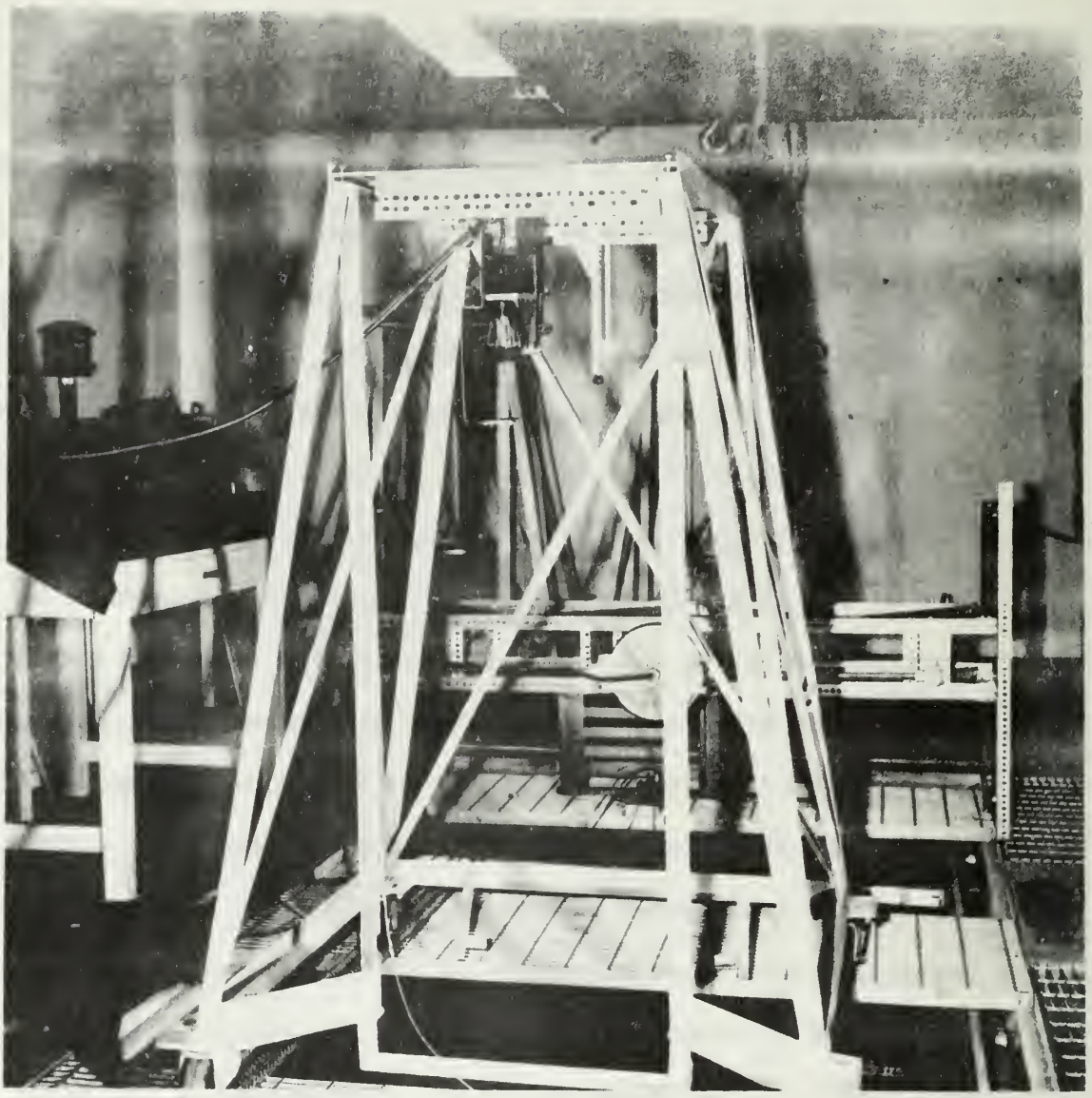

Fig. 3.21 Wave Slope Measuring Device

Fig. 3. [illegible] bearing device details

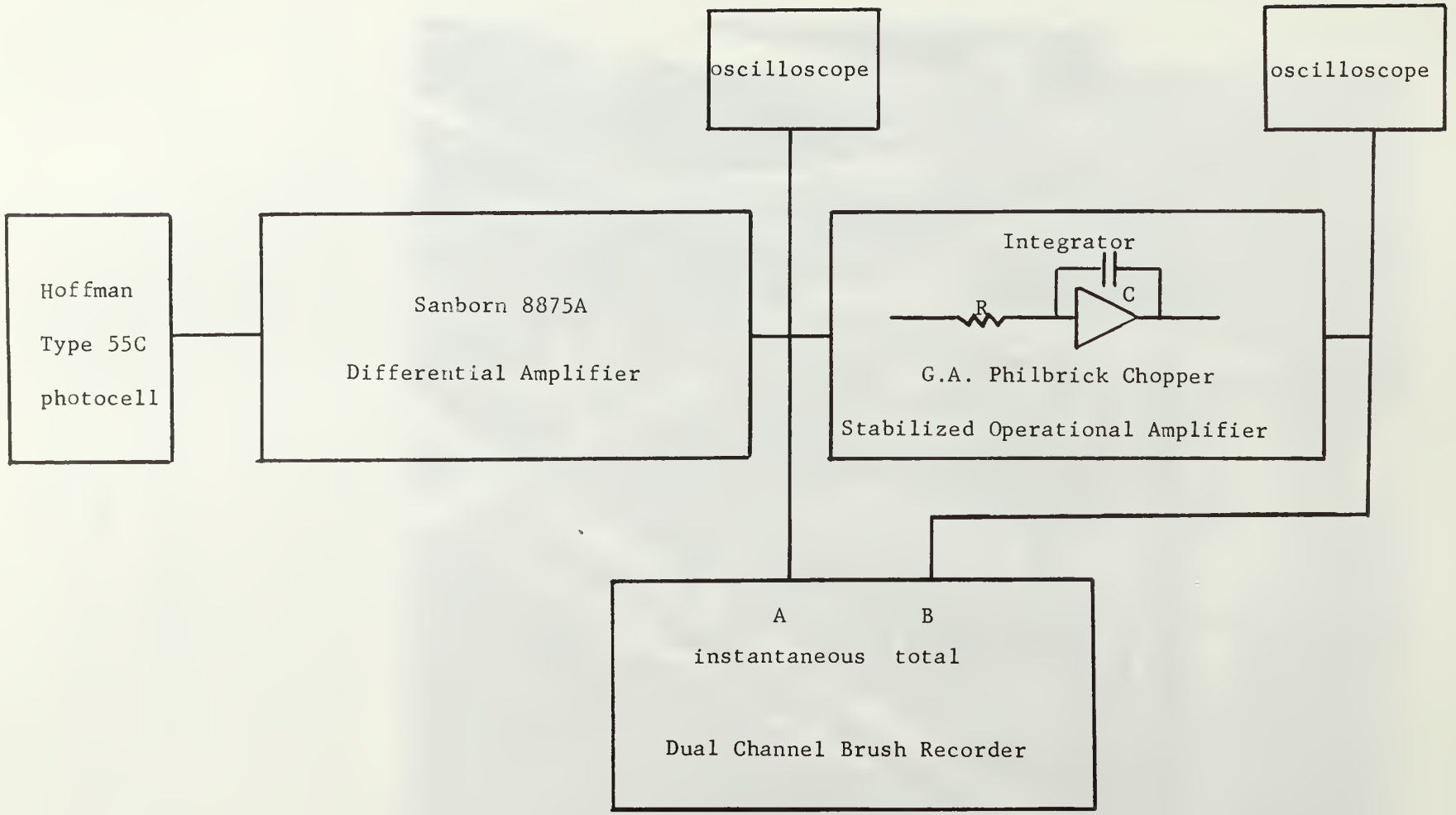

Fig. 3.23 Wave Slope Signal Processing Diagram

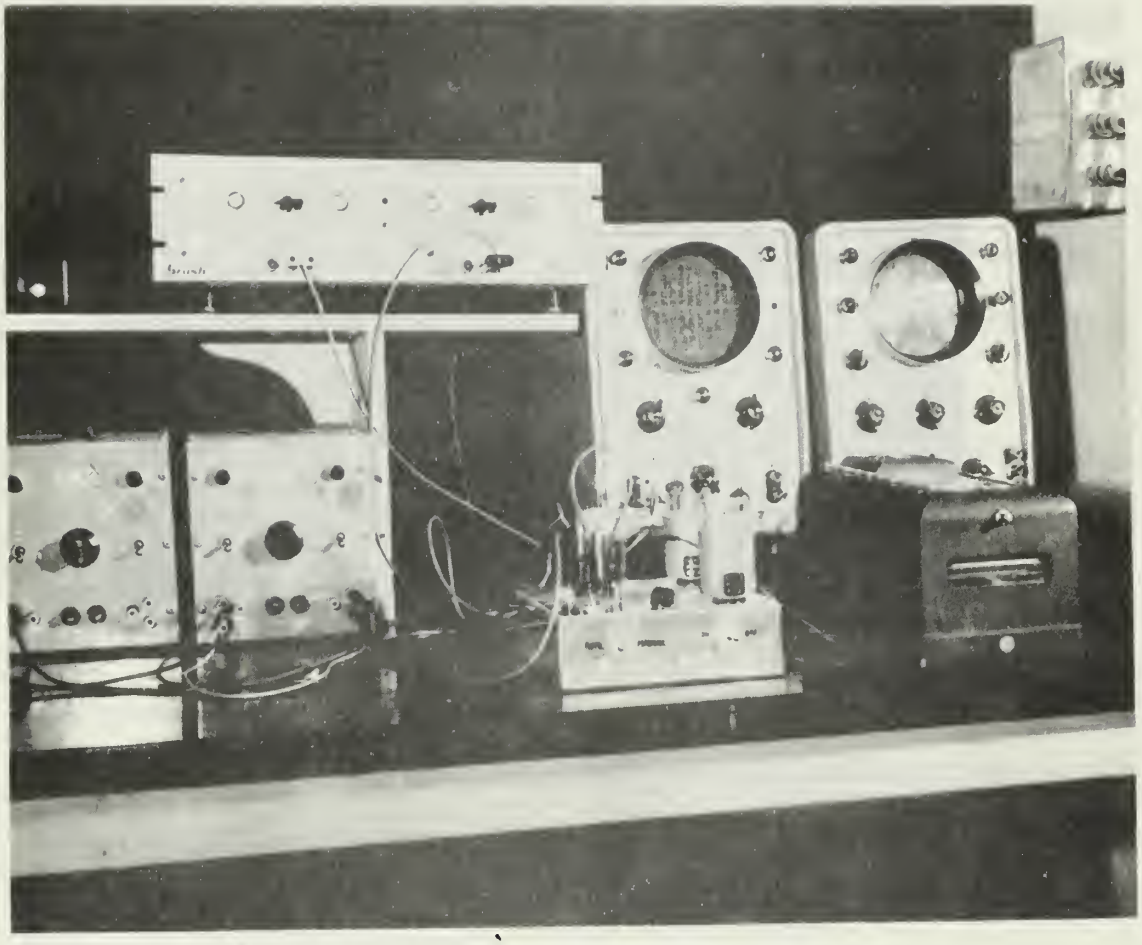

Fig. 3.24 Wave Slope Digital Processing Apparatus

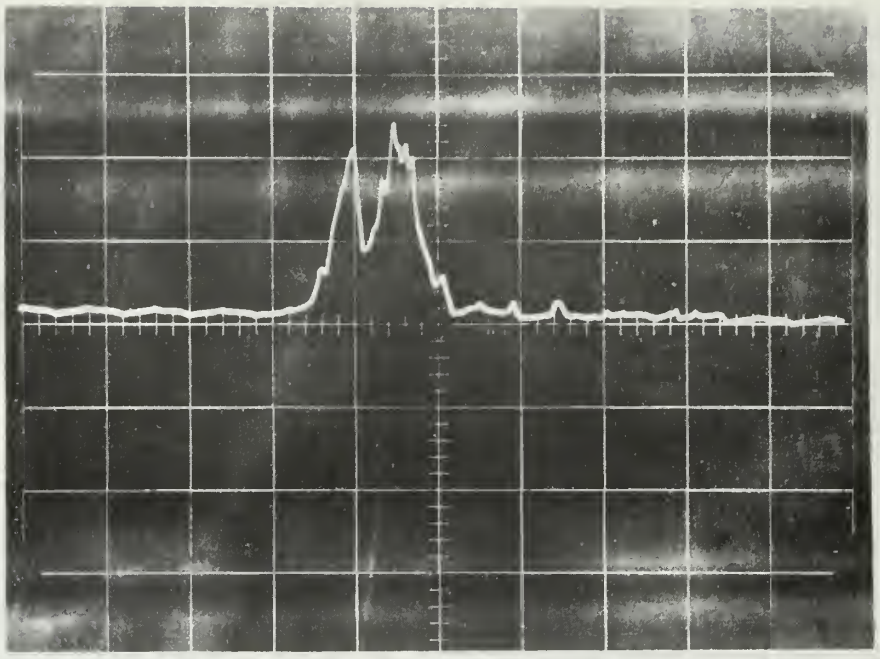

Fig. 3.25 Typical Voltage Signal from Photocell

vertical .5 volt/cm.

horizontal 100 ms/cm.

on it and the partial area illuminated, varied with the movement of the water surface. The signal was essentially zero when the cell was dark, rising and falling rapidly (Fig. 3.25) every time a sparkle of light was received from the surface of the water. The signal was recorded directly, and after integration, for a two minute period to obtain the average value. This value was then plotted on a histogram for wave slope angles. The position of the camera was changed to a new slope angle and the process repeated until the complete histogram was obtained.

The instantaneous signal from the photocell was approximately 50 to 500 microvolts varying with the slope angle. This was amplified with a Sanborn D. C. differential amplifier set with a gain of 1200 and then integrated with a G. A. Philbrick Operational Amplifier configured for integration (Figs. 3.23 and 3.24). The differential amplifier made this whole technique possible by reducing the noise level sufficiently to give a suitable signal-to-noise ratio. Both the instantaneous signal and its integrated value was recorded with a Brush Recorder oscillograph (Fig. 3.26).

There was a bit more involved in the technique used to integrate the signal due to the small drift in the zero level of the output of the differential amplifier. This zero level drift was a major problem and several D. C. amplifiers were tried before one with a tolerable drift was found. After the differential amplifier was adjusted to minimize the D. C. component a small and variable D. C. component still existed. The signal from the photocell was superimposed on this "noise" so it had to be corrected in the integration process. This was done by integrating the background level (point source off) for 30 seconds before and after each one minute integration of signal.

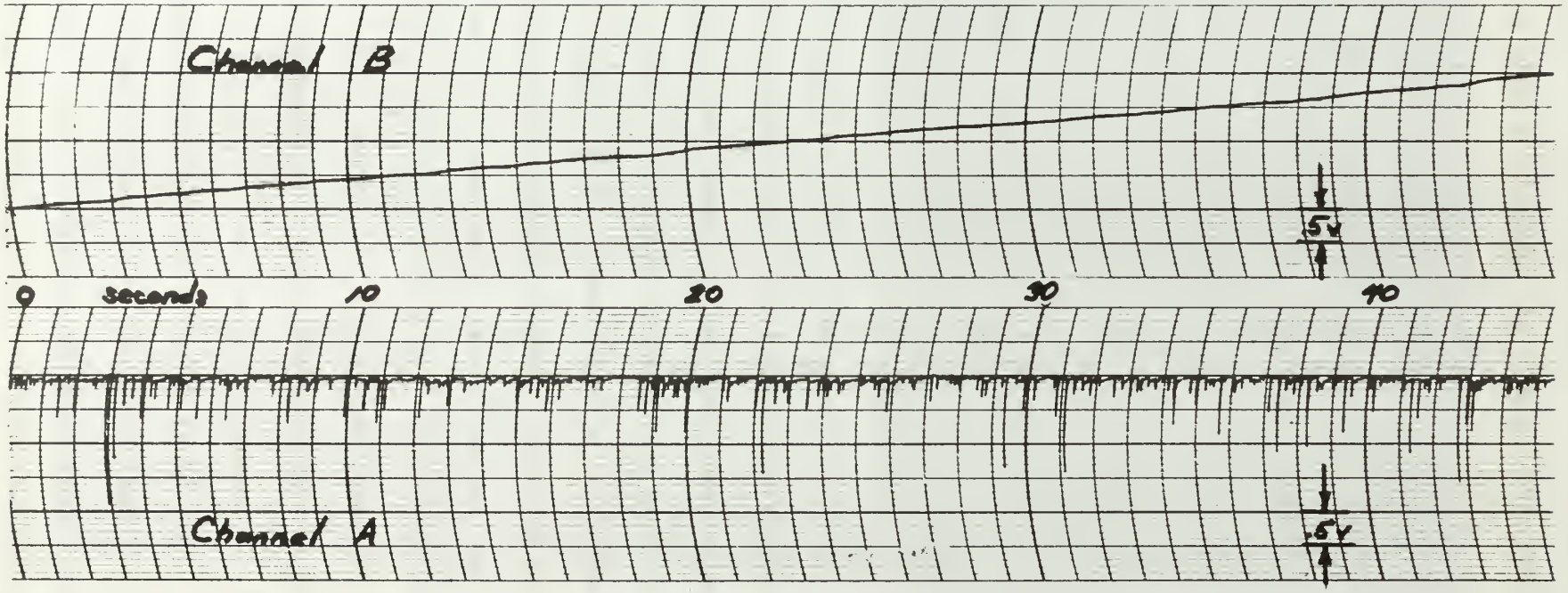

Fig. 3.26 Typical Brush Recorder Trace

Channel B integrated photocell voltage

Channel A amplified photocell voltage

The signal plus background was integrated for two one minute periods and was then corrected for the background level integration. The average of these two corrected readings was plotted on the histogram for the slope angle. To find the accuracy of each point plotted on the histogram the standard deviation for several readings at a given angle was measured. These errors were found to vary from 4% to 9% and are noted on the histograms presented.

Calibration

The output voltage of the cell was assumed to be directly proportional to the portion that was illuminated (at constant light intensity). The plot of voltage output as a function of exposed area was found to be linear.

The change of light intensity at the photocell due to increased spherical divergence loss for the increased range of the source and lens at large slope angles was measured. It was found that the 5% increase in range for the maximum slope angle resulted in a 2% decrease in voltage. This allowed the distance from the lens to the rough sea surface, and therefore the intensity, to be treated as a constant so no corrections had to be made to the photocell's output voltage.

To obtain better slope angle resolution the photocell was partially masked with opaque masking tape. With the masked photocell the resolution for slope angle was $\pm$ .2 degree.

Results and Conclusions

The slope angle distribution was taken in both the upwind-downwind direction and the crosswind direction for both scattering areas with two and three blowers on. The results are tabulated in Table 3.2.

TABLE 3.2 MEAN SQUARE SLOPE

Station I	$\sum^2_{udw}$	$\sum^2_{cw}$	$\sum^2$	$\sum^2_{udw}/\sum^2_{cw}$
2 blowers	.00769	.00238	.01007	3.23
3 blowers	.00975	.00680	.01655	1.44
Station II				
3 blowers	.00935	.00364	.01299	2.57

The general results (Figs. 3.27 - 3.32) found for our model compare favorably with those measured at sea by Cox and Munk (12). The skewness in the downwind direction of the slope distribution reported by them was observed for our rough surface (Fig. 3.29). The crosswind distributions as well as the upwind-downwind distribution for the relatively smooth surface were all found to be approximately Gaussian as at sea. The ratios of the up-downwind to the crosswind component of mean square slope varied from 1.44 to 3.23 whereas those found by Cox and Munk (12) at sea ranged from 1.0 to 1.9. Our ratios were somewhat larger than at sea because of the channeling effect of our model. The mean square slope in our model corresponded to a wind speed of approximately 5 knots.

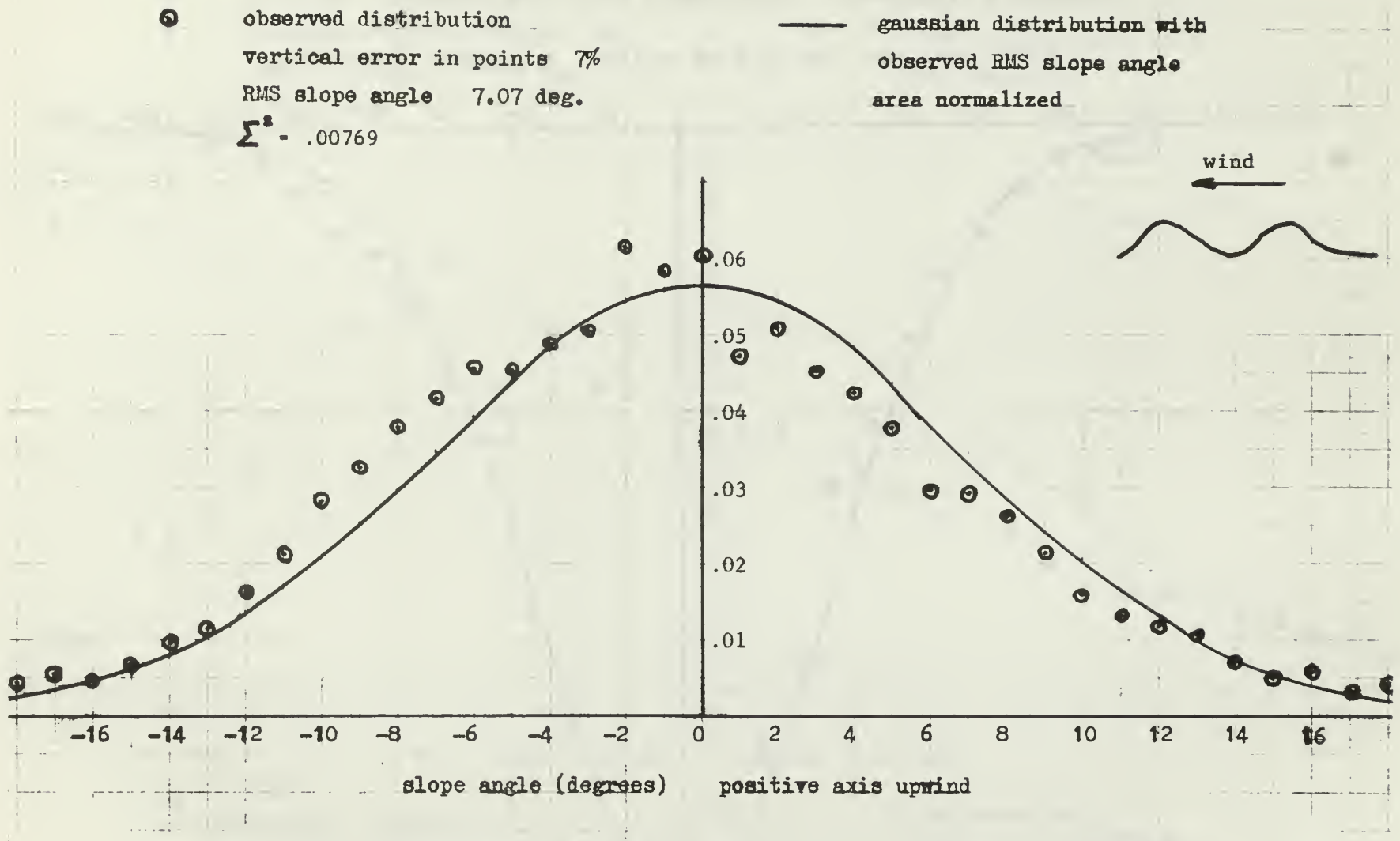

Fig. 3.27 Upwind-Downwind Wave Slope Distribution Station 1, 2 blowers

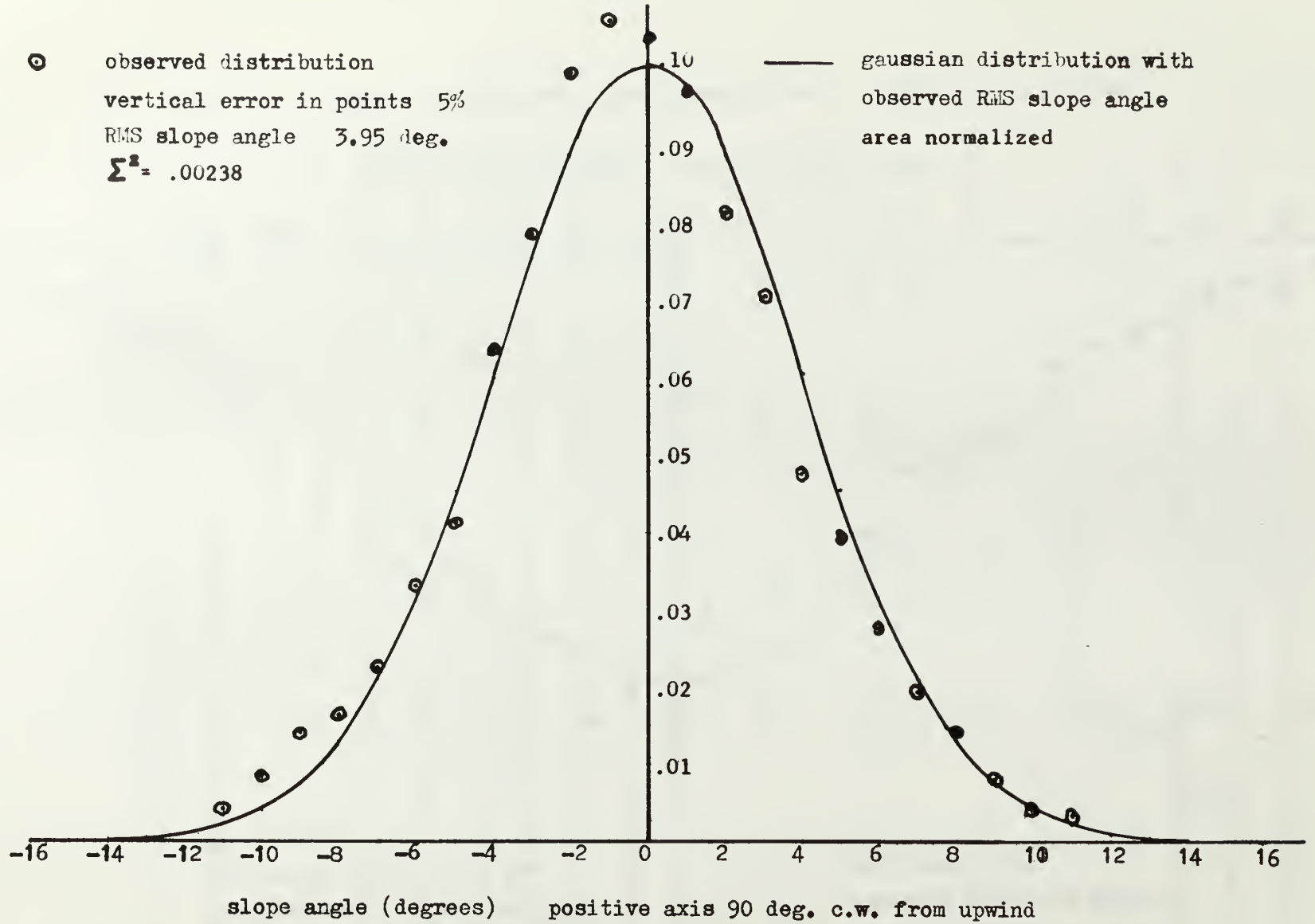

Fig. 3.28 Crosswind Wave Slope Distribution Station 1, 2 blowers

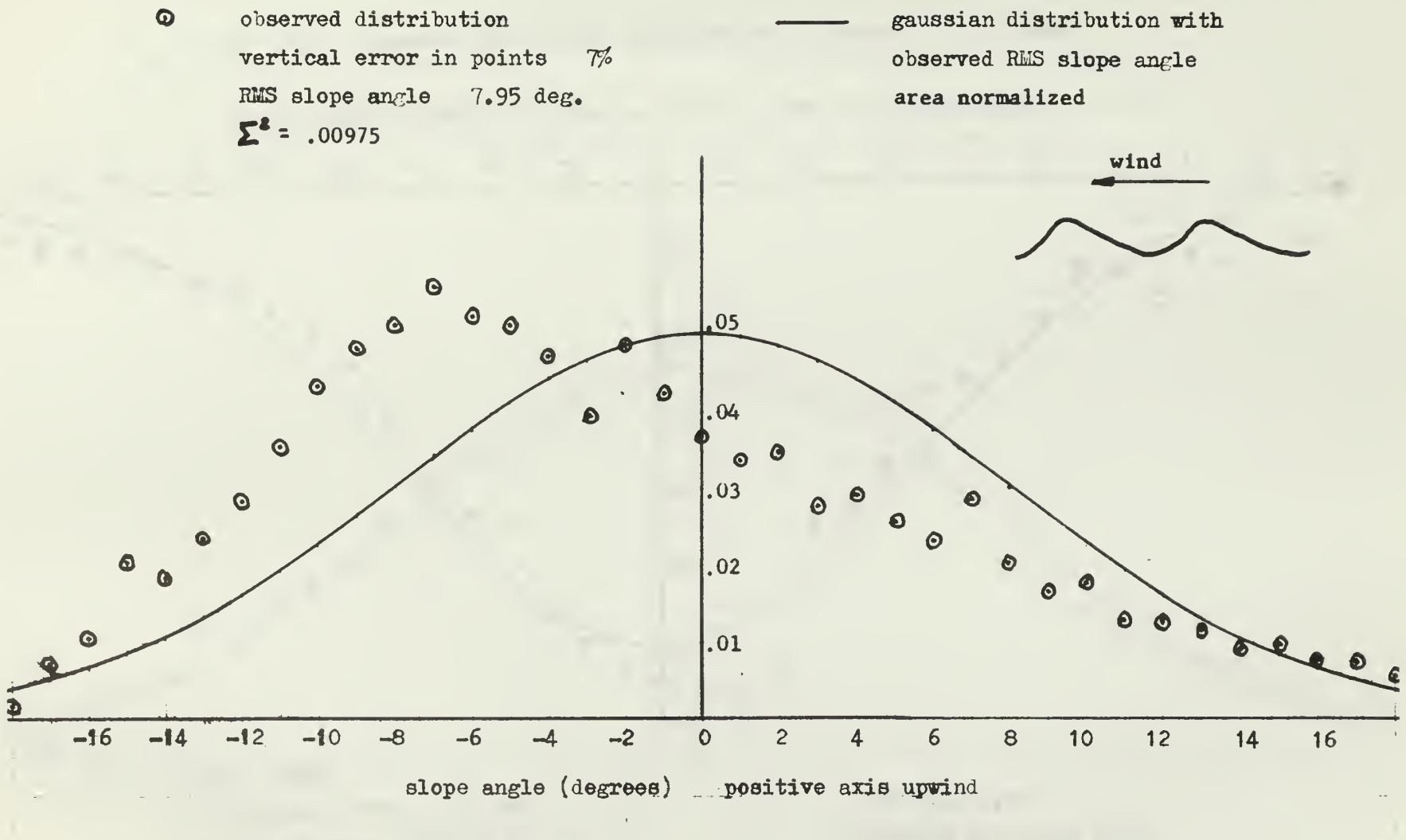

Fig. 3.29 Upwind-Downwind Wave Slope Distribution Station 1, 3 blowers

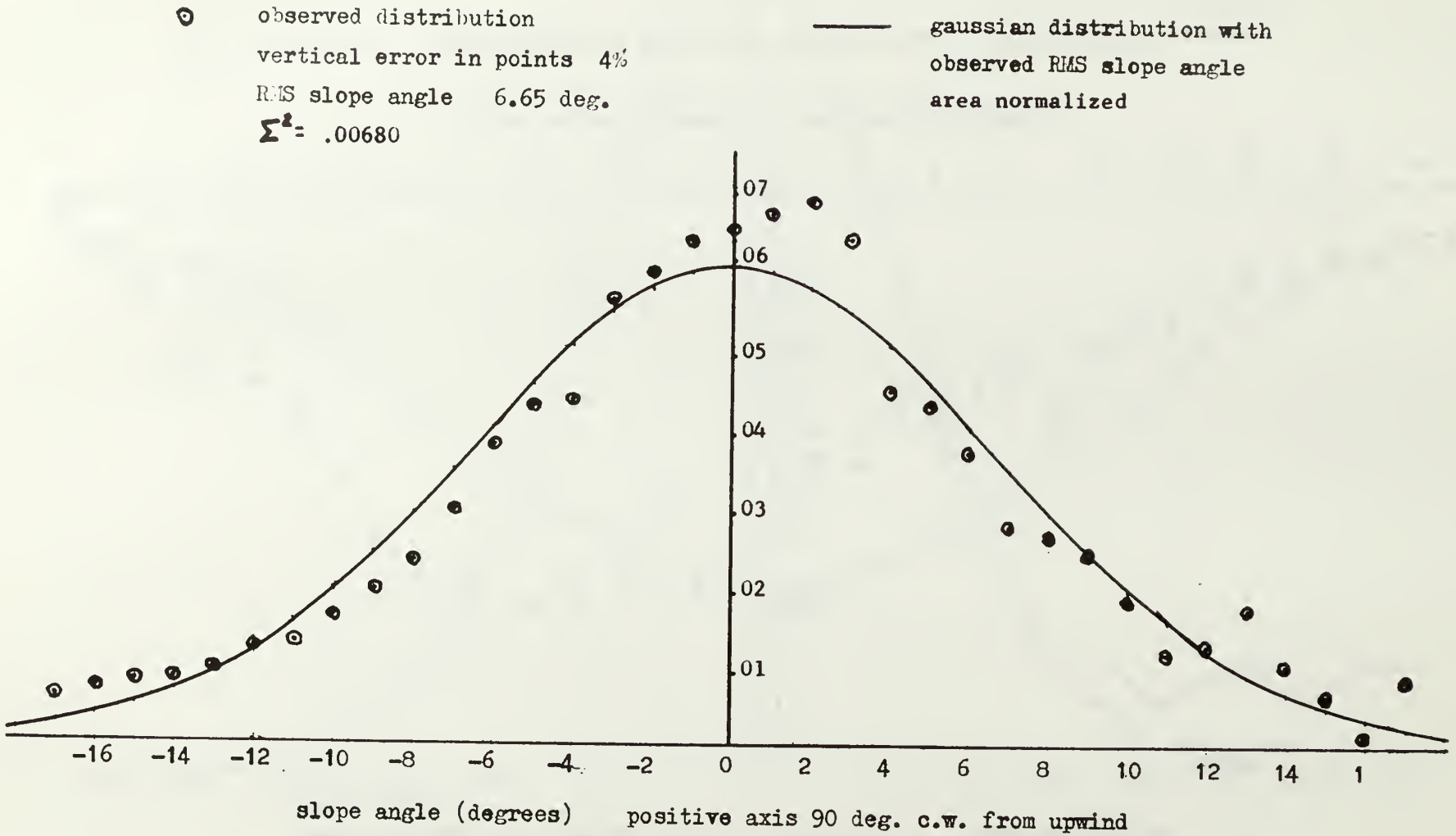

Fig. 3.30 Crosswind Wave Slope Distribution Station 1, 3 blowers

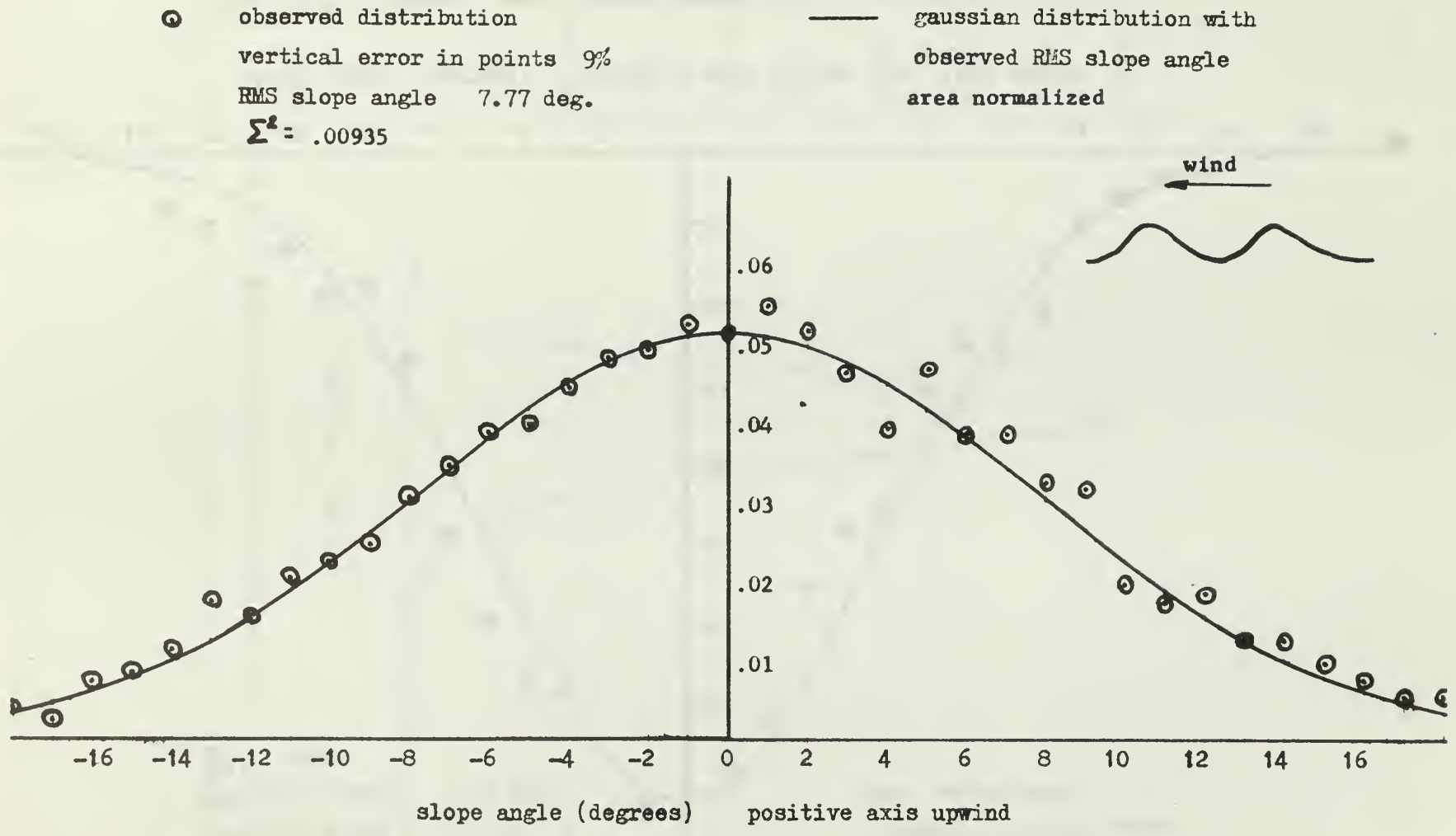

Fig. 3.31 Upwind-Downwind Wave Slope Distribution Station 2, 3 blowers

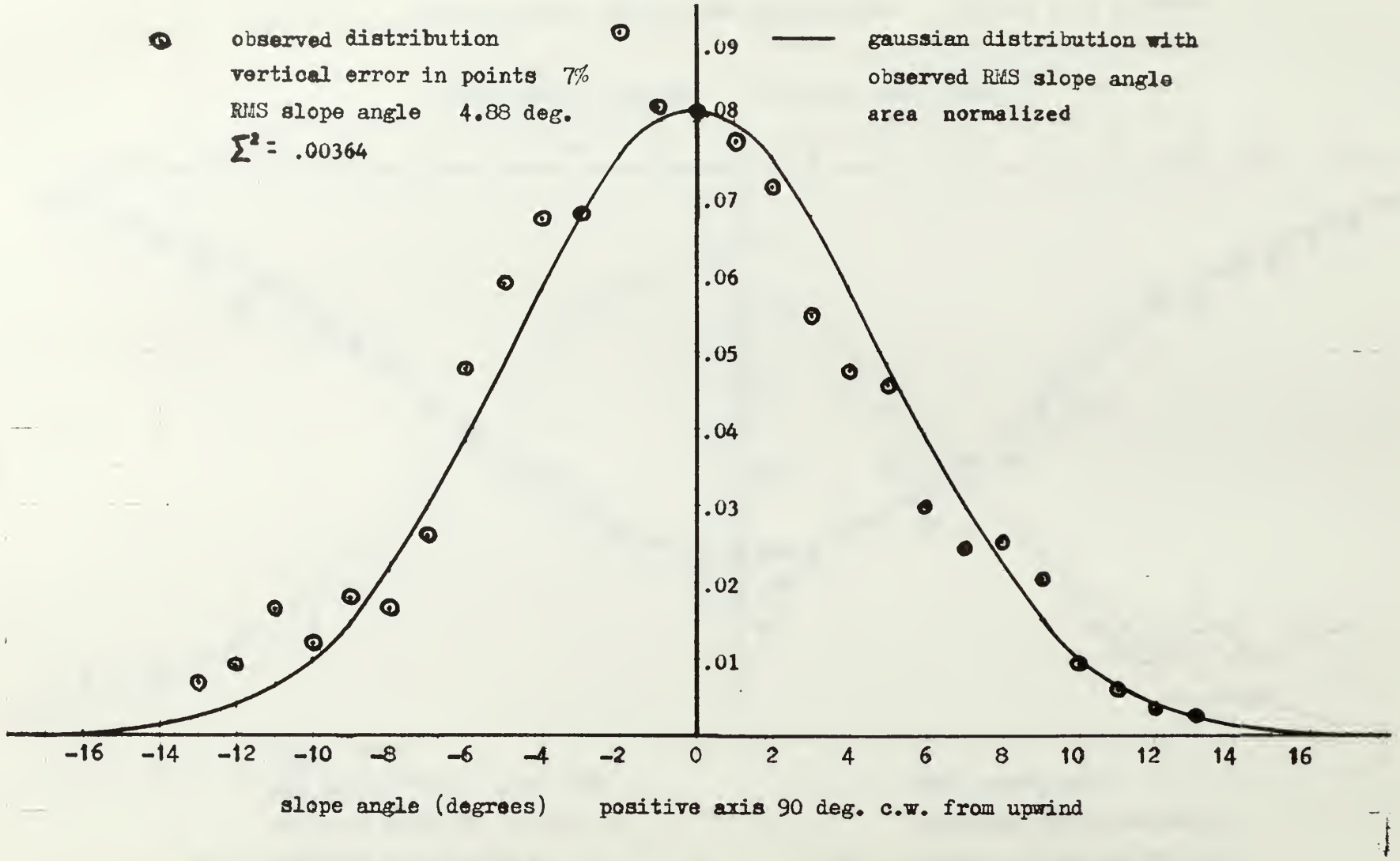

Fig. 3.32 Crosswind Wave Slope Distribution Station 2, 3 blowers

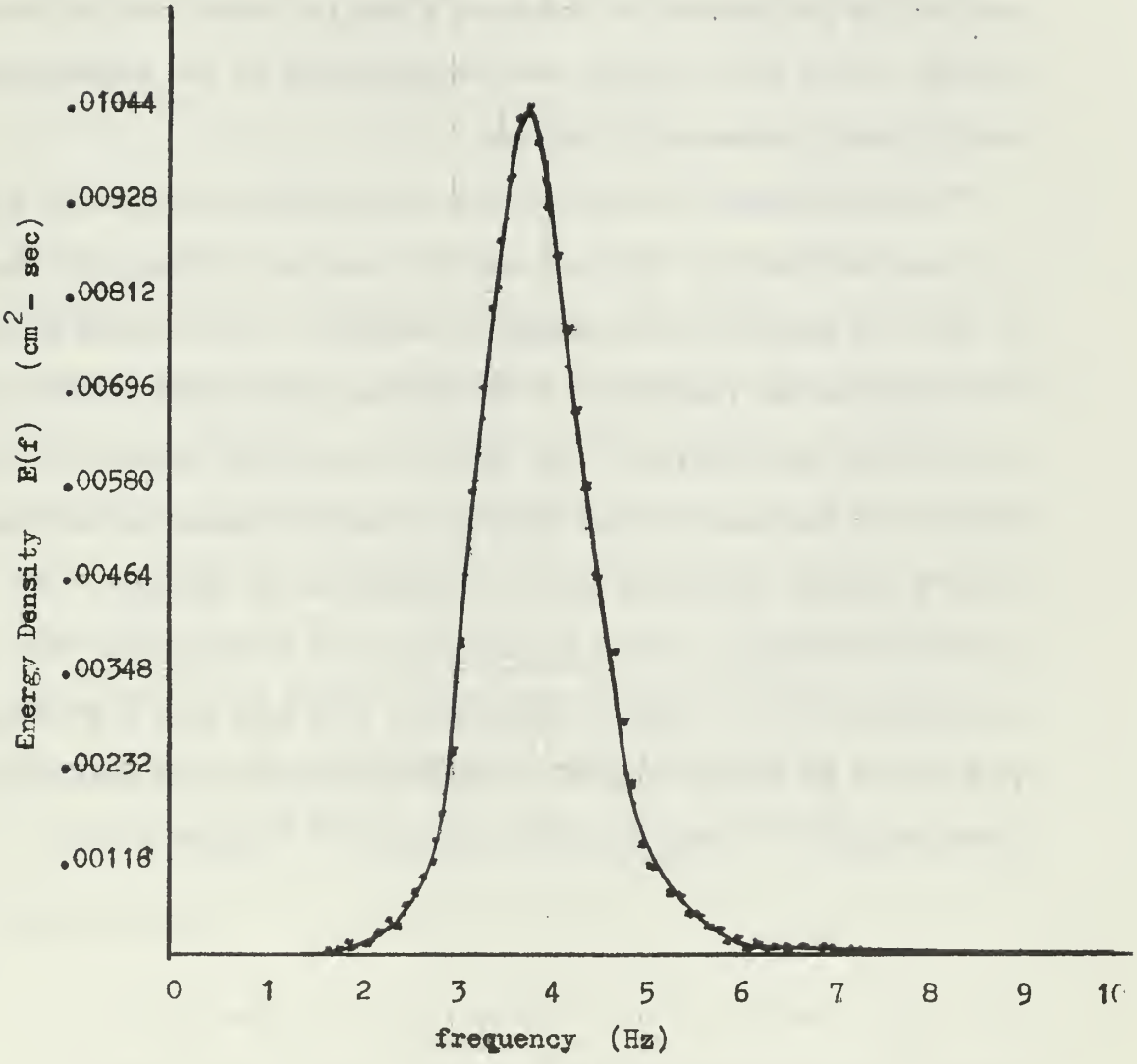

Fig. 3.33 Energy Spectrum of Rough Surface

Surface Wave Spectrum

The wave height signal from the wave height measurement system can be analyzed to determine the wave spectrum. This description of the rough model sea surface allows comparison with ocean wave spectra for the purpose of assessing a scaling factor for the model surface and is also included for identification of the backscattered energy spectra measured in Section 4.

This experiment was carried out as an advanced laboratory project by Cohen and Scheible (17) who used the identical system described in Fig. 3.6 except for the method of analysis. The detected modulation envelope was recorded at 0.375 ips and then played back at 37.5 ips into the wave analyzer with the fixed bandwidth selected at 3 Hz. In this way the spectrum was shifted to audio frequencies and expanded so that greater resolution within the spectrum is achieved. The resultant spectrum is shown in Fig. 3.33. It is noted that the energy is concentrated in a band of frequencies 6 Hz wide with a pronounced peak at 3.8 Hz and falling off at frequencies above the peak with an approximately f^{-10} dependence to 6 Hz and $f^{-4.2}$ beyond 6 Hz.

4. The Backscattered Radiation

The statistical scattering theory predicts a relation between the backscattered intensity and the surface statistics and the frequency of the acoustic energy scattered. It also predicts the existence at normal incidence of a coherent and an incoherent component of backscattered sound. (At normal incidence, backscatter and specular scatter are identical). For a relatively smooth ($g \ll 1$) surface, the distribution of the heights of the pulses scattered in the specular direction is predicted to be Gaussian. The distribution of energy scattered in other than the specular direction is predicted to be Rayleigh since the scattered energy is incoherent. For rough ($g \gg 1$) surfaces, the specular scattering is predominately incoherent and all distributions are expected to be nearly Rayleigh. The measurement of the scattered echoes has been designed to display the distribution of echo strengths and to determine the average backscattered itensity. The latter is calculated from the square of the mean plus the variance of the scattered pulse amplitude distribution.

Experimental

In the conduct of the experiment, it is extremely important to identify the received signal as backscattered energy from the particular angle considered. It is possible to measure noise, echoes from other portions of the tank or transducer support or from the side lobes or even off-axis in the main beam. Particular care must be taken with the geometry of the apparatus and with choice of electronics equipment to discriminate against all signals

which are not truly surface backscatter. With respect to electrical noise, low noise figure electronic apparatus is essential as is the use of bandpass filters to reduce the effects of wideband noise. So far as the geometry is concerned, any pulsed technique can discriminate against echoes from the tank walls or floor by the simple expedient of making the distance to the scattering area shorter than any other distance in the tank, or at least making the distance to the scattering area different from the distance to other possible targets so that the surface scattering and the spurious echoes do not coincide in time. However, in a model study of backscatter, there is a spurious echo from the surface for which this is not always possible. At angles near normal incidence, the normal incidence reflection from off-axis in the main beam may be very close in time to the scattered echo, and the amplitude of this reflection may be larger than the scattered echo. To reduce the errors, the projector must have a very narrow beam pattern, yet, in a tank experiment this dictates that the dimensions of the scattering area will not be large with respect to the surface correlation distance. For a beam incident on a relatively smooth surface the strength of the backscattered echoes near normal incidence is very sensitive to small changes in the angle of incidence. Since all other backscattered intensities at other angles of incidence are referenced to the reading at zero incidence, errors in the measurement of the scattering intensity at this sensitive spot will affect the level of all results. It is considered that this is a principal source of experimental error in this work. The level of electrical noise and spurious echoes was measured and these effects are indicated by a noise line on the curves of backscattering factor vs. angle of incidence (Figs. 4.17 to

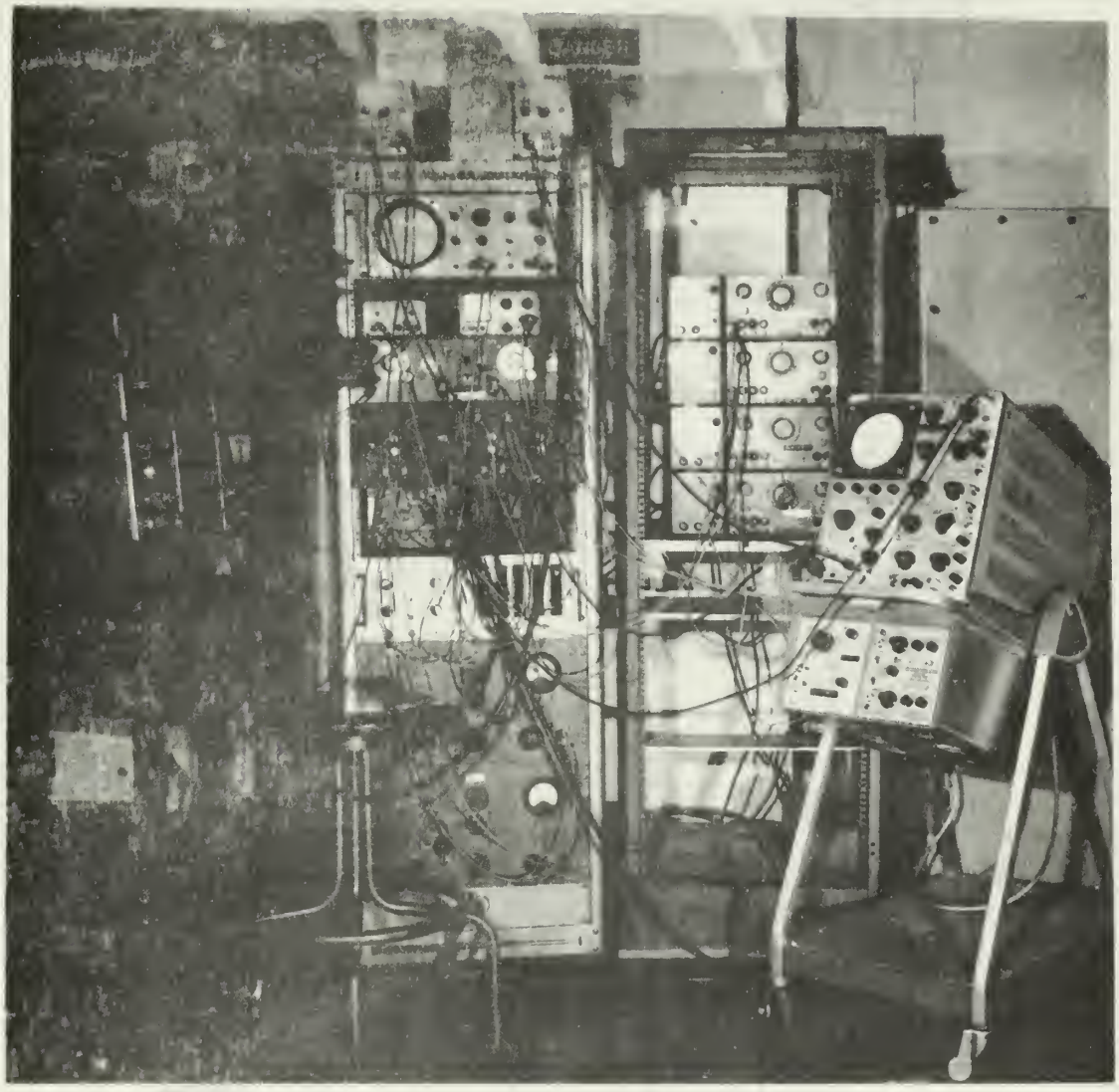

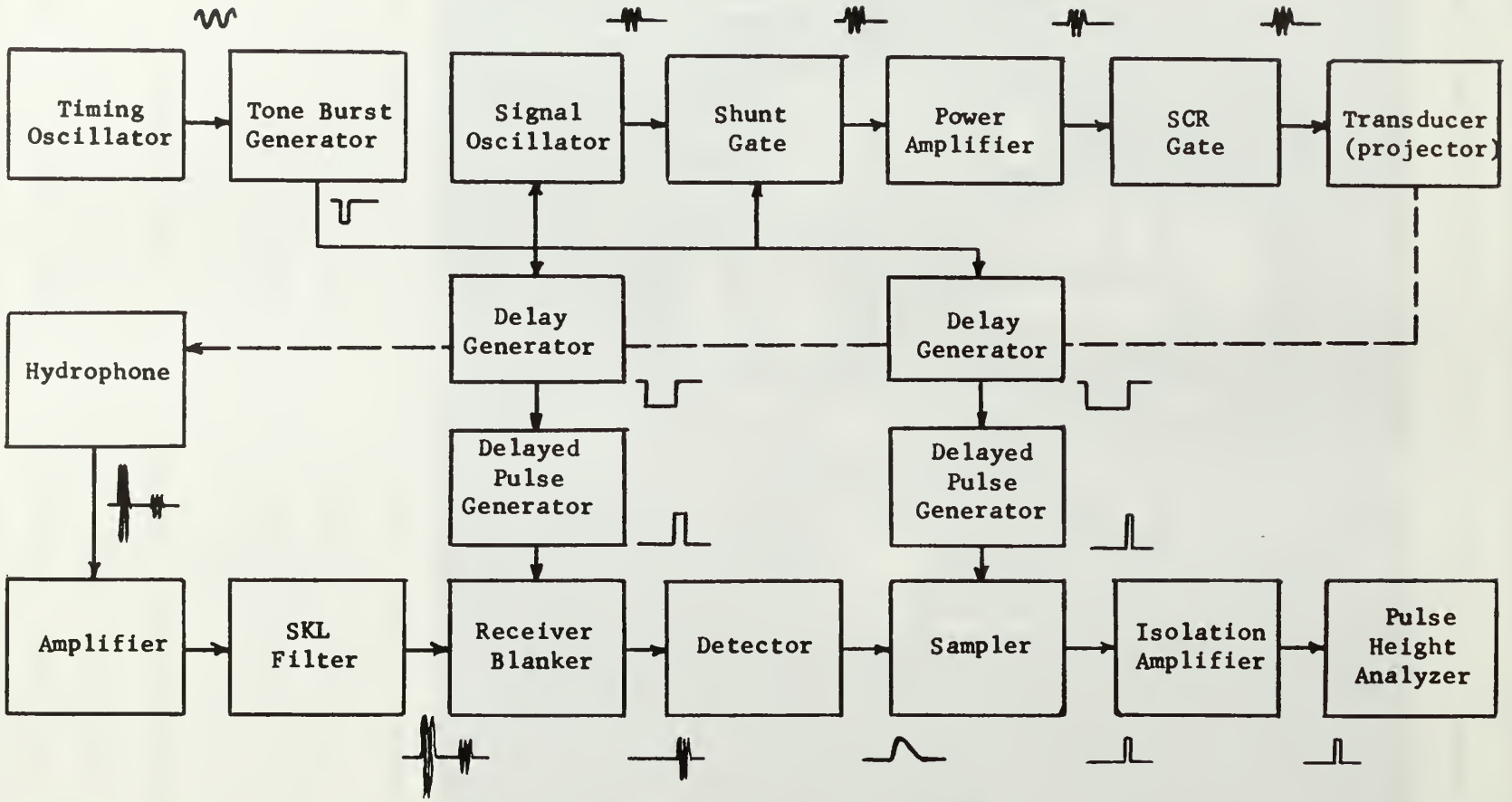

Fig. 4.2 Transmitter and Receiver System - 70 kHz

Timing Oscillator	HP 650A Test Oscillator
Tone Burst Generator	GR 1396A Tone Burst Generator
Signal Oscillator	HP 3300A Function Generator
Plug in Unit	HP 3302A Trigger/Phase Lock Module
Shunt Gate	see Fig. 4.4
Power Amplifier	GR 1233A Power Amplifier
SCR Gate	see Fig. 4.5
Projector	EDO Model 327 Transducer
Delay Generator (2)	GR 1217B Unit Pulser
Delayed Pulse Generator (2)	GR 1217B Unit Pulser
Hydrophone	Atlantic Research LC-32
Amplifier	HP 463A Precision Amplifier
SKL Filter	Spencer Kennedy Model 302 Electronic
Receiver Blanker	see Fig. 4.6
Detector	see Fig. 4.7
Sampler	see Fig. 3.8
Isolation Amplifier	HP 467A Power Amplifier
Pulse Height Analyzer	RCLiac 128 Scaler Analyzer

Fig. 4.2(a) Equipment List for

Transmitter and Receiver System - 70 kHz

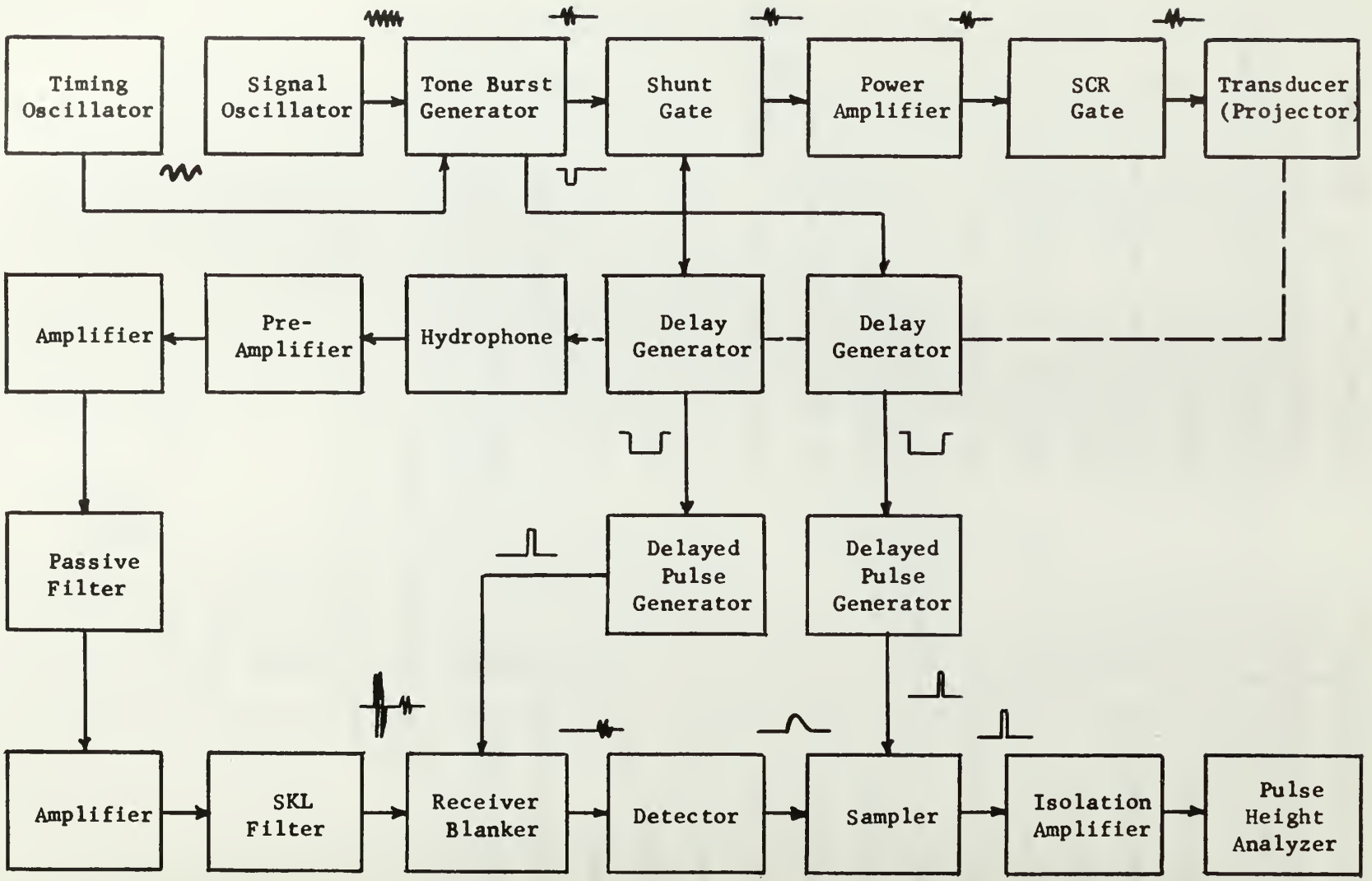

Fig. 4.3 Transmitter and Receiver System - 450 kHz

Timing Oscillator	HP 650A Test Oscillator
Signal Oscillator	HP 650A Test Oscillator
Tone Burst Generator	GR 1396A Tone Burst Generator
Shunt Gate	see Fig. 4.4
Power Amplifier	GR 1233A Power Amplifier
SCR Gate	see Fig. 4.5
Projector	4 x 4 array $BaTiO_4$ special NPGS
Delay Generator (2)	GR 1217B Unit Pulser
Delayed Pulse Generator (2)	GR 1217B Unit Pulser
Hydrophone	3 x 3 array $BaTiO_4$ special NPGS
Pre-Amplifier	HP 463A Precision Amplifier
Amplifier (2)	HP 467A Power Amplifier
Passive Filter	Allison Model LC Variable
SKL Filter	Spencer Kennedy Model 302 Electronic
Receiver Blanker	see Fig. 4.6
Detector	see Fig. 4.7
Sampler	see Fig. 3.8
Isolation Amplifier	HP 467A Power Amplifier
Pulse Height Analyzer	RCLiac 128 Scaler Analyzer

Fig. 4.3(a) Equipment List for
Transmitter and Receiver System - 450 kHz

4.21). Unless these particular precautions are observed in any scattering experiment, the small grazing angle effects, which depart from theory, and which have been observed by several experimenters (1,2,3) may well be illusory.

Electronics. Fig. 4.1 shows the electronic equipment used in this part of the experimental work. Figs. 4.2 and 4.3 are block diagrams of the systems used in measuring the backscattered radiation from the rough surface at 70 kHz and 450 kHz. They differ only in the use of additional amplifiers at the higher frequency to compensate for attenuation inherent in the sampling circuits at the higher frequency, and in the use of a different signal generator in each of the experiments.

The tone burst generator used in the experiment at 70 kHz was a HP 3100A Function Generator with a 3302A Trigger/Phase Lock plug-in-unit. This provided 67 db separation between the tone burst level and the output noise. For the experiment at 450 kHz, a separate signal oscillator was used and the tone burst formed by a GR 1396A Tone Burst Generator. The GR tone burst generator provides only 44 db separation between tone burst level and leak-through signal. Particularly in the case where the transducer is used both as a projector and a hydrophone, there must be at least 80 db separation between the tone burst level and the noise or leak-through signal. An additional 27 db was provided by a supplementary shunt gate, and in both cases, noise from the power amplifier during the off period was suppressed by use of a switch incorporating a silicon control rectifier.

The supplementary shunt gate is shown in Fig. 4.4. It is a simple emitter follower followed by a shunt switch with provision for pedestal adjustment. The switching circuits of the GR Tone Burst Generator are very similar. With the transistors used, one stage provides 27 db separation between the signal levels measured in the on and off modes. The key factors in determining this ratio are the transistor resistances in the saturated and cut-off modes.

The power amplifier used in the pulsed experiments was a GR 1233A Power Amplifier. This unit provides a high gain and a wide frequency response with signal levels up to 120 volts peak-to-peak. This amplifier is subject to oscillation unless particular care is taken in location and layout of input and output circuitry to avoid feedback. It is also particularly sensitive to poor pedestal adjustment in the input signal. Any amount of pedestal voltage causes distortion of the output pulse.

The Silicon Control Rectifier (SCR) gate is used at the higher power level to isolate the power amplifier when the system is in the listen mode. The low output impedance of the power amplifier is an advantage when supplying power to the transducer, but it is a decided liability if the transducer is being used as a hydrophone as well, since the signal is shunted by the power amplifier output impedance. Secondly, the noise output of the power amplifier with zero input signal is still sufficient to mask the scattered radiation and must be isolated. Fig. 4.5 shows the SCR gate. The gate is self operating and requires no external gating pulse. The diode bridge ensures that the SCR faces signals of the correct polarity for both positive and negative halfcycles of the tone burst. Initially the SCR is not conducting. The positive rise of the input signal biases the cathode

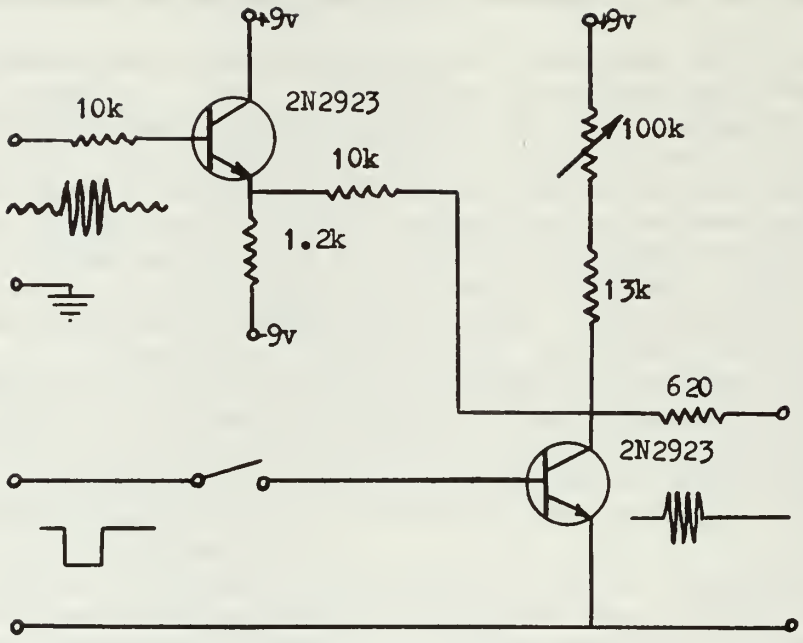

Fig. 4.4 Shunt Gate

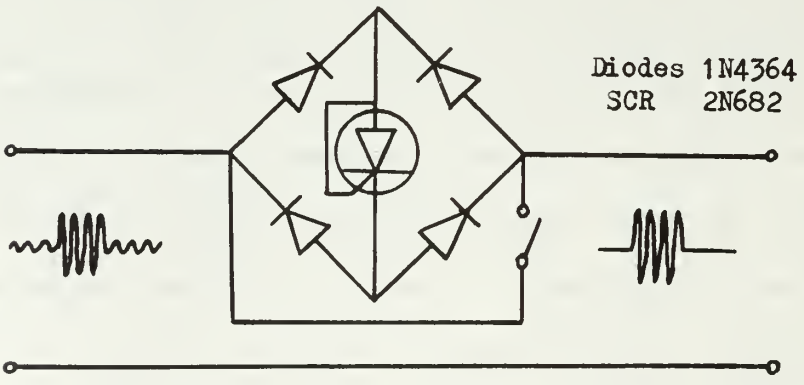

Fig. 4.5 SCR Gate

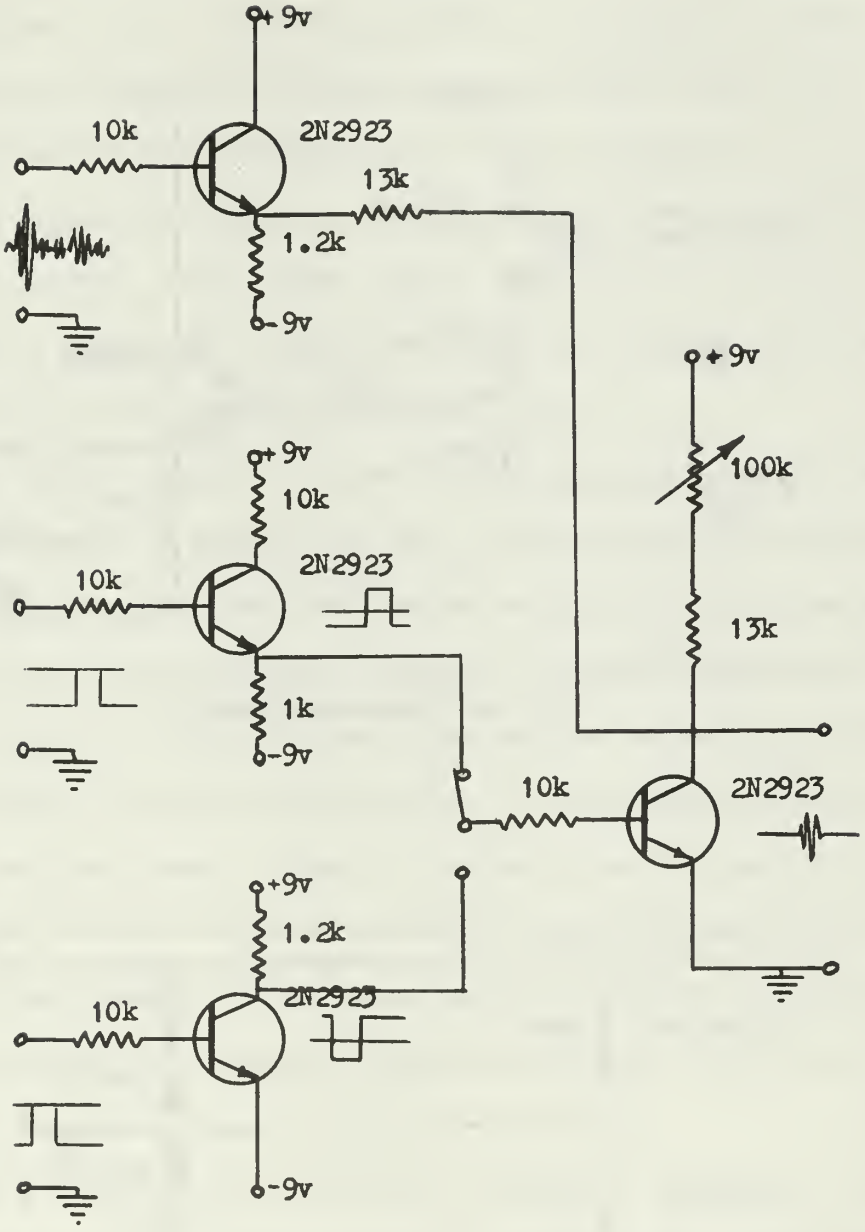

Fig. 4.6 Receiver Blanker Circuit

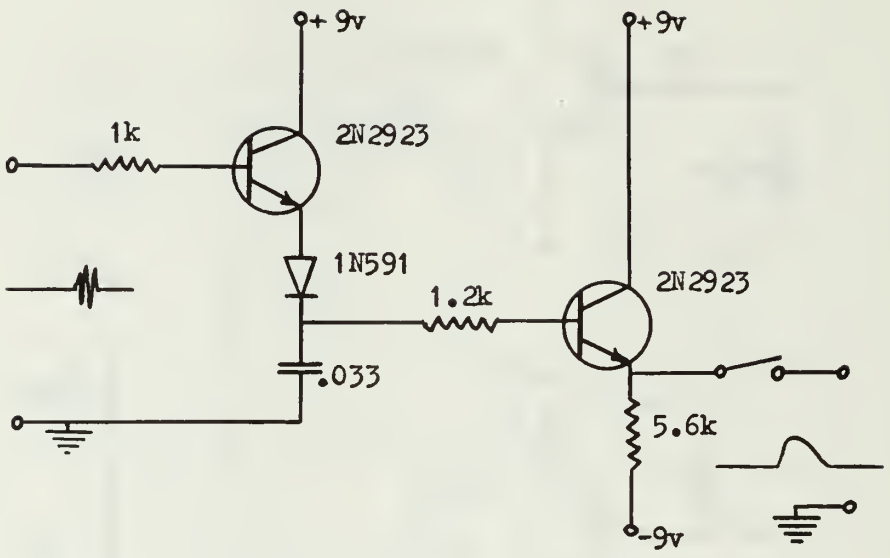

Fig. 4.7 Detector Circuit

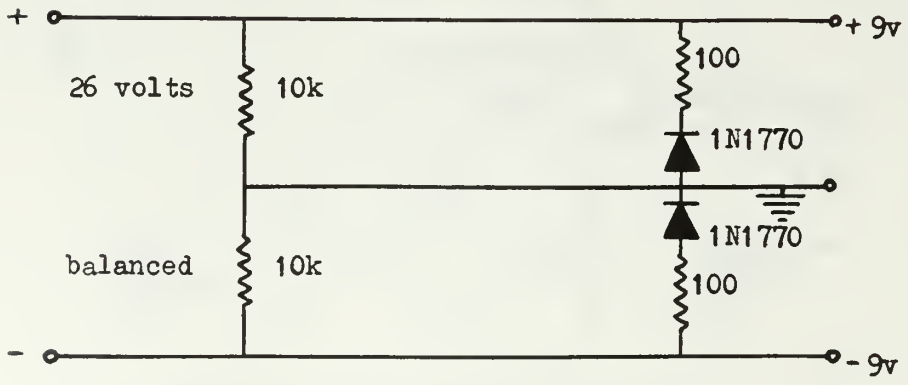

Fig. 4.8 Regulated Power Supply

gate and the SCR turns on. As the current falls after the first half-cycle, the critical hold-on current is passed and the device turns off. If the tone burst continues, the process is repeated for each half-cycle. If the tone burst is finished, the device stays turned off. The resistance in the on mode is very low (10 ohms) and in the off mode is very high (2 megohms). It should be noted that the gate voltage required to turn the SCR on is about 2 volts. For a large signal, this causes negligible distortion. For a small signal, the distortion may not be tolerable. The device will not work at low signal levels.

The receiver blanker is used to eliminate any signals other than those received at a preset time for a preset period after the main pulse is transmitted. The unit may be switched to use the pulse from the tone burst generator, inverted, to cause blanking only during the main pulse. It may also be triggered from an externally generated delayed pulse in order to discriminate in time against spurious echoes in the received signal. Under all circumstances the main pulse must be blanked in order to prevent sensitive receiving amplifiers from being driven into saturation which can cause unwanted transients for some time after the saturating signal is removed. This circuit is shown in Fig. 4.6.

The detector circuit is shown in Fig. 4.7. This unit will provide a rapid rise time to follow the leading edge of the echo pulse and a long fall time to hold the maximum voltage reached by the pulse. The emitter follower input provides the low charging resistance with isolation from the input device. The emitter follower output provides the high resistance discharge path to hold the signal and isolates the detector from the effects of low input impedance of any possible following stage.

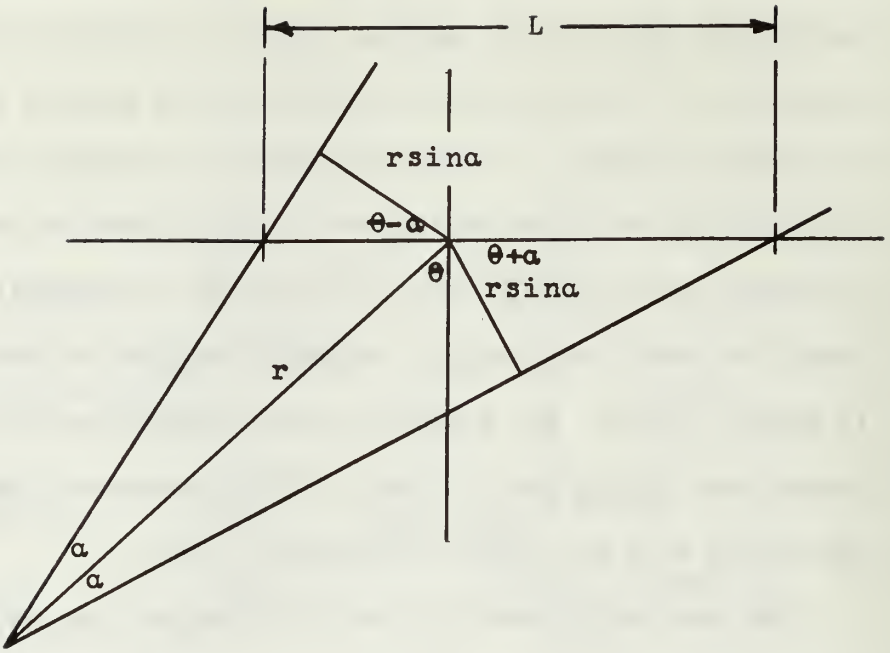

$$L = r\sin\alpha \left[\frac{1}{\cos(\theta-\alpha)} + \frac{1}{\cos(\theta+\alpha)}\right]$$

$$A = \frac{\pi r^2 \sin^2\alpha}{2\cos\alpha}\left[\frac{1}{\cos(\theta-\alpha)} + \frac{1}{\cos(\theta+\alpha)}\right]$$

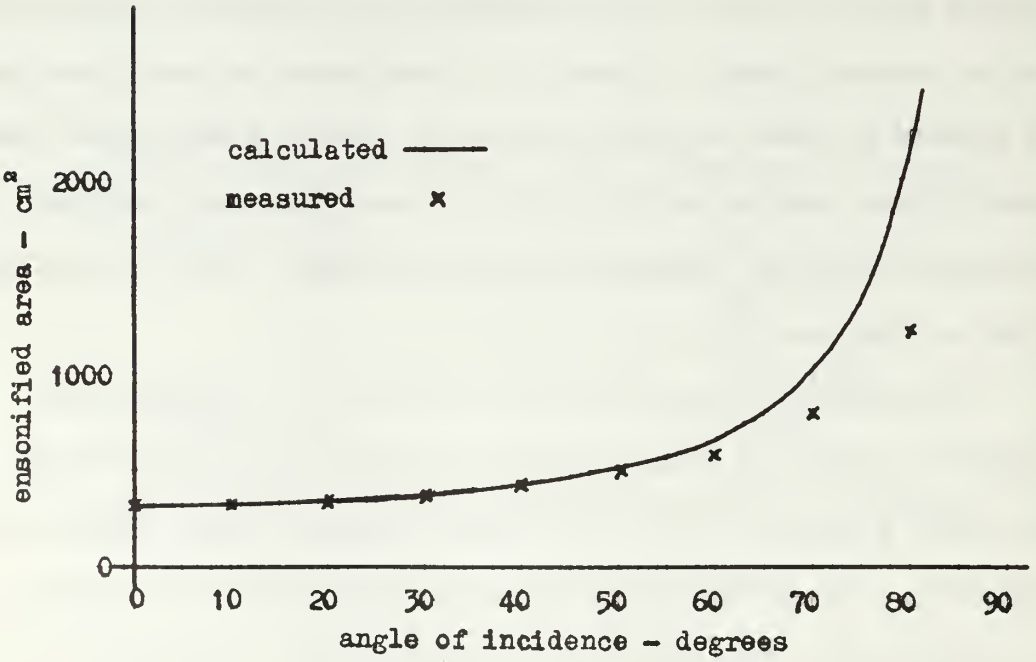

Fig. 4.9 Calculation of Scattering Area

The sampler unit is connected to the detector by a simple SPST switch. This allows the detector to be isolated when the sampler is used for other purposes such as in the sampling of the wave height signal. This unit has been fully described in Section 3 in the discussion of the electronics apparatus used for measurement of the wave height distribution. The delayed pulse units and the pulse height analyzer have also been described in the same section. In this application the analyzer measures the distribution of pulse voltages and hence gives a measure of the average backscattered intensity from the mean and variance of the recorded distribution.

The regulated power supply for all the supplementary transistorized gating and sampling circuits is shown in Fig. 4.8. The unit incorporates two zener diodes to regulate the voltage at a balanced +9v and -9v. The voltage supply is a HP 471A Power Supply.

Transducers. For the experiments conducted at frequencies from 20 to 100 kHz, the projector used was an EDO Model 327 transducer. This 30 cm diameter transducer contains two concentric arrays of ADP crystal piezoelectric elements. When both arrays are used simultaneously, the beam width to the 3 db down points at 180 cm distance is as shown in Table 4.1. The beam angle for these 3 db down points is also calculated. Similar data are included in the table for the transducer used in the experiment at 450 kHz. Fig. 4.9 shows the geometry of the calculation of the scattering area from the beam measurements. The beam is conical and the area of the intersection with the surface is an ellipse. The 3 db down points were actually measured for the 70 kHz case and the comparison of theoretical and measured data is given in Fig. 4.9.

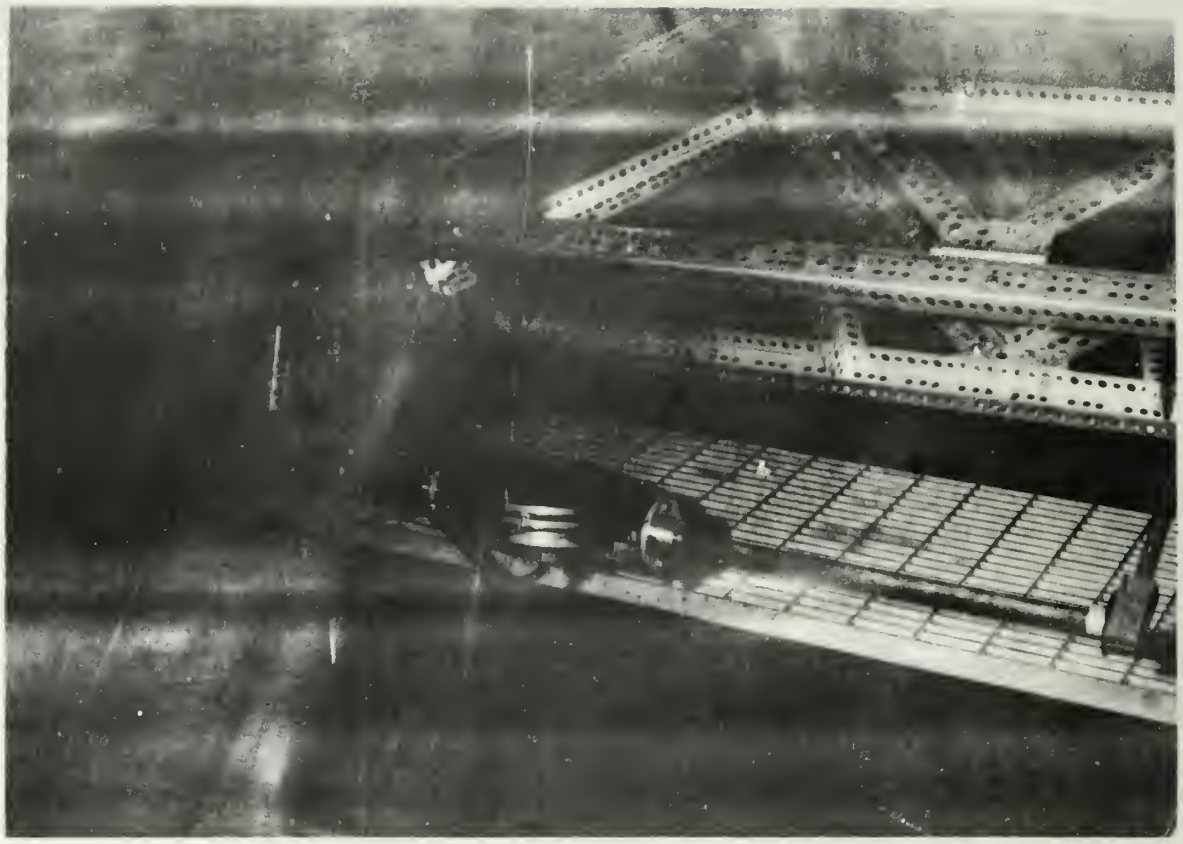

Fig. 1.10 Positioning Jaws for Transducer
Showing DX 327 Transducer

TABLE 4.1

BEAM ANGLES TO 3 db DOWN POINTS

Frequency	kHz	20	50	70	100	450
Beam diameter at 180 cm	cm	80	43	21	14	10*
Beam angle	deg	12.5	6.8	3.3	2.2	4.0

*measured at 72 cm from source.

In Fig. 4.9 there is a marked departure of the calculated area from the measured area. This is due to the effect of spreading losses and of the very wide aperture which were neglected in this oversimplified model. In the actual calculation of the backscattering factor, the measured area was used. Since this area enters the expression for the backscattering factor in the denominator, the noise line drawn on Figs. 4.17 to 4.21 must be modified to show the downward shift the calculation would cause for a constant signal.

In the experiments at the lower frequencies, it was found that the noise level due to interference from the projector power amplifier was high enough to mask scattered echoes that could be discerned by filtering the broad band signal from a separate hydrophone. Consequently, during the entire run of experiments a separate Atlantic Research LC-32 hydrophone, placed at the center of the EDO projector, was used. This hydrophone is omnidirectional. The beam pattern was modified by placing it against the diaphragm of the EDO transducer but in all measurements, this geometry was kept constant. Since the backscattering factor is a ratio of scattered to incident intensity and both were measured with the same equipment and geometry, these effects were effectively cancelled out.

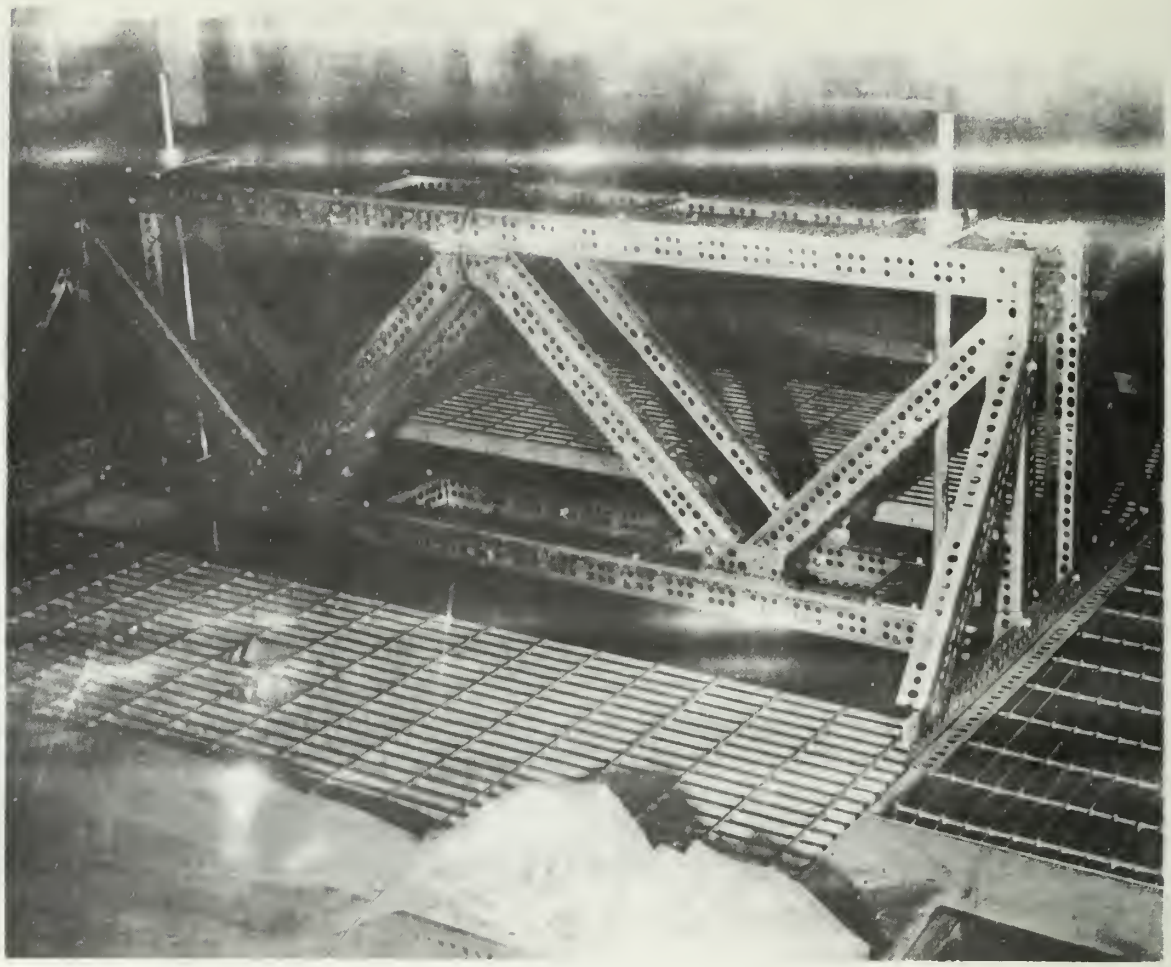

For the experiments at 450 kHz, both transducers were 3 cm diameter units specially constructed at the Naval Postgraduate School. The active elements in each are barium titanate units vibrating in a thickness mode. The transducers were mounted side by side. As shown in Table 4.1, (at a distance of 72 cm), the three db down points on the surface were 10 cm apart making a beam angle of 4.0 degrees. Areas calculated from this width and modified for the effects of spreading losses at grazing incidence were used in the calculation of the backscattering factor.

Transducer Support and Positioning Gear. The transducers were held in specially constructed clamps and secured to a horizontal bar which could be accurately (1 degree) positioned to provide any angle of incidence for the acoustic beam. The EDO transducer and clamp on the bar is shown in Fig. 4.10. The horizontal bar is supported by vertical elements which are positioned in height by ring clamps. By this means it was possible to maintain the transducer at a constant distance from the scattering area. The whole was supported by a slotted angle steel bridge which could be accurately positioned and leveled at any position over the tank. This support bridge is shown in Fig. 4.11.

Calibration. The need for absolute calibration of the equipment is avoided by the nature of the backscattering factor defined in terms of the ratio of scattered to incident intensity. Only the amplifiers in the system with gains to be varied during the experiment needed to be calibrated. Particular care was taken to ensure that no element in the system was driven into saturation

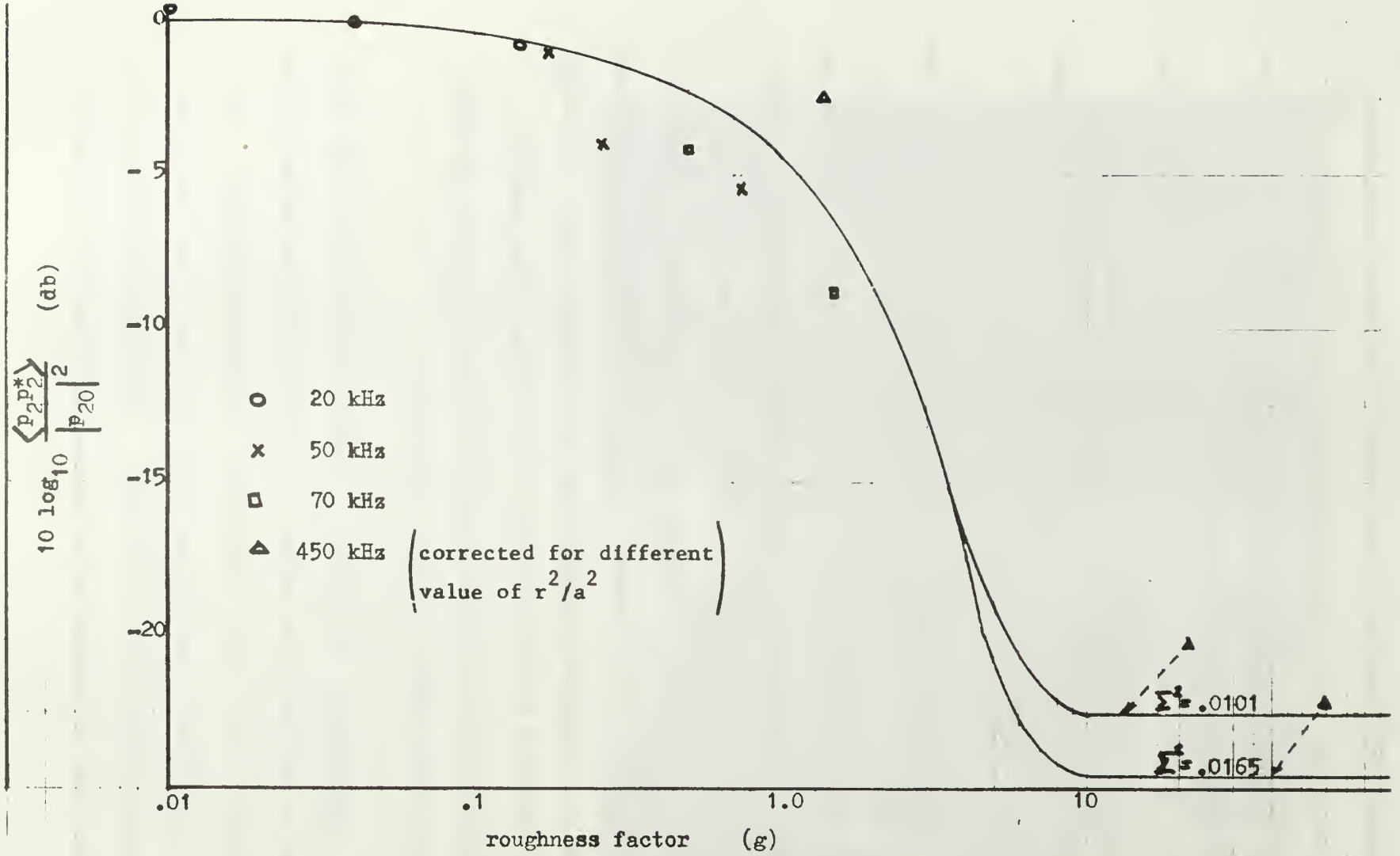

Fig. 4.12 Mean Square Pressure vs. Roughness Factor (Normal Incidence)

either during the experiment or during the calibration, since such an occurrence would cause a change in effective gain even if the distortion went unnoticed.

Comparison With Theory

Normal Incidence. Equations 9 and 10 in Section 2 show a relation between the backscattering factor and the system parameters. The roughness parameter (g), is particularly important in these equations. The first experiment shows a comparison of this theory which predicts the backscattering factor at normal incidence, a specular reflection phenomenon, as a function of the roughness parameter. The statistical theory was tested for this case by Medwin (15) in 1966. This particular experiment compliments that work in that here are statistics determined from thousands of echo pulses, and the surface height statistics were measured directly. A range of roughness parameter from very smooth (g=0.01) to rough (g=60) was explored by altering the surface roughness with different combinations of blowers and by changing the frequency. The theoretical curve and data points are shown in Fig. 4.12. The data fit the smooth surface theoretical curve closely. The principal source of error is the sensitivity of the measurement of the sound reflected from the smooth surface to the positioning of the transducer. The actual scattering levels were 60 db above the noise. The 450 kHz data at the large roughness end of the scale are too large. This is considered to be caused by the fact that the RMS slope calculated from the optical glitter experiment was used to calculate the theoretical curve. Due to the large acoustic wavelengths, there are portions of the waves

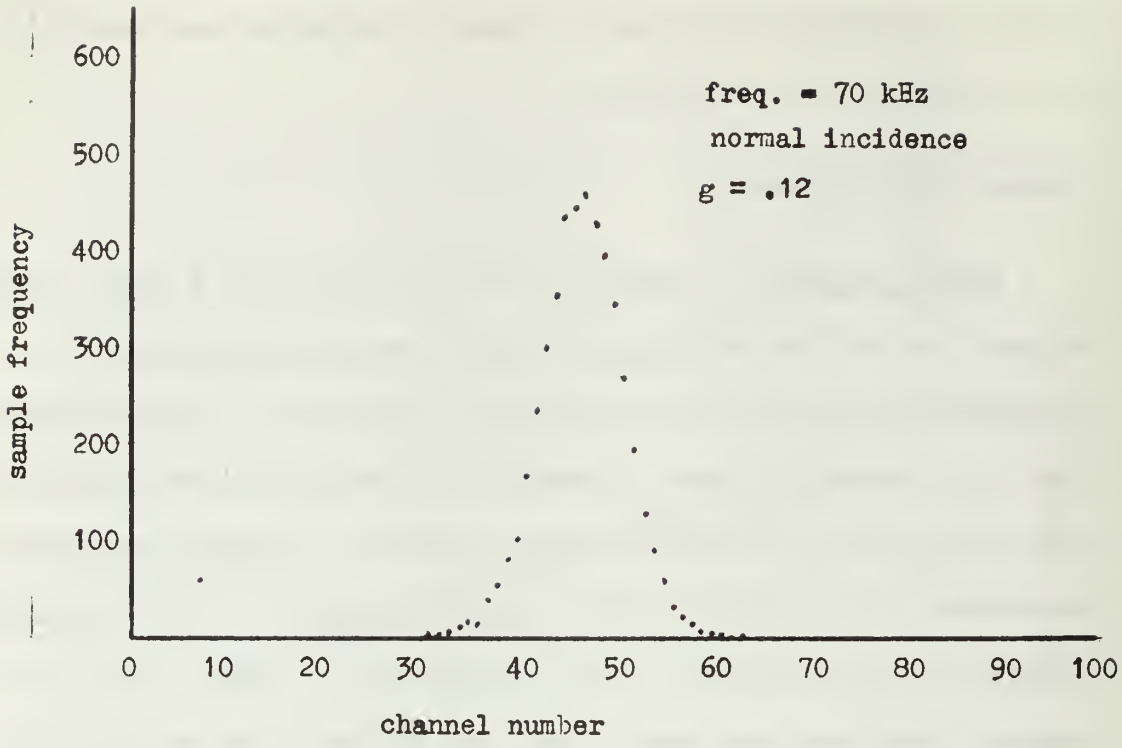

Fig. 4.13 Pulse Height Distribution Station 1 1 blower

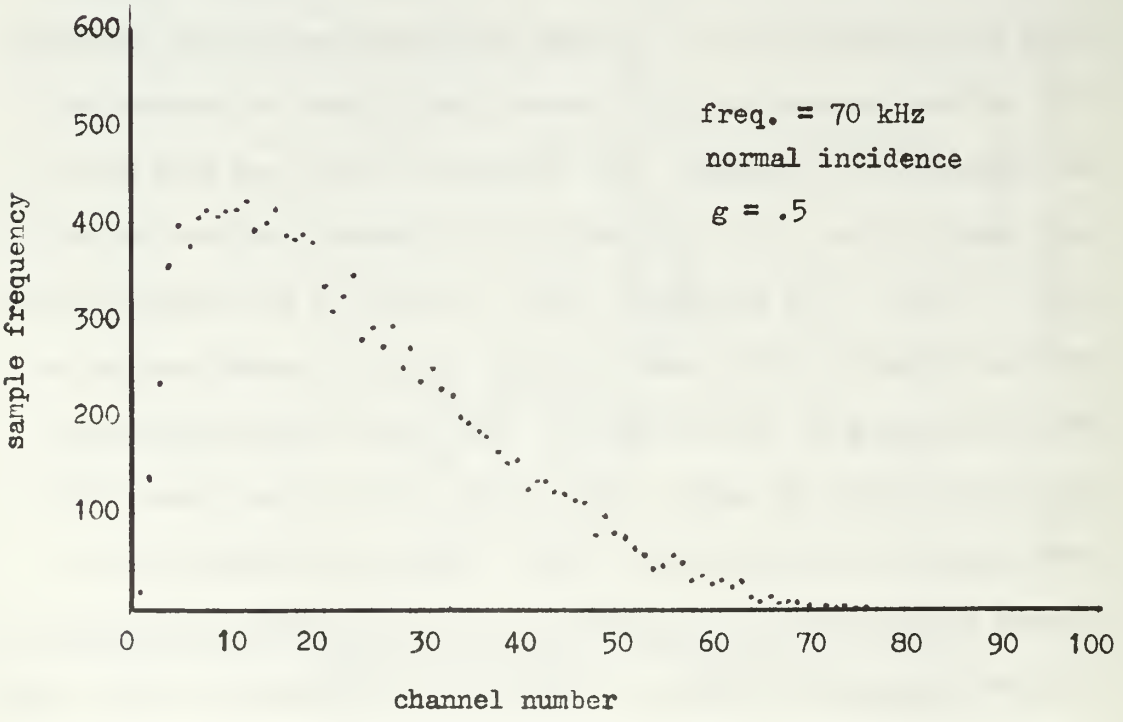

Fig. 4.14 Pulse Height Distribution Station 1 2 blowers

presumably due to capillaries which scatter the light but which would not affect the sound. The RMS slope used is too large for the acoustic application.

Backscattered Pulse Distribution. This experiment affords a real insight into the nature of the distributions of the scattered echoes for specular reflection and for backscatter. Figs. 4.13, 4.14, and 4.15 show the echo distributions for normal incidence specular scatter at 70 kHz for the rough surfaces with one, two, and three blowers in operation. The transition from a normal distribution to a Rayleigh distribution as the roughness parameter increases is readily apparent. The positions of the 70 kHz data on the curve of Fig. 4.12 show that the three different wind conditions give rise to roughness parameters occurring over the region of transition from smooth scattering to rough scattering.

Fig. 4.16 is drawn for backscattering data for 20^{o} incidence at 70 kHz with one blower operating. This is a smooth surface condition at 70 kHz, as the specular scatter distribution in Fig. 4.13 shows, yet the backscattered distribution is Rayleigh, indicating that the backscattered radiation is incoherent.

Backscattered Pulse Magnitude. Figs. 4.17 to 4.21 show the data for backscattering at various angles of incidence under various conditions of surface roughness with incident sound projected in the upwind direction. On these curves, the predictions of the statistical scattering theory are shown. In Figs. 4.17 and 4.18 the prediction of the Wetzel resonance theory is also shown. This curve is not shown in the other figures since the surface wave

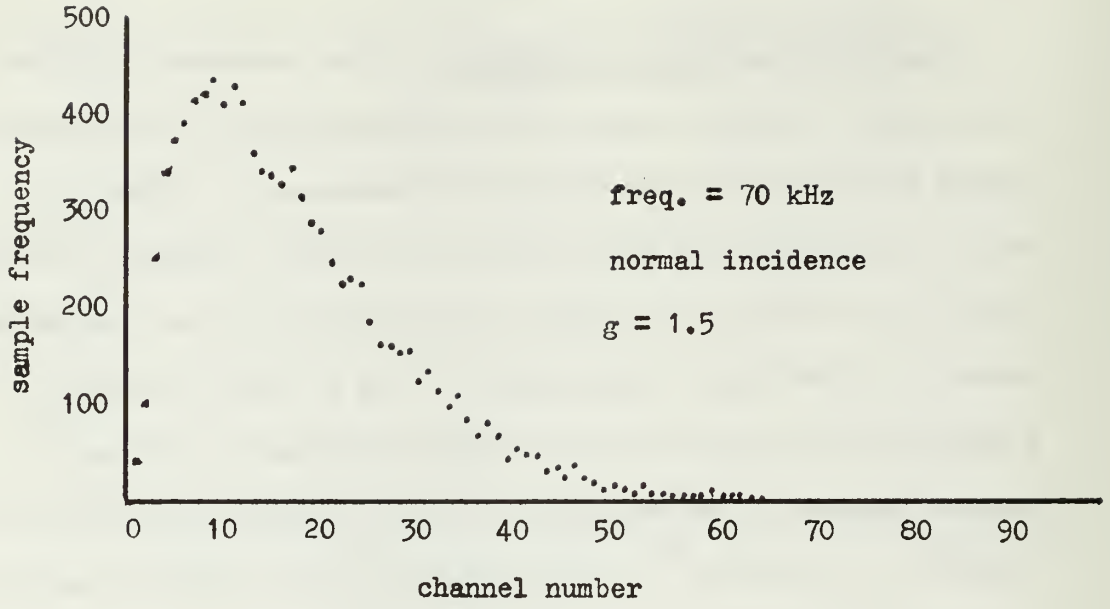

Fig. 4.15 Pulse Height Distribution Station 1 3 blowers

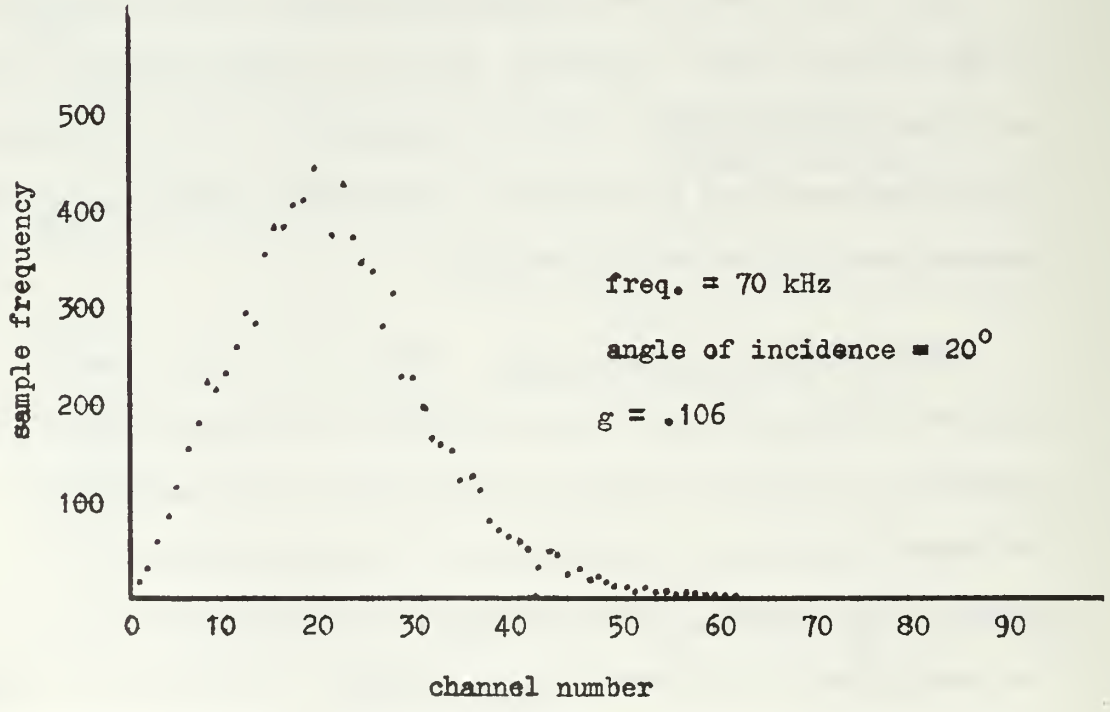

Fig. 4.16 Pulse Height Distribution Station 1 1 blower

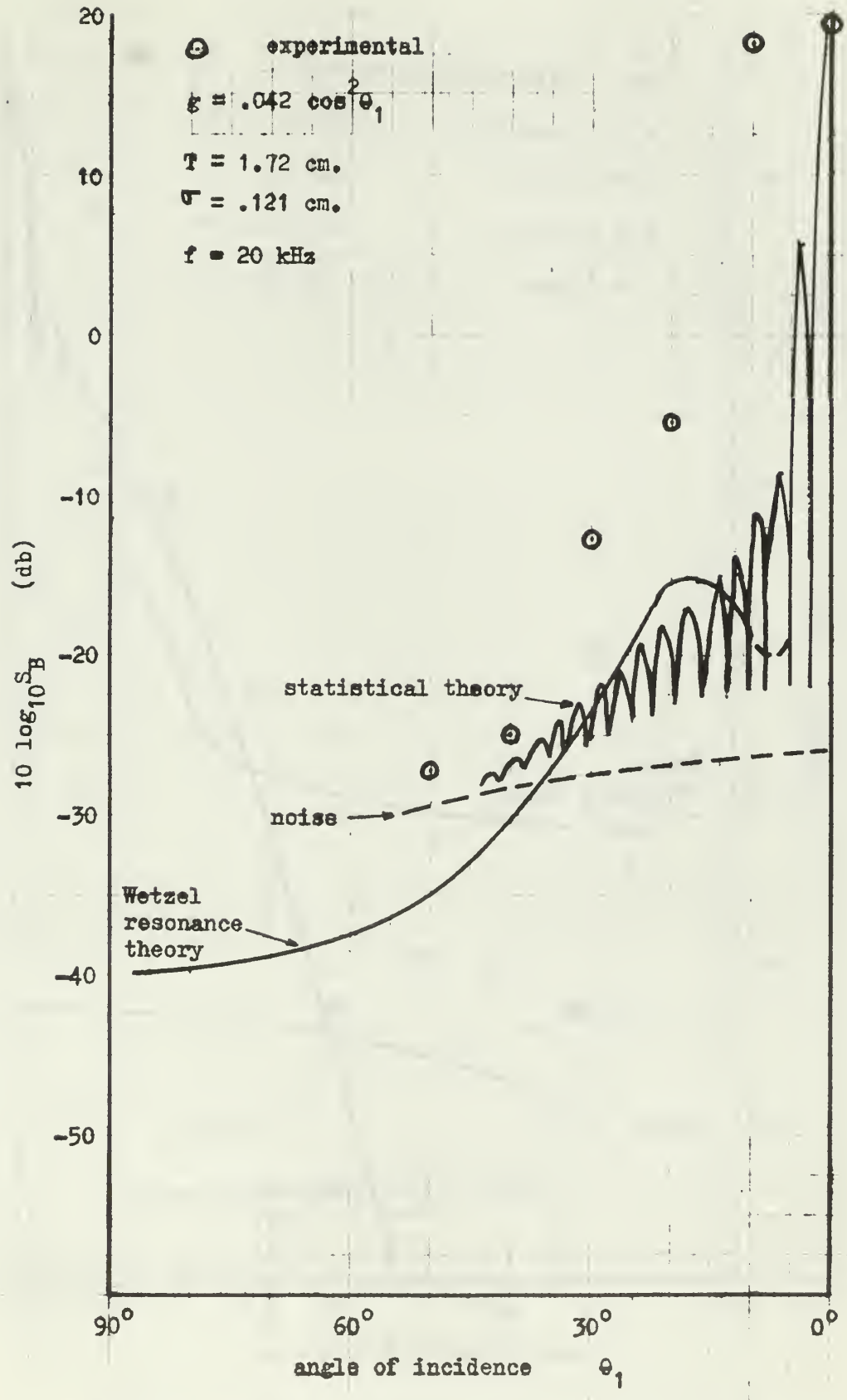

Fig. 4.17 Backscattering Factor - Relatively Smooth Surface

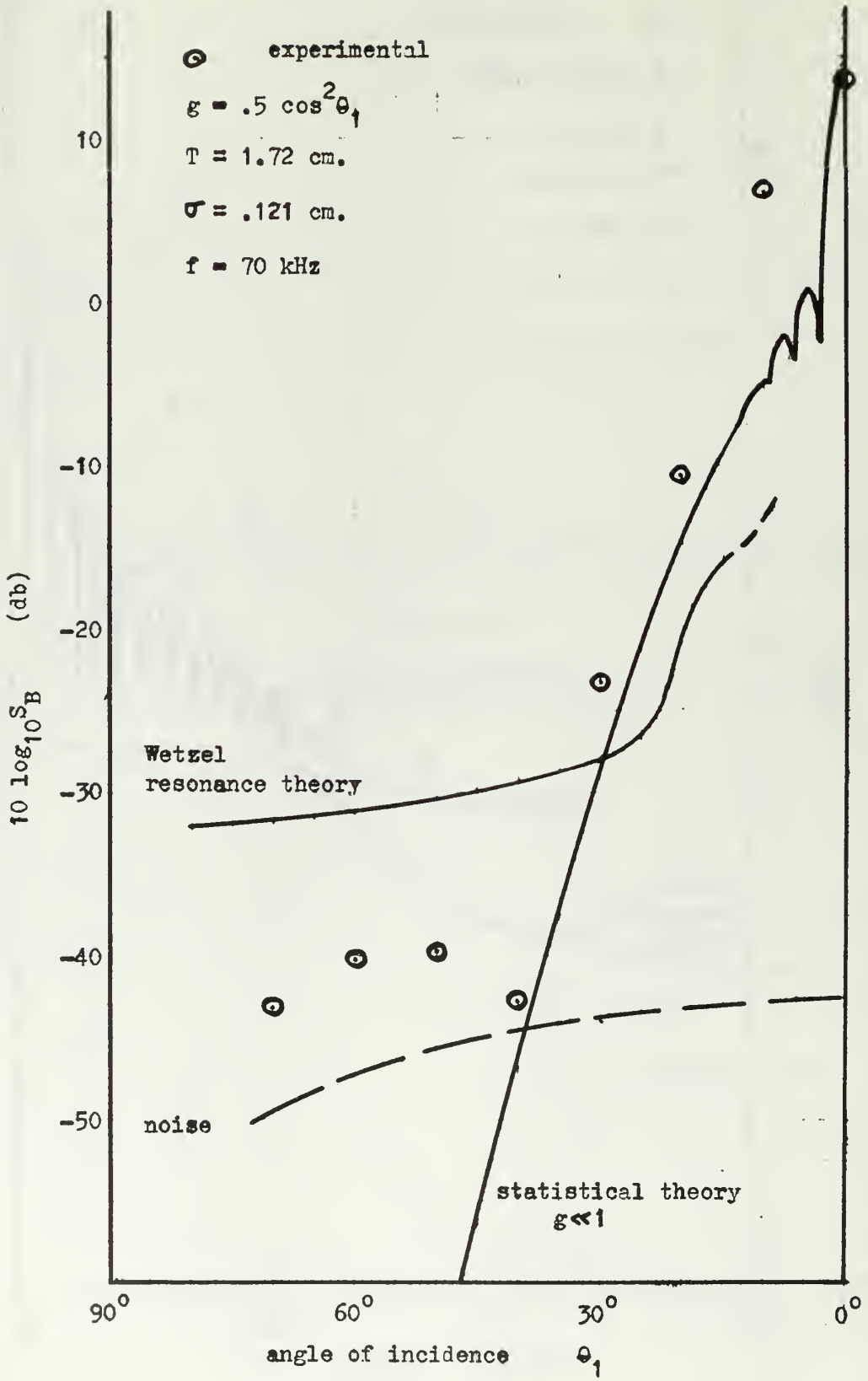

Fig. 4.18 Backscattering Factor - Transition Surface

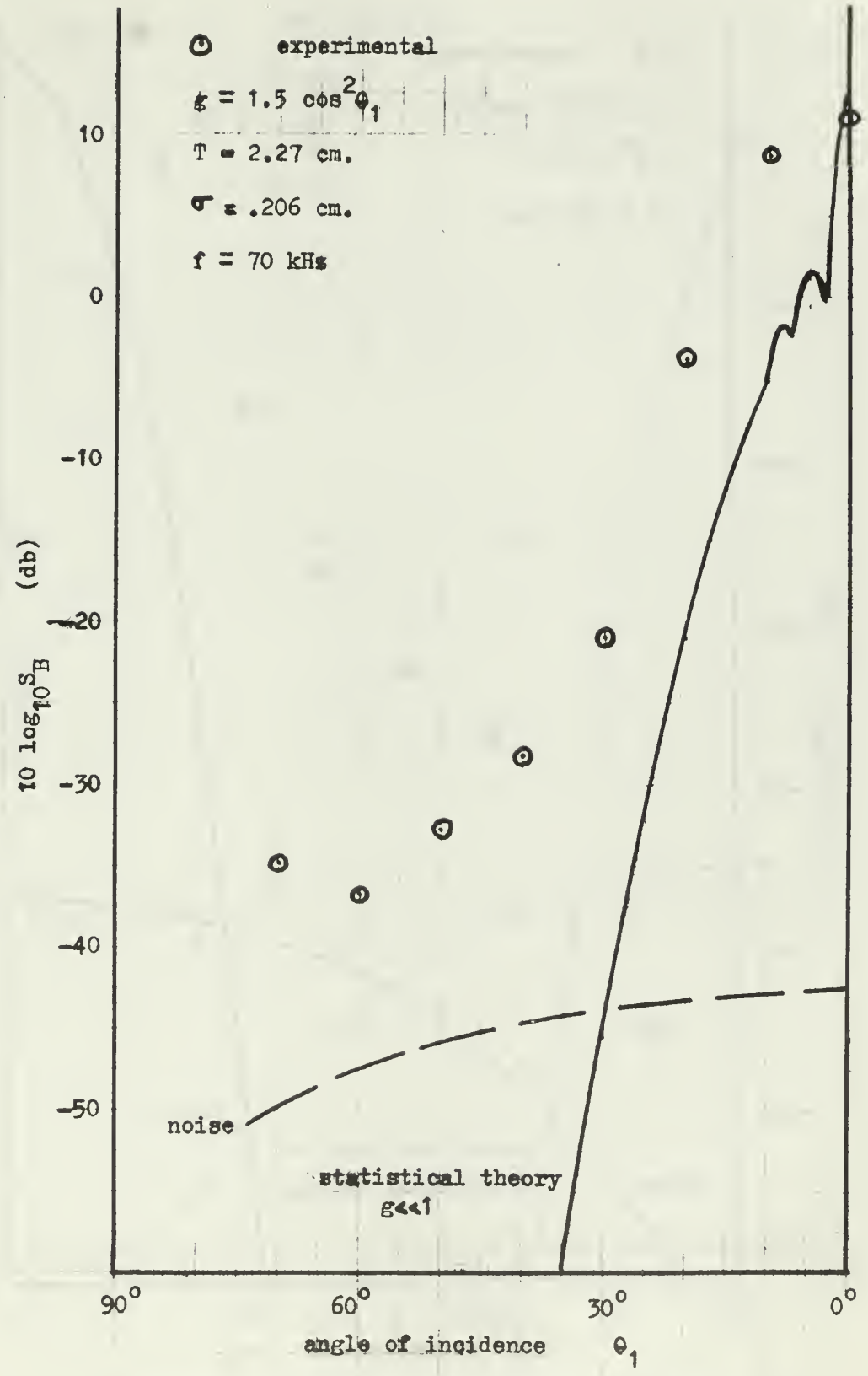

Fig. 4.19 Backscattering Factor - Transition Surface

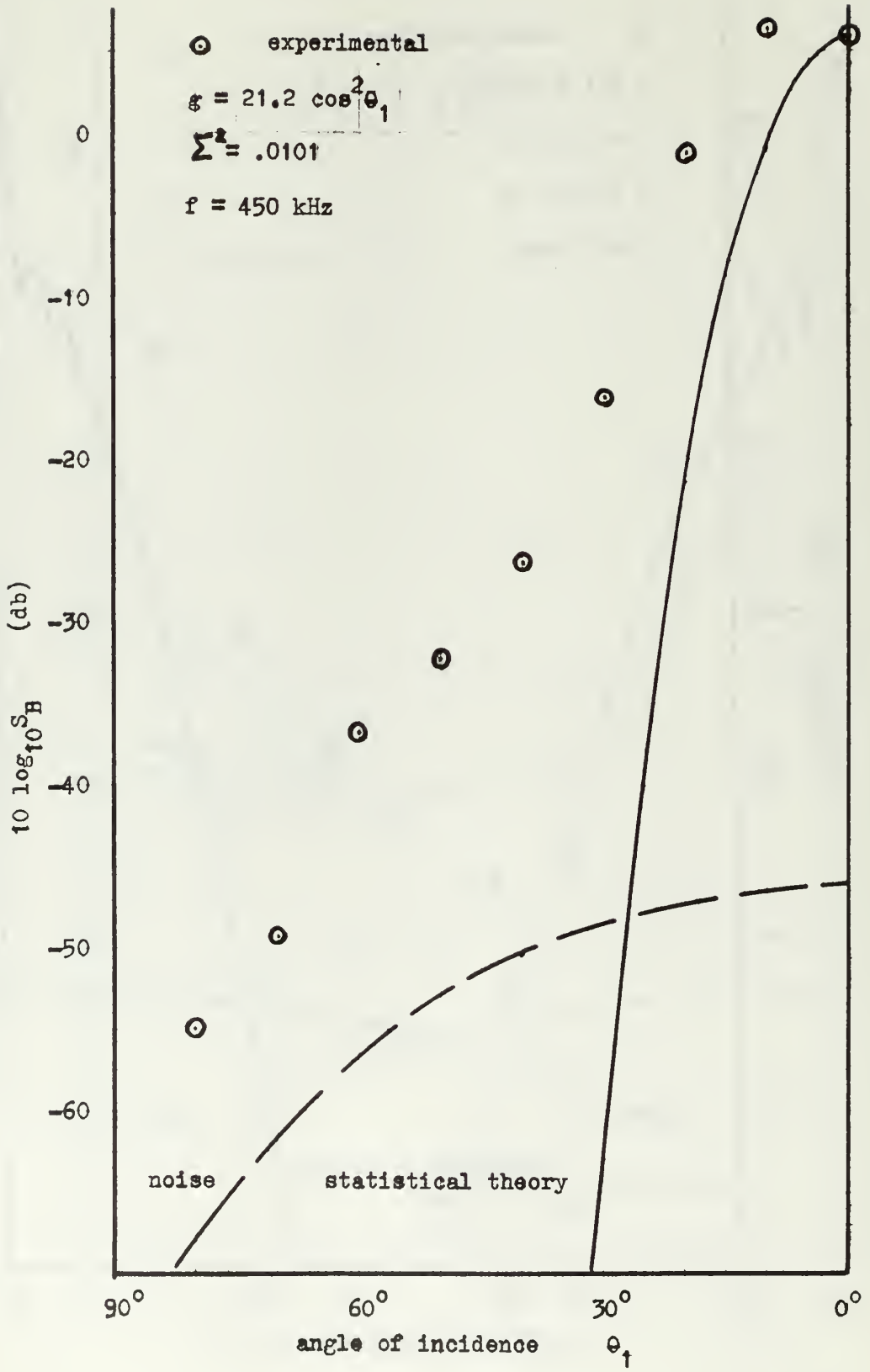

Fig. 4.20 Backscattering Factor - Rough Surface

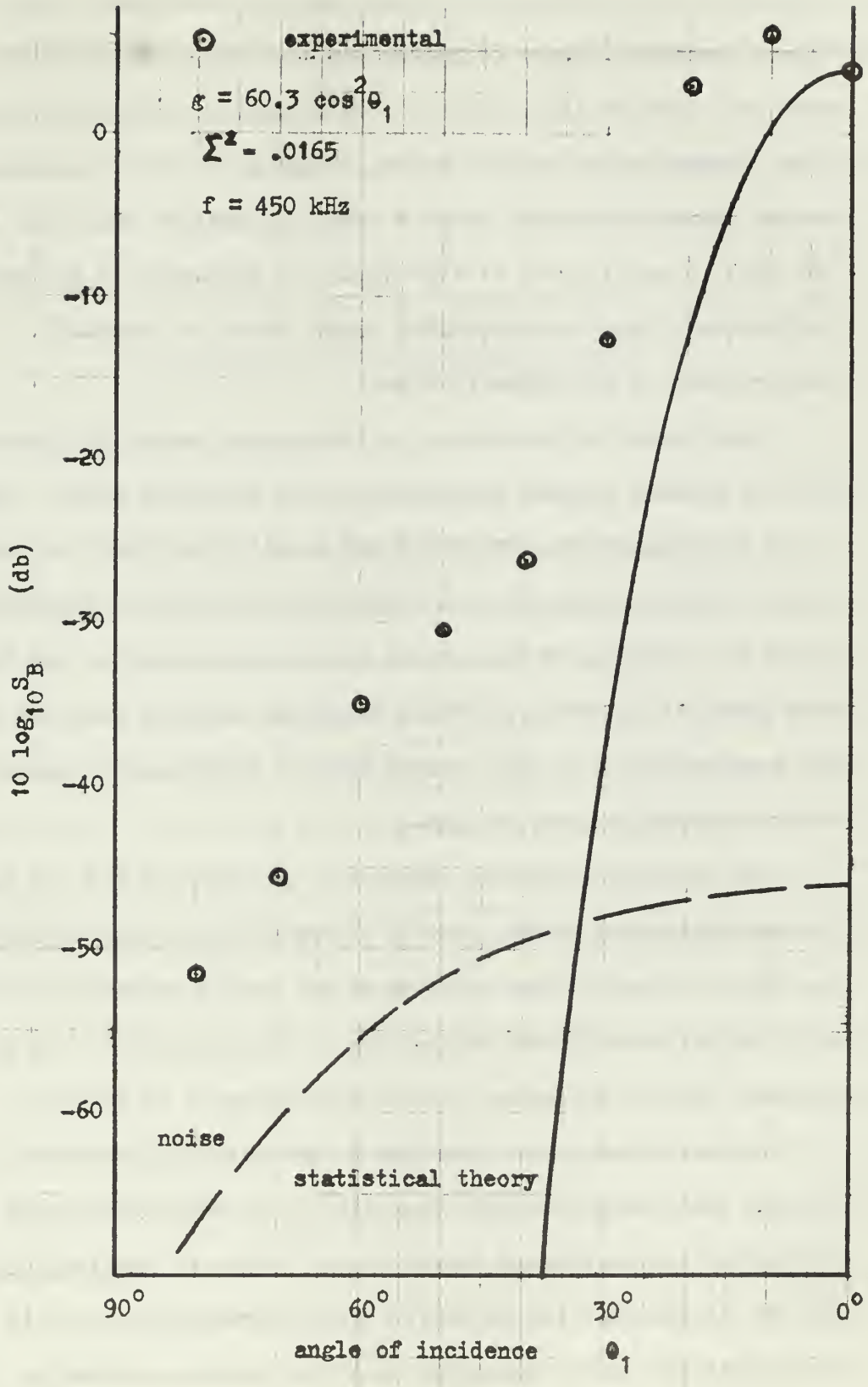

Fig. 4.21 Backscattering Factor - Rough Surface

spectrum was not measured for those surface conditions. The Wetzel resonance theory is derived only for relatively smooth surfaces. The noise curves are also given to indicate how one might inadvertantly measure noise, thinking it to be scattered sound, unless particular care is taken to identify the noise level. The drop in noise level at high angles of incidence is due to the definition of the backscattering factor which is inversely proportional to the ensonified area.

The "tails" of the curves at low grazing angles are observed, for the rougher surface conditions, 15 db above the noise. This is in an environment free of marine and animal life likely to cause volume scattering and free of bubbles by dint of the care taken to allow the tanks to settle without agitation or filling, and the care taken in filtering to avoid discharge directly into the tank. The wind agitation of the surface was not sufficiently violent to introduce bubbles into the tank.

The statistical theory (Section 2, equations 9 and 10) predicts the backscattering factor closely at angles near normal incidence but fails to predict the leveling of the curves at grazing incidence. Although the statistical curves have an inflexion point, it is not anywhere near to the actual data above angles of 30 degrees.

The resonance theory (Section 2, equation 13) using the surface wave energy spectrum from Fig. 3.33, has less success in predicting the scattering levels in its region of application than did the statistical theory in its area of application, yet it is clear that the theory resulting from the resonance mechanism of backscattering at grazing incidence has the right shape. The theory fails the actual measured levels by as much as 10 db, in one case

coming too low and in the other case coming too high. The scattering predicted by the resonance theory for the predominant frequencies in the surface wave spectrum fails to rise to the level of the actual scattering in Figs. 4.17 and 4.18 at near normal incidence, indicating that the resonance mechanism is unsatisfactory to explain the back-scattering in this region.

Backscattered Continuous Wave Spectra

The resonance theory of backscattering from a moving surface requires the existence of doppler shifts in the scattered radiation and further requires that the doppler shifted radiation be due principally to certain frequencies in the surface spectrum that would give rise to resonances in accordance with Bragg's law. The equations for resonance backscattering as developed by Wetzel [9], and modified to be consistent with the definition of backscattering factor used herein, were used in the last sub-section to predict the backscattering near grazing incidence in two of the scattering experiments where the data were felt to be sufficiently above the noise level. There it met with some success in its predictions. However, it was considered that some of the assumptions of the resonance theory should be studied experimentally. Some of the results obtained, though largely qualitative, yield new insight into scattering analysis and raise some questions worthy of consideration in future research in this area. Primarily, then, this experiment is directed to three features of scattering: to find if the doppler shifts can be measured; to find a way to relate the spectrum of the continuous wave scattering to the surface wave spectrum; to find if there are specific resonances that can be identified.

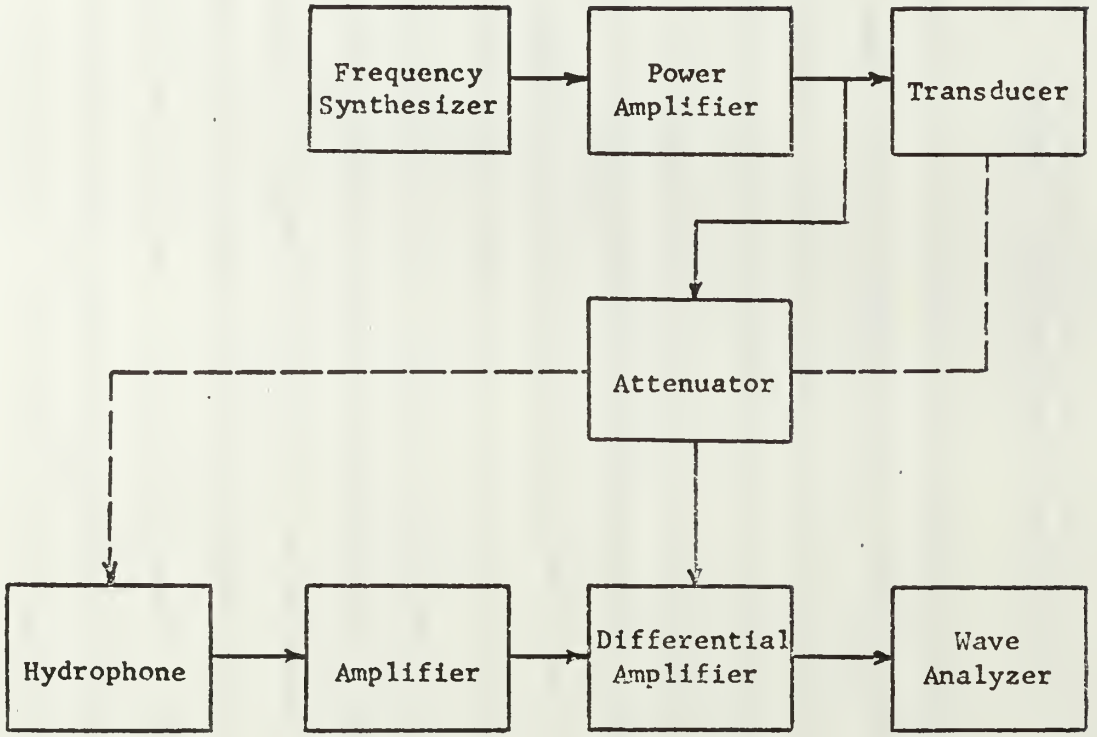

Fig. 4.22 Continuous Wave Spectra Measurement System

Frequency Synthesizer	GR 1161A Coherent Decade Frequency Synthesizer
Power Amplifier	HP 467A Power Amplifier
Transducer	EDO Model 327 Transducer
Attenuator	HP 350A Attenuator Set
Hydrophone	Atlantic Research LC-32
Amplifier	HP 463A Precision Amplifier
Differential Amplifier	Tektronix 1A7 in Tek 545 Oscilloscope
Wave Analyzer	GR 1900A Wave Analyzer

Fig. 4.22(a) Equipment List for
Continuous Wave Spectra Measurement System

Experimental

The system used in this experiment is described in the block diagram of Fig. 4.22. The frequency synthesizer was stable to better than one part in 10^{10}. The wave analyzer local oscillator was stable to one part in 10^{6} for short terms of the order of a few hours. The CW signal at 48.3 kHz was amplified and supplied to the EDO transducer previously described. If there is a doppler shift to be detected due to the moving wave system, it should be clearly identified by its dependence on the direction of radiation from the transducer, whether downwind or upwind. The scattering experiment was conducted with the transducer directed for normal incidence and subsequently at 60 degrees upwind and downwind to scatter from station 3 as shown in Fig. 3.1. The hydrophone was placed approximately 30 cm from the face of the transducer in clamps to keep the distance to the transducer constant. Since the major component of the received spectrum would be due to the acoustic radiation incident by a direct path on the hydrophone, and since this signal would have a constant phase and amplitude relationship to the signal supplied to the projector, it could be removed by subtracting a suitably attenuated signal derived from the power amplifier, whenever the path difference from hydrophone to projector was the correct multiple of half-wave lengths to provide the necessary phase relationship. This restricted the frequencies that could be used to a set of discrete frequencies, but there was sufficient freedom to choose suitable frequencies despite this limitation. This incident signal was reduced to the point where the signal passing the "skirts" of the bandpass filter was much less than any shifted frequency signal in

the backscattered spectrum. Since the object of the experiment was to look for the doppler shifted frequencies, the loss of information concerning any unshifted component of the spectrum was of no great consequence. In practice the received signal was initially observed under quiet conditions, that is with a smooth surface. The difference spectrum under such conditions is shown in Fig. 4.23. The specified bandpass characteristic of the wave analyzer is superimposed to show that the signal is a single frequency so far as can be determined by the analyzer. A second component of the signal observed under quiet conditions was the reflected signal from the surface. Unless the surface height is kept constant during the experiment, the phase relationship of this signal to the supplied signal will change and the unshifted frequency component measured by the analyzer will vary in amplitude.

Since the filtered component of the scattered spectrum at any frequency is not constant in time but varies widely, the measured spectrum is necessarily the result of some sort of averaging process. A long time constant filter of the wave analyzer damps the meter response. However, the output in this experiment still varied one or two db, and the final reading was the result of an averaging by eye. In this way, all of the temporal information in the spectrum is ignored, yet the process is identical to that which is carried out when the surface wave spectrum is analyzed. Hence it is not expected that this averaging will invalidate conclusions made about relations between the backscattered spectrum and the surface wave spectrum.

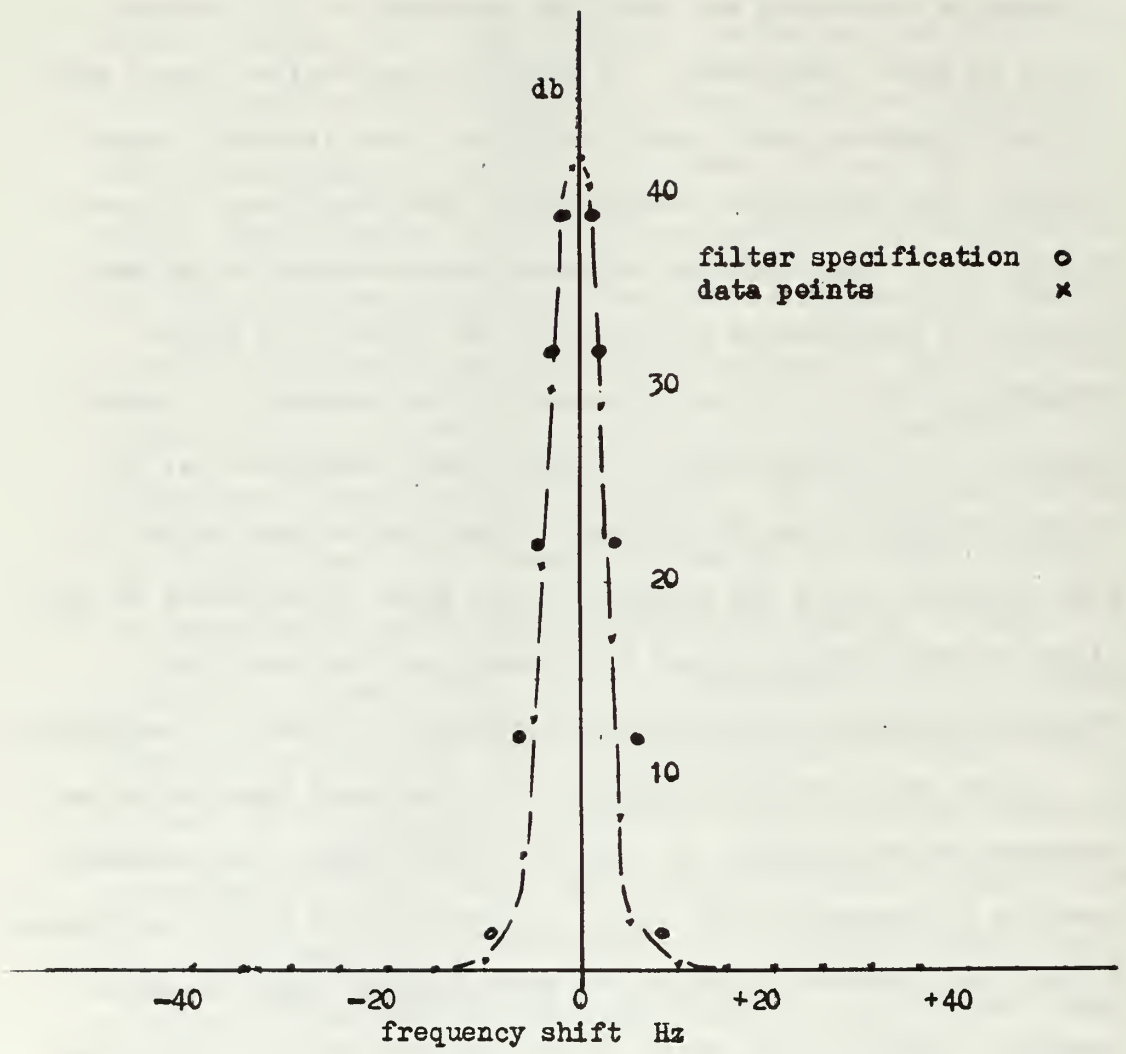

Fig. 4.23 Difference Spectrum - Smooth Surface

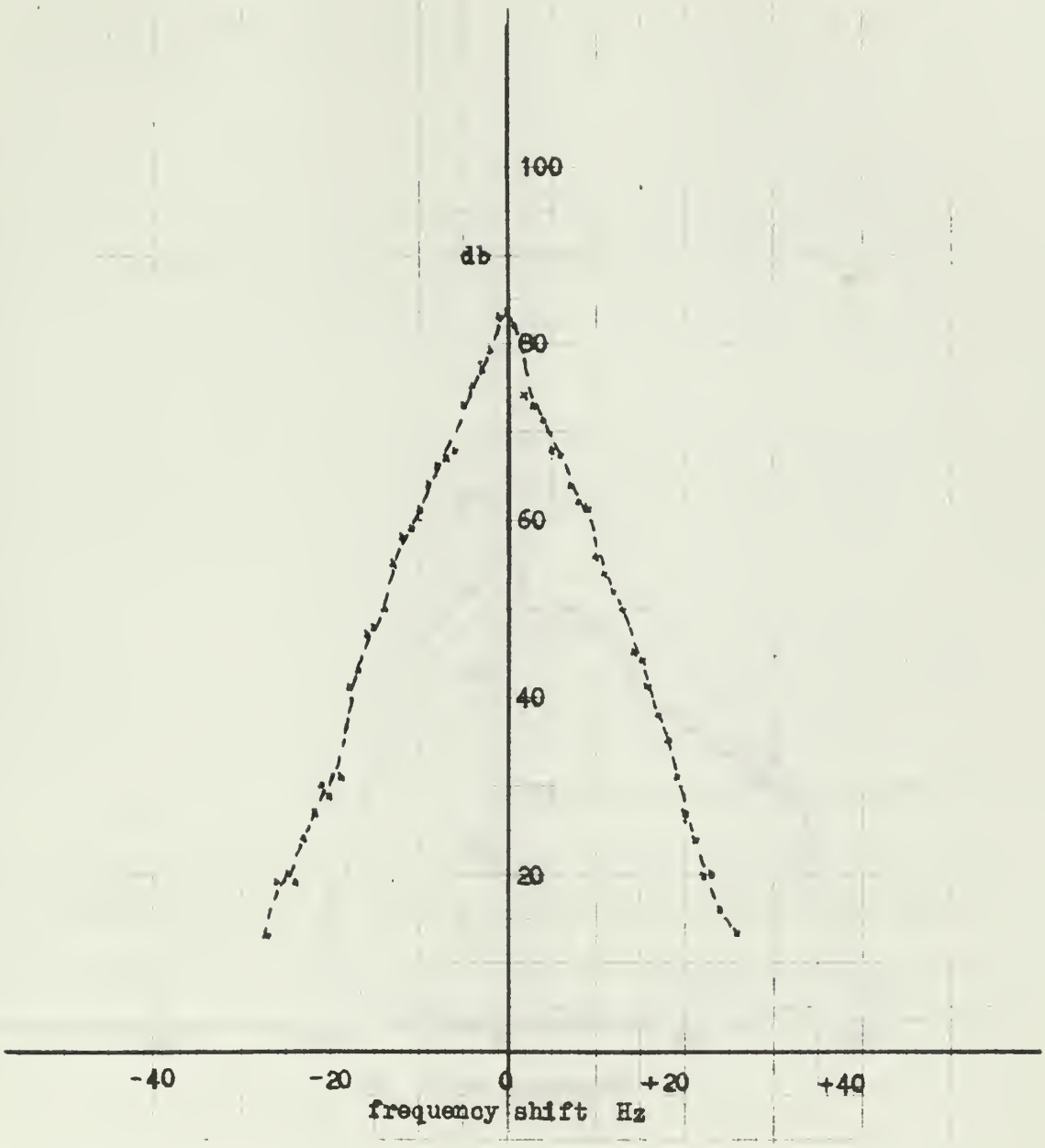

Fig. 4.24 Difference Spectrum - Rough Surface - Normal Incidence

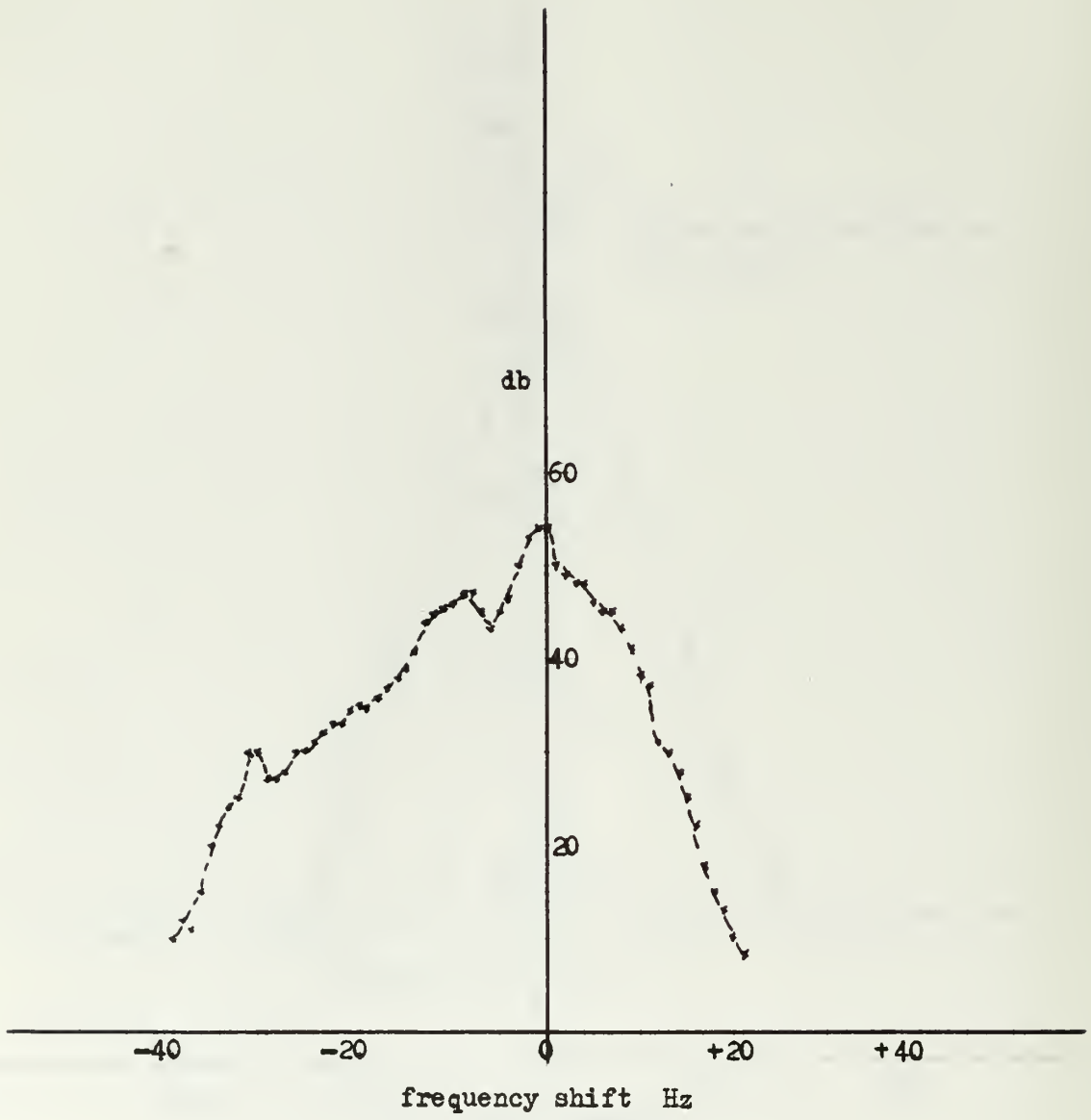

Fig. 4.25 Difference Spectrum - Rough Surface
60° Incidence - Looking Downwind

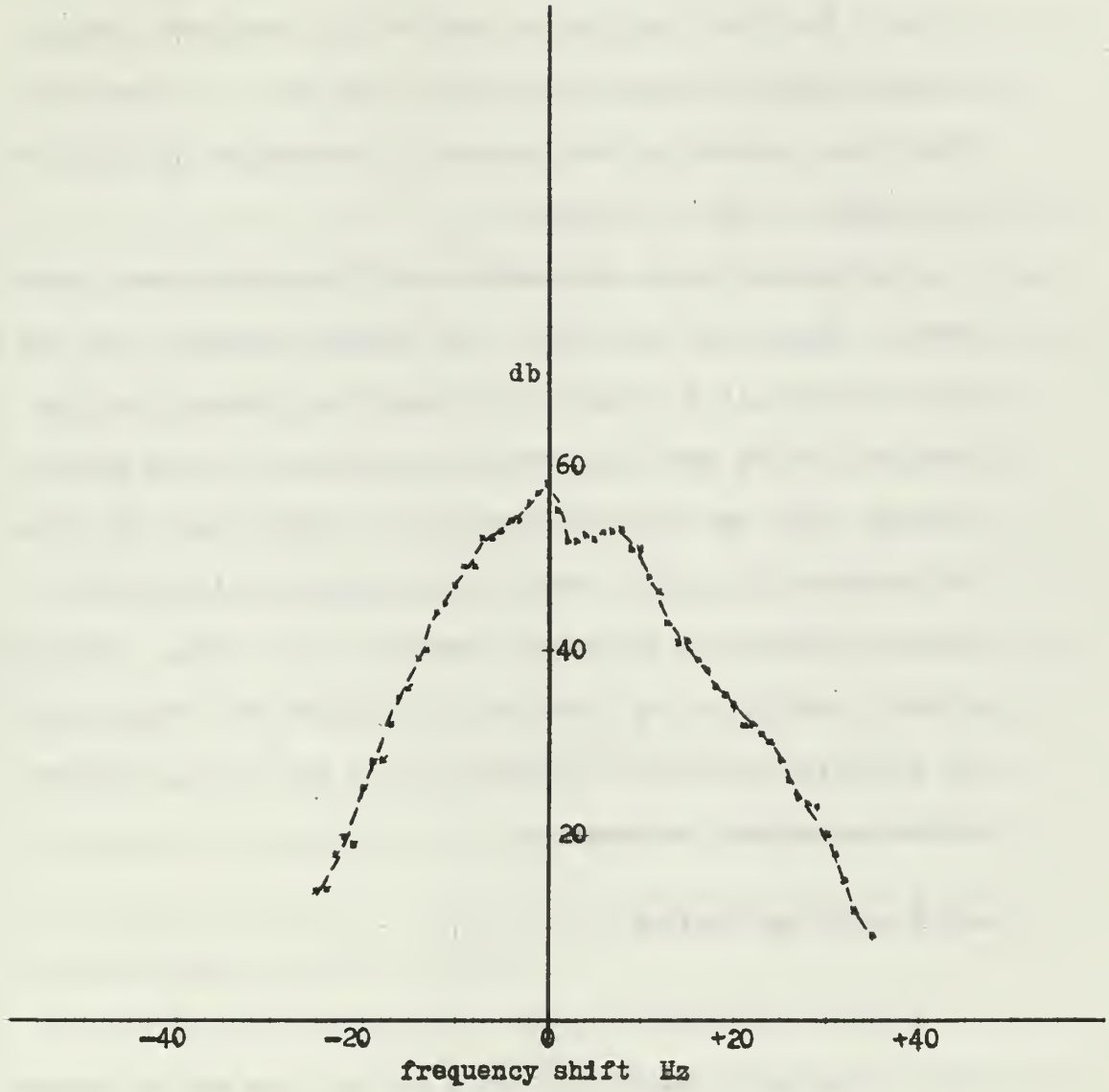

Fig. 4.26 Difference Spectrum - Rough Surface
60° Incidence - Looking Upwind

Observations

The result of the spectrum analysis at normal incidence is shown in Fig. 4.24. This spectrum is considerably broadened from that observed under quiet conditions (Fig. 4.23) and it is generally symmetrical, indicating the presence of frequencies shifted from the incident acoustic frequency.

On the other hand, the spectra at 60^{o} incidence both upwind and downwind (Figs. 4.25 and 4.26), show decided asymmetry. In the downwind case there is a "bulge" in the negative frequency shifted direction; in the upwind direction, the bulge is in the opposite direction. The two curves are not mirror images since the downwind spectrum (Fig. 4.26) contains more energy in the shifted frequencies than does the upwind spectrum (Fig. 4.25). The slopes of these spectra, on the sides not affected by the "bulges", are very close to the slope of the spectrum of Fig. 4.24, which was obtained at normal incidence.

Analysis and Speculation

There is no theory to apply to this particular phenomenon other than general theory concerning surface wave motion, doppler shift and frequency domain analysis techniques. In the following analysis there are many steps based on conjecture which must be examined in greater detail in some future experiment.

Consider the broadening of the spectrum from the smooth to the rough conditions at normal incidence. A number of possible mechanisms come to mind. The surface is moving and it should be expected that there would be doppler shifts in the echoes from various parts of the

surface due to its up and down motion. Since the wave propagation is at right angles to the acoustic beam, no doppler shift from this motion can be expected. If we consider the received signal in the time domain, it is amplitude modulated and, with reference to the incoherent nature of the backscatter already considered, it is likely that the signal is also angle modulated. It appears plausible, then, that the broadening of the spectrum for normal incidence may be interpreted completely as a modulation phenomenon with simultaneous amplitude and angle modulation. The spectrum at normal incidence was observed to be symmetrical. Since it is possible to generate asymmetrical spectra by combined amplitude and angle modulation, but not by amplitude modulation alone, it appears that the angle modulation must be small. This would be reasonable if the wave height variation were small with respect to the acoustic wavelength, a relatively smooth surface, but bears examination for rough surfaces. The assumption of symmetry of the backscattered spectrum at normal incidence is important to the identification of the identification of the doppler shifted spectrum.

Consider the asymmetries which occur in Figs. 4.25 and 4.26. It is expected that any doppler shifts due to the moving wave system would not be simple since the motion itself is anything but simple. However, the wave motion in the rough surface is in one direction and the doppler shift must show the correct sign of shift if it is to be identified as such. With the wave motion away from the sound source, the doppler shift must be negative. In the downwind direction the bulge appears on the negative side hence it is an acceptable candidate for identification as doppler shift. For sound propagated

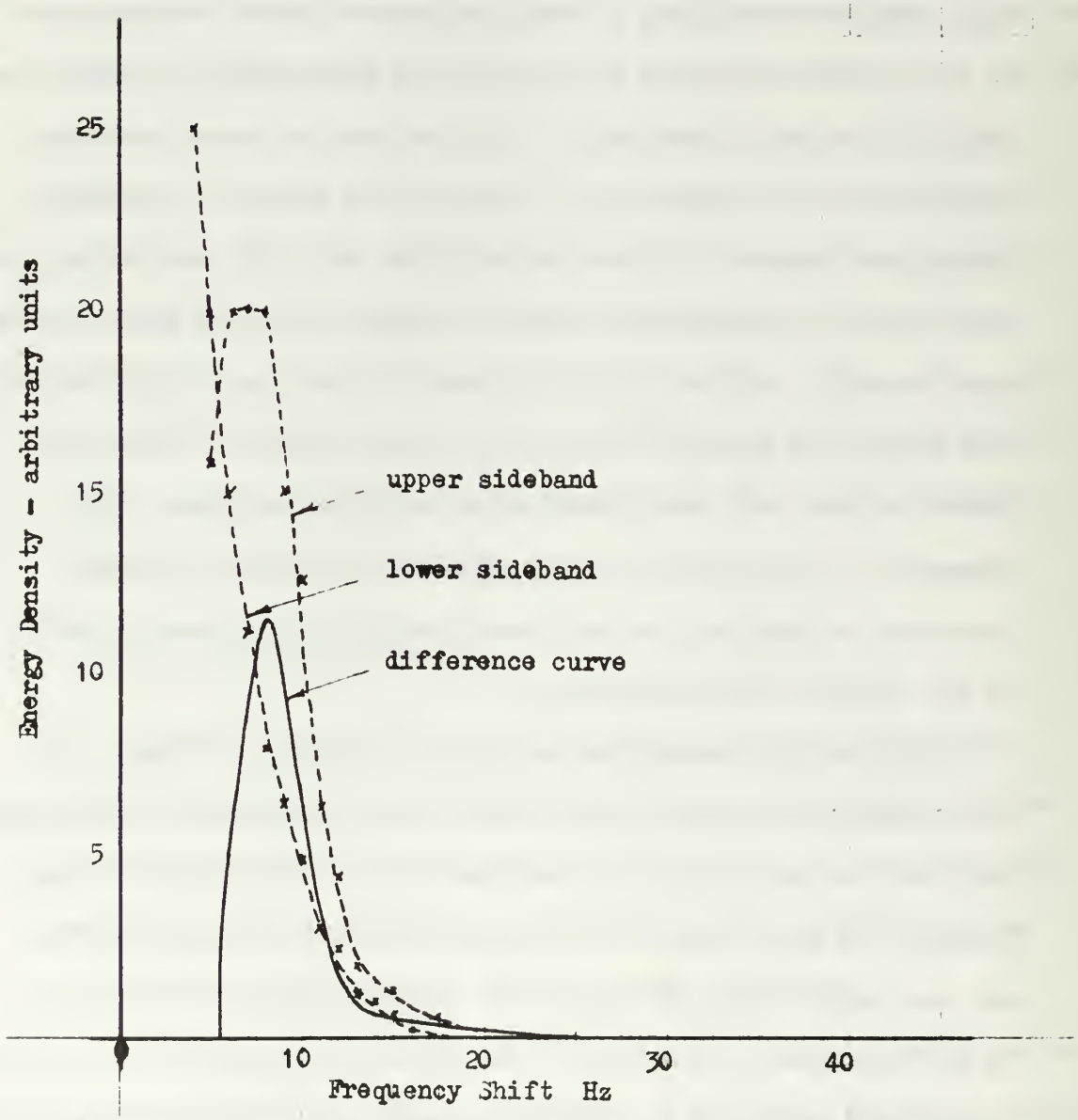

Fig. 4.27 Graphical Construction of Doppler Spectrum
Upwind Direction

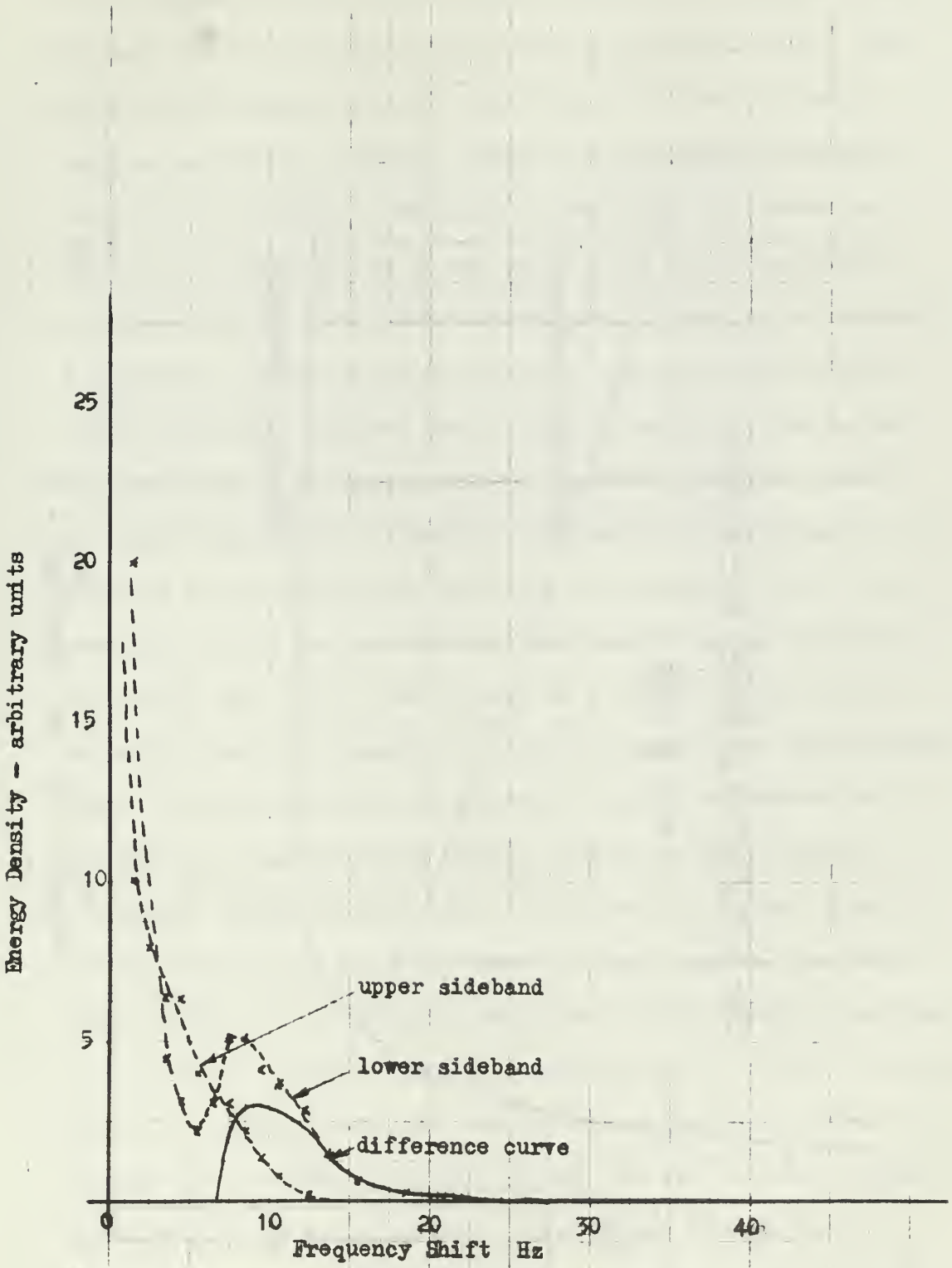

Fig. 4.28 Graphical Construction of Doppler Spectrum
Downwind Direction

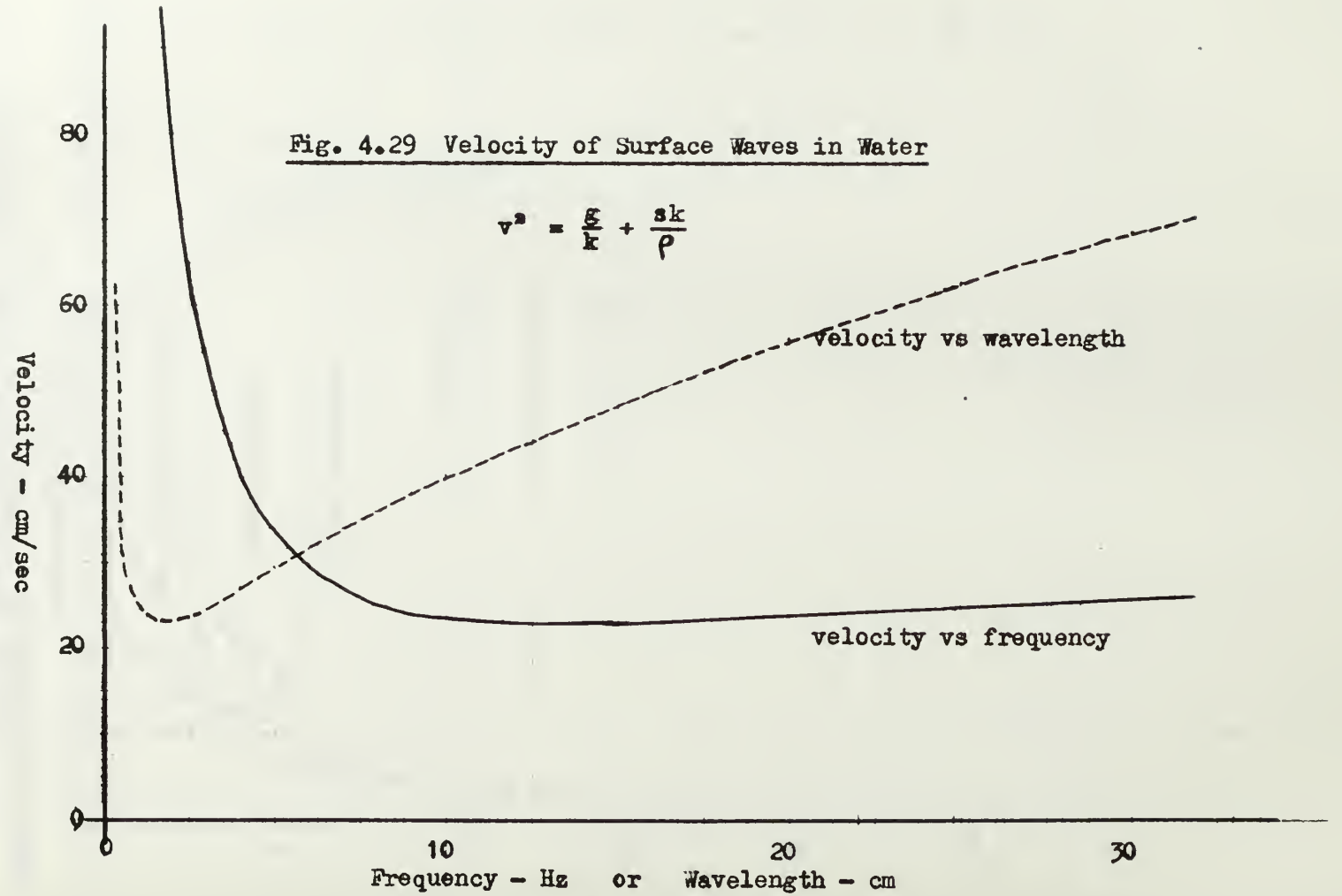

Fig. 4.29 Velocity of Surface Waves in Water

$$v^2 = \frac{g}{k} + \frac{sk}{\rho}$$

in the upwind direction, the bulge appears on the positive side; further justification for identification as doppler shift. The spectra at 60 degrees contain something of the shape of the spectrum at normal incidence. This is the broadened spectrum about the CW frequency. There is a symmetry that is preserved about the CW frequency up to the point where the bulge appears. It is postulated, then, that this spectrum is made up of two parts: a symmetrical spectrum due to modulation of the backscattering and an additional spectrum due to doppler shift from the moving wave structure. It appears to be a reasonable step to attempt to separate these two spectra. On the basis of the assumption of symmetry of the backscatter spectrum, the spectral values of the unbulged side of the spectrum are subtracted from the values on the bulged side. This must be done on a linear scale, not on a db scale since the assumption is that the spectra are superimposed. Figs. 4.27 and 4.28 show the graphical process of subtraction of one sideband from the other (dashed lines) and the resultant difference spectra (solid lines). They are ill-defined from 0 to 6-7 Hz because they are differences of large numbers, and thereafter appear to have a regular shape not unlike a typical surface wave spectrum. However, such an assumption here is totally invalid, since the frequency scale is that of the doppler shift. This is related to the surface spectrum through the wave velocity, which is not related in a simple manner to the surface frequencies.

In the surface wave velocity curve of Fig. 4.29, it is seen that there is a minimum velocity for waves in water due to the combined effects of gravity and surface tension on the wave formation. Since there is a minimum velocity, there must be a

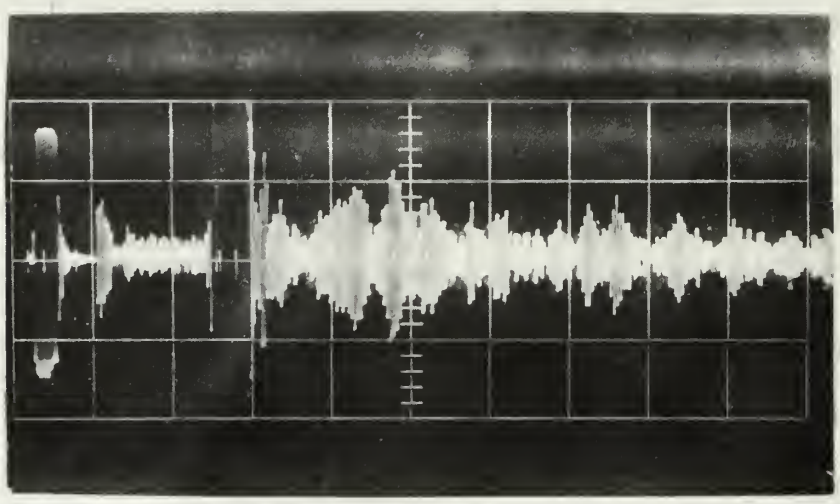

0.5 msec/cm

Fig. 4.3 Backscatter from 0.2 msec Pulse at 48 kHz

doppler shift frequency. This minimum frequency is readily calculated from the minimum velocity of surface waves which is 23.1 cm/sec. This corresponds to a surface wave frequency of approximately 12 Hz. From Fig. 3.33 it is seen that there is very little energy in the surface wave spectrum at this frequency, hence the doppler shifted spectrum can be expected to rise from a zero at or near the calculated minimum frequency. The doppler shift equation is

$$\Delta f = \frac{2v\sin\theta f}{c} \qquad (11)$$

For a frequency of 48.3 kHz and a minimum velocity of 23.1 cm/sec, the minimum doppler shift is 15.1 $\sin\theta$ where θ is the angle of incidence.

From the photograph of a typical backscatter at 60^{o} angle of incidence for a 0.2 msec pulse at 48 kHz, (Fig. 4.30), it is seen that there are a number of echoes received at times other than the time at which the scattered echo in the main beam is expected. The time base is 0.5 msec/cm. There is a very large echo starting at 1.22 ms due to the reflection of the side lobe facing the surface at normal incidence. This echo is very wide compared to the 0.2 msec pulse width indicating that there are two echoes here. The first at normal incidence would produce symmetrical frequency shifts as in Fig. 4.24. The other large pulse commences at about 1.3 msec. Another pulse is seen at 2.1 msec and the actual pulse from the center of the main lobe scattering area occurs at 2.4 to 2.5 msec. In the face of this type of scattered return, it is almost impossible to make sense of the continuous wave doppler shifted frequencies until further consideration is given to the nature of the doppler shift. Since the echo at 1.3 msec is very large, the contributions

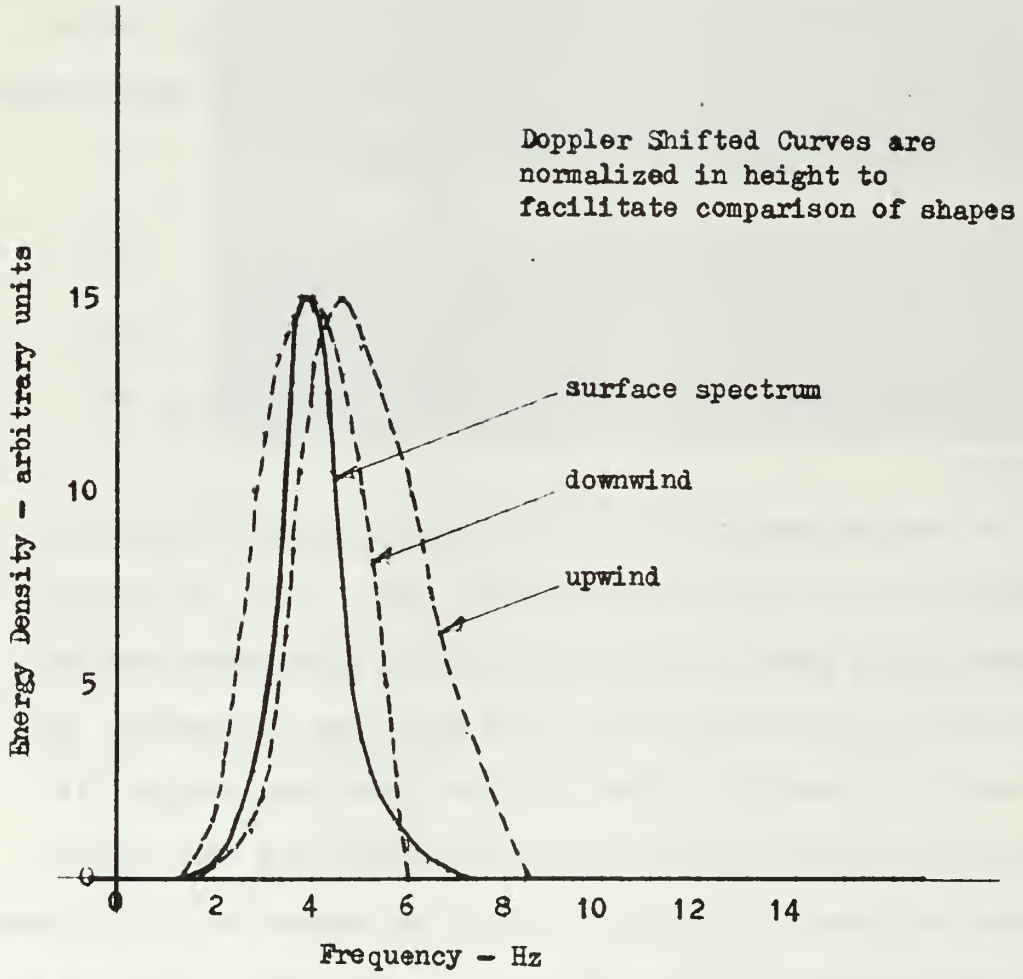

Fig. 4.31 Doppler Shifted Energy vs Surface Wave Frequency

of the pulses at 2.1 and 2.4 msec can be temporarily ignored. The effective angle of incidence can then be calculated from the times of the return of the normal incidence echo and the major scattered echo. Since $1.22 = 1.3 \cos\theta$, $\cos\theta = 0.94$ from which it is seen that the effective angle of incidence is about 20^{o}. Using this angle in the doppler shift equation above (1) predicts a minimum doppler shift of 5.2 Hz. This compares favorably with the minimum frequency of the curves derived in Figs. 4.27 and 4.28. It must be noted that it is very difficult to determine the effective angle of incidence.

The surface wave spectrum (Fig. 3.33) shows very little energy below 1.75 Hz. This indicates that there would be very little doppler shifted sound corresponding to velocities associated with waves of lower frequency than this. Since the wave velocity of gravity waves increases with decrease in frequency, this predicts an approximate maximum for the doppler shift spectrum. From Fig. 4.29, the velocity corresponding to a frequency of 1.75 Hz is 90 cm/sec. This predicts that there will be very little doppler shifted sound above 20 Hz. Once again this is in close agreement with the maximum observed in the curves constructed in Figs. 4.27 and 4.28.

With a certain amount of numerical justification for the derived curves, it is possible to speculate on how one might relate the doppler shift spectrum, which was constructed graphically, to the surface wave energy spectrum. When equation (11) is combined with the equation for the velocity of the surface waves as a function of frequency

$$v^2 = \frac{gv}{2\pi f} + \frac{2\pi s f}{\rho v} \qquad (14)$$

where g is the acceleration of gravity, v is the velocity of the surface wave, and s is the surface tension, a relation is found between the doppler shift frequency and the surface wave frequency. Due to the implicit nature of (14) this is most easily evaluated graphically from Fig. 4.29. By means of this change of abcissa, a curve of backscattered doppler shifted energy is plotted against the surface wave frequency. This curve is shown in Fig. 4.31 to facilitate comparison. The heights of the doppler shifted curves for upwind and downwind cases have been set equal to that of the surface wave spectrum which is also plotted. The curves fit the actual spectrum fairly closely. From the spread of the two derived curves it is seen that there is some experimental error. The principal source of error is the determination of the effective angle of incidence.

This conjecture seems to go no further, with profit, until the assumptions made are subjected to experimental and theoretical confirmation. It should be noted that it has been assumed that the energy in the doppler shifted spectrum is simply related to the energy in the surface spectrum. There is a resonance phenomenon which causes the doppler shifted spectrum to alter shape at some frequencies. Since there are very few wavelengths of surface waves in the scattering area, this resonance has been ignored.

Conclusion

There is a definite asymmetry produced in the backscattered spectrum at other than normal incidence, produced by the doppler shifts in the backscattered spectrum. An analysis technique has

been presented based on assumptions concerning the nature of the angle modulation in the backscattered signal and concerning the superposition of doppler shifted and symmetrical modulation spectra. An assumption was implicitly made that the surface wave produces doppler shifts from each of the spectral components moving at its phase velocity. This assumes a linear system for the surface waves. The resultant curves of doppler shifted energy vs surface wave frequency show some regularity, but there is a need for further experimental work and theoretical study before such a curve might be used to argue the existence of resonances to explain its deviation of shape from the surface wave spectrum.

5. Summary

The phenomenon of backscattering of acoustic radiation from a random rough surface has been studied from several points of view. A statistical theory and a resonance theory have been examined, and backscattering measurements made to determine whether the predicted backscattering factors are close to experimentally determined values. The assumptions in theory that the wave heights of a rough water surface are Gaussian distributed have been validated for this surface as they have been in the ocean itself. In this sense, then, the rough surface in the tank is a good model of the sea surface. The wave slopes have been shown to be distributed in a Gaussian distribution with the upwind-downwind slope being skewed in the downwind direction. The upwind-downwind to crosswind slope ratios are slightly higher than those experienced at sea when the rougher surfaces are used. This is a measure of the effect of creating the rough surface in a channel.

Over a very wide range of roughnesses ($0.01 < g < 60.0$), the specular scattering at normal incidence is closely predicted by a statistical theory due to Beckmann and Spizzichino (5). The statistical theory predicts near-normal backscatter reasonably well, but it fails completely to predict backscatter for incidence angles greater than 30°. The predictions concerning the distributions of scattered pulse heights have been substantiated by actual measurements: the near coherent scattering is Gaussian distributed and the incoherent is Rayleigh distributed.

At grazing incidence, the shape of the backscattering factor curve is fitted closely by the resonance theory prediction. There is

some discrepancy in the predicted levels which may be due to inaccuracies in measuring surface wave spectrum and in the measurement of backscattering factor from experimental data. A theory of backscattering would do well to consider both mechanisms for scattering as have been studied. Each mechanism has a dominant effect in its own region of application, and the actual backscattering phenomenon is closely predicted by a summation of backscattering factors from the two theories.

Further consideration of backscattered signals as a modulation phenomenon may yield a method of extracting the surface wave spectrum from the backscattered spectrum. An analytical method has been suggested, but it is based on several assumptions which have not yet been validated from theory or in experiment.

BIBLIOGRAPHY

1. Urick, R. J. and Hoover, R. M. Backscattering of Sound from the Sea S urface: Its Measurement, Causes and Application to the Prediction of Reverberation Levels. J. Acoust. Soc. Am. v. 28, No. 6, November,1956.

2. Garrison, G. R., Murphy, S. R. and Potter, D. S. Measurements of the Backscattering of Underwater Sound from the Sea Surface. J. Acoust. Soc. Am. v. 32, No. 1, January, 1960.

3. Chapman, R. P. and Harris, J. H. Surface Backscattering Strengths Measured with Explosive Sound Sources. J. Acoust. Soc. Am. v. 34, No. 10, October, 1962.

4. Eckart, C. The Scattering of Sound from the Sea Surface. J. Acoust. Soc. Am. v. 25, No. 3, May, 1953.

5. Beckmann, P. and Spizzichino, A. The Scattering of Electromagnetic Waves from Rough Surfaces. Macmillan Co., New York, 1963.

6. Schulkin, M. and Shaffer, R. Backscattering of Sound from the Sea Surface. J. Acoust. Soc. Am. v. 36, No. 9, September, 1964.

7. Clay, C. S. and Medwin, H. High-Frequency Acoustical Reverberation from a Rough-Sea Surface. J. Acoust. Soc. Am. v. 36, No. 11, November, 1964.

8. Barnhouse, P. D. C., Stoffel, M. J. and Zimdar, R. E. Instrumentation to Determine the presence and Acoustic Effect of Microbubbles Near the Sea Surface. M.S.E.E. Thesis, Naval Postgraduate School, June, 1964.

9. Wetzel, L. HF Sea Scatter and Ocean Wave Spectra. Research Report, Institute for Defense Analyses, April, 1966.

10. Marsh, H. W. Sound Reflection and Scattering from the Sea Surface. J. Acoust. Soc. Am. v. 35, No. 2, February, 1963.

11. Fante, R. L. Discussion of a Model for Rough Surface Scattering. IEEE Trans.on Antennas and Propagation. v. AP-13, No. 4, July, 1965.

12. Cox, C. and Munk, W. Measurement of the Roughness of the Sea Surface and Photograph's of the Sun's Glitter. J. Opt. Soc. Am. v. 44, No. 11, November, 1954.

13. Schooley, A. H. A Simple Optical Method for Measuring the Statistical Distribution of Water Surface Slopes. J. Opt. Soc. Am. v. 44, No. 1, January, 1954.

14. Farmer, H. G. and Ketchum, D. D. An Instrumentation System for Wave Measurements, Recording and Analysis. Proc. 7th Conference on Coastal Engineering, Berkeley, Calif., Council on Wave Research, Univ. of California, 1961.

15. Medwin. H. Specular Scattering of Underwater Sound from a Wind-Driven Surface. unpublished paper accepted for publication, J. Acoust. Soc. Am. v. 39, May, 1967.

16. Medwin, H. The Helmholtz Integral, Reflection, Rough Surface Scattering. unpublished class notes for use at Naval Postgraduate School, October, 1966.

17. Cohen, S. R. and Sheible, J. W. Measurement of Surface Spectra. Advanced Acoustics Laboratory PH 471, Naval Postgraduate School, May, 1967.

18. Phillips. O. M. The Equilibrium Range in the Spectrum of Wind-Generated Waves. J. Fluid Mech. v. IV, pp. 426-434, 1958.

19. Fung, A. K. and Moore, R. K. The Correlation Function in Kirchhoff's Method of Solution of Scattering of Waves from Statistically Rough Surfaces. J. Geoph. Res. v. 71, No. 12 June, 1966.

INITIAL DISTRIBUTION LIST

		No. Copies
1.	Defense Documentation Center Cameron Station Alexandria, Virginia 22314	20
2.	Library Naval Postgraduate School Monterey, California 93940	2
3.	Commander, Naval Ordnance Systems Command Department of the Navy Washington, D. C. 20360	1
4.	Professor H. Medwin Department of Physics Naval Postgraduate School Monterey, California 93940	6
5.	LCDR Ernest Charles Ball, RCN Director Marine Combat Systems Canadian Forces Headquarters Ottawa, Ontario, Canada	2
6.	LT John Algot Carlson, USN USS DEALEY, (DE 1006) c/o Fleet Post Office New York, New York 09501	2
7.	Commander, Anti-Submarine Warfare Systems Project Office Department of the Navy Washington, D. C. 20360	1
8.	Commander Naval Ships Systems Command Attention Code 1610 Department of the Navy Washington, D. C. 20305	1
9.	Mr. Marvin Lasky Director, Acoustic Programs, Code 468 Office of Naval Research Washington, D. C. 20360	1
10.	Chief Superintendent, Defense Research Board Attention Mr. C. W. Bright Naval Research Establishment Fleet Mail Office Hallifax, Nova Scotia, Canada	1
11.	Commander, Naval Ships Systems Command Attention PMS 88 Department of the Navy Washington, D. C. 20305	1

DOCUMENT CONTROL DATA - R&D

(Security classification of title, body of abstract and indexing annotation must be entered when the overall report is classified)

1. ORIGINATING ACTIVITY (Corporate author)
Naval Postgraduate School
Monterey, California 93940

2a. REPORT SECURITY CLASSIFICATION
Unclassified

2b. GROUP

3. REPORT TITLE
Acoustic Backscatter From a Random Rough Water Surface

4. DESCRIPTIVE NOTES (Type of report and inclusive dates)
Master's thesis

5. AUTHOR(S) (Last name, first name, initial)
Ball, Ernest C., LCDR, Royal Canadian Navy
Carlson, John A., LT, USN

6. REPORT DATE
June 1967

7a. TOTAL NO. OF PAGES
134

7b. NO. OF REFS
19

8a. CONTRACT OR GRANT NO.

b. PROJECT NO.
Underwater Physics Research

c. NSSC 17257

d.

9a. ORIGINATOR'S REPORT NUMBER(S)
N.A.

9b. OTHER REPORT NO(S) (Any other numbers that may be assigned this report)
N.A.

10. AVAILABILITY/LIMITATION NOTICES
[redacted]

11. SUPPLEMENTARY NOTES

12. SPONSORING MILITARY ACTIVITY
Naval Ships Systems Command

13. ABSTRACT
Acoustic backscattering from a random rough water surface has been studied experimentally to test the application of two scattering theories, a statistical description and a resonance approach. The rough surface was created by wind agitation over an anechoic tank. The wave height distribution was measured with a resistive probe and the wave slope distribution by optical glitter detection using a photocell. The distributions of backscattered sound pressures were recorded for surface roughnesses and sound frequencies corresponding to a very wide range of roughness conditions. Both statistical and resonance theories have regions of applicability and regions where they fail to predict the backscatter. Backscattering may be considered to be due to these two mechanisms, since a summation of the predictions of the two theories fits the experimental data fairly well over the complete range of angles of incidence studied. A method of analysis is suggested to relate the doppler shifted continuous wave sound spectrum to the surface wave spectrum.

14. KEY WORDS	LINK A		LINK B		LINK C	
	ROLE	WT	ROLE	WT	ROLE	WT
Scattering						
Backscattering						
Acoustic Scattering						
Rough Water Surface						
Wave Height Distribution						
Wave Slope Distribution						
Wave Spectra						
Surface Reverberation						
Doppler Shift						

thesB1794
DUDLEY KNOX LIBRARY
3 2768 00407058 1
DUDLEY KNOX LIBRARY